1. The Classification of Exact Quantum Methods for Nonreactive Scattering.

2. Quantum Mechanical Calculations of Rotational-Vibrational Scattering in Homonuclear Diatom-Atom Collisions.

3. The Effect of the Potential Well on Vibrational Scattering and the Validity of SSH Theory.

Thesis by
Albert F. Wagner

In partial fulfillment of the requirements
for the degree of
Doctor of Philosophy

California Institute of Technology
Pasadena, California
1972
(submitted January 18, 1972)

Dedication

This thesis is dedicated to my wife Arlene, who put up with loneliness, very real poverty and a scudsy blue jacket, but gave out snickerdoodles, Old Man Hat and lots of TLC; to my parents from whom I inherited a basic optimism and peace of mind so necessary for survival in this loony bin; to my advisor, Vincent McKoy, for his encouragement and guidance, and for his efforts in getting me a job; to my fellow inmates who are married, in particular: Woody and Kathy Wilson, Dick and Barbara Blint, Ed and Isabel O'Brien, Luis and Hazel Kahn, Frank and Pat Bobrowicz, Tim and Catie Surratt - Arlene and I thank you for the friendship and we hope you all find jobs; to my fellow inmates who are single, in particular: "Lafite" Bob Ladner, Vince Gutschick (currently flying paper airplanes at Berkeley), Al Mortola (Natomas never had a better friend), Steve Guberman (from whom I learned something of baseball, classical music and procrastination), John Rose (the okapi never had a better friend) - Arlene and I will never forget such a motley crew; to my noninmate teachers who taught me the difference between physics and formulas; to the interesting and almost always friendly people I have met in and around Caltech; and to the fervent hope that, after all this education, I may regain a sense of compassionate involvement in the real world.

My ninety-five rejection slips I dedicate to graduate students everywhere who persist in writing a purely theoretical thesis.

Abstract

Part 1. The exact quantum methods for the calculation of nonreactive scattering are classified. The classification is based on the essential characteristics of methods, not their detailed technical aspects. As a result the potential efficiency of each class of methods can be determined. Methods derived from differential formalism (time-independent and time-dependent Schroedinger equations) and from integral formalism (Lippmann-Schwinger equation) are reviewed. The most efficient class of differential methods are found to be time-independent perturbation propagation channel methods. Integral and differential methods are found to be very similar. There seems to be no room for any further dramatic improvements in exact nonreactive quantum methods.

Part 2. Most calculations of the vibrational scattering of diatom-atom collisions use the breathing sphere approximation (BSA) of orientation-averaging the intermolecular potential. The resulting angularly symmetric potential cannot cause rotational scattering. We determine the error introduced by the BSA into observables of the vibrational scattering of low-energy homonuclear diatom-atom collisions by comparing two quantum mechanical calculations, one with the BSA and the other with the full angularly asymmetric intermolecular potential. For reasons of economy the rotational scattering of the second calculation is restricted by the use of special incomplete

channel sets in the expansion of the scattering wavefunction. Three representative collision systems are studied: H_2-A, O_2-He, and I_2-He. From our calculations we reach two conclusions. First, the BSA can be used to analyze accurately experimental measurements of vibrational scattering. Second, measurements most sensitive to the symmetric part of the intermolecular potential are, in order, elastic cross sections, inelastic cross sections and inelastic differential cross sections. Elastic differential cross sections are sensitive to the potential only if the collision is "sticky", with scattering over a wide range of angles; I_2-He is such a collision. Otherwise the potential sensitivity of elastic differential cross sections is concentrated in the experimentally difficult region of very small angle scattering.

Part 3. The vibrational deexcitation probability, P_{10}, is calculated quantum mechanically over a large energy range for models of three collision systems: O_2-O_2, Cl_2-Cl_2, and Br_2-Br_2. The vibrational deexcitation cross section, σ_{10}, is similarly calculated for the Cl_2-Cl_2 model. P_{10} and σ_{10} are obtained for the Lennard-Jones intermolecular potential and three other "well-less" potentials designed to duplicate the scattering of the Lennard-Jones potential. The results emphasize the adiabatic nature of potentials with wells and indicate that the acceleration approximation for the effect of the well is not valid. The curves of P_{10} and σ_{10} as a function of initial trans-

lational energy are used to obtain exact collision numbers. These numbers are compared to the results of SSH theory. SSH theory is found to predict collision numbers with reasonable accuracy except at low temperatures. SSH theory is also not suitable for analyzing experimental collision numbers for the well depth potential parameter.

Table of Contents

Part 1

Part 2

Part 3

Forward

In this forward I would like to discuss informally the work reported in this thesis within the context of larger developments in the theory of chemical dynamics. Consider theoretical chemical dynamics divided into two groups. In one group I place all theories that explicitly involve the calculation, from given intermolecular forces, of the motion of the chemical system during collision; in the second group I place all other theories. This latter group is by far the largest, for it contains most of the semiempirical and phenomenological theories often used by experimentalists. In contrast, the first group is a rather new development used mainly by molecular beamists and some spectroscopists. My thesis work belongs to the first group, which I label chemical scattering theory. By definition chemical scattering theory is the fundamental investigation of the relationship of dynamics to structure as revealed by intermolecular forces. Many hope that the theory will eventually be able to explain why semiempirical or phenomenological theories work by revealing in detail the relationship of intermolecular forces to collision observables. At present the theory is a long way from significant achievements. An example is the fact that the three dimensional quantum mechanical calculation of the dynamics of the low-energy collision $H + H_2$ in the gas phase is considered a major development. To the organic and inorganic synthetic chemist this must seem like so much malarky. While there is no doubt that chemical scattering theory is in its infancy, like all infants it is growing fast. I

would like to review some of the developments in this field since 1966 and then indicate how my thesis work is involved.

Binary collisions involving only two partners are the simplest type of collision and therefore the type that receives the most theoretical consideration. Binary collisions may be classified as elastic, nonreactive inelastic, reactive and dissociative. Except for the elastic class, each class of binary collisions contains examples whose dynamics are so complicated that they are not susceptible to practical calculations now or in the forseeable future. In fact even the simplest examples of each of the last three classes of binary collisions are not susceptible to practical calculation without highly efficient computational methods. The question of efficient methods is complicated by the presence of three mechanics in chemical scattering theory:classical, semiclassical and quantum mechanics. Each mechanics has its own formalism which gives rise to a variety of computational methods. Although quantum mechanics is the only universally valid mechanics, classical and semiclassical mechanics are often operationally and conceptually easier to use. Therefore the development of highly efficient methods must proceed in two stages: first, the most efficient methods of each mechanics must be discovered; second, the regions of applicability of classical and semiclassical methods must be determined. When efficient methods are available the simplest cases of each type of binary collision can be studied and approximations de-

veloped that will allow the accurate, if not exact, calculation of the dynamics of more complex cases. Since 1966 the greatest effort has been in the first stage of the development of methods. In 1966 essentially exact quantum methods existed only for elastic scattering. Now highly efficient methods for nonreactive scattering are available. Although there has been little progress in the development of quantum methods for dissociative scattering, there are several quantum methods for reactive scattering under intensive development. In 1966 semiclassical mechanics as it is presently known did not exist. In the last two or three years its formalism and computational methods have been developed. In 1966 classical methods existed, but had never been applied on the scale required to study chemically interesting systems. Now classical trajectory studies of simple collisions and of severe models of complex collisions are fairly routine. In the future, further development of reactive and dissociative quantum methods and the thorough comparison of the three mechanics should be expected.

When a new computational method is developed, it is usually applied to the study of some chemical system; little or no effort is expended in comparing the efficiency and accuracy of the method to other methods. Unfortunately, my thesis suffers in this regard. I examine quantum mechanically the rotational-vibrational scattering of diatoms with themselves and with other atoms. I use one of the most efficient quantum methods, but make no attempt to de-

termine whether more efficient classical or semiclassical methods may apply. The thorough comparison of the three mecnanics for the calculation of rotational-vibrational scattering would be a thesis project in itself and, by rights, one that should have preceded my work. But at the time my thesis work was begun, the comparison of the three mechanics was not envisioned. My work is divided into three parts. In the first part I summarize and evaluate recent developments in exact nonreactive inelastic quantum methods. I conclude that there will be no new conceptual developments that will lead to dramatic improvements in existing methods, because the most efficient methods currently available have optimally reduced all the dimensions of the space over which a scattering solution must be calculated. The results of the last two parts of my thesis are made economically feasible by the use of one of the best available methods, the Gordon propagation method. In the second part of the thesis I evaluate an often used approximation regarding the effects of rotations on vibrational scattering. Almost all approximate theories of the vibrational scattering of molecules begin with the assumption that the rotationally averaged vibrational scattering by an angular asymmetric intermolecular potential is equivalent to the vibrational scattering by a rotationally averaged (i.e. spherically symmetric) intermolecular potential. In other words, rotationally averaging the scattering can be done by rotationally averaging the forces. If this assumption is true, there is no need to consider ex-

plicitly rotational motion and the calculation is therefore drastically simplified. My evaluation of this assumption involves other assumptions, but of a much less severe and more readily verifiable nature. I study only homonuclear diatom-atom collisions at low energy and conclude that the assumption introduces little error into the calculations. In the last part of the thesis I examine the effect of the well on vibrational excitation. The modeling of the collision system is more severe than in the second part and, as a result, the conclusions are less quantitative. The calculation also affords an opportunity to evaluate SSH theory, a commonly used set of formulas for the evaluation of vibrational relaxation times. My calculations indicate that potentials with wells are more adiabatic than "well-less" potentials and that SSH theory is accurate except at low temperatures.

My work has used the most recent developments in computational methods to study the simplest examples of nonreactive inelastic binary collisions. The work has led to the verification of often-used approximations of previously unknown validity and to the isolation of the effects on vibrational scattering of certain features of intermolecular forces.

Part 1: The Classification of Exact Quantum Methods for Nonreactive Scattering

INTRODUCTION

The major purpose of the study of collisions is to discover the relation between scattering observables and intermolecular forces. When this relation is known, the dynamics of chemical systems can be related to the structure of the molecules and atoms. In gross observations at low energies and in precise observations at low and higher energies, the quantum nature of scattering is apparent. Therefore, the major purpose of collision studies is furthered by the development of exact quantum methods for the calculation of scattering observables from intermolecular forces. The most common type of collision in low density fluids is the binary collision. Binary collisions can be classified as nonreactive (energy and momentum are changed), reactive (particles are exchanged between collision partners), and dissociative (one or both of the collision partners breaks up). Collisions in which Pauli forces are important must be either reactive or dissociative, because the identical particles can not be claimed by either collision partner. This article will deal only with nonreactive collisions.

There are many methods, presently available or readily developed, which can quantitatively describe the exact quantum mechanical scattering of nonreactive collisions. In this article we will identify several classes of methods on the basis of each method's essential characteristics. Essential characteristics answer such questions as: does the method involve the inversion of a matrix, the solution to a partial differential equation, the

evaluation of a transcendental function, etc. A method's essential characteristics can be contrasted with its technical aspects: how a matrix is inverted, which numerical method is used to solve the partial differential equation, etc. There will be no examination of a method's technical aspects. Therefore, we will be able to determine only the potential efficiency of each class of methods. However, it is doubtful that technical considerations would reverse our major conclusions. The rest of the article is divided as follows. Section I compares global to channel methods. Section II contrasts time-independent and time-dependent channel methods based on Schroedinger's differential formalism. Sections III, IV, and V discuss in greater detail time-independent channel methods. Section VI examines channel methods based on the Lippmann-Schwinger integral formalism. Section VII summarizes our conclusions.

I. GLOBAL VERSUS CHANNEL METHODS

There are two generalized coordinates that describe a nonreactive collision: $\vec{r}_1$ represents all the internal coordinates of the collision partners and $\vec{r}$ is the translational or external coordinate vector between the centers of mass of the two partners. Basically, three different but equivalent equations of motion exactly describe the quantum mechanical dynamics of a nonreactive collision; the Lippmann-Schwinger equation and the time-independent and time-dependent Schroedinger equations. The nature of a method for calculating nonreactive scattering depends upon the equation from which

the method is derived. Briefly, each equation must be solved for some function which contains all the scattering information. The generalized space over which the function must be known is $\vec{r}_1$, $\vec{r}$, and possibly t (time). Methods which directly solve for the function over this space we call global methods.[1]

For any collision system whose intermolecular forces are known well enough to make a scattering calculation possible, we know or can readily determine all the eigenstates for the internal motion of both collision partners. Through a partial wave expansion, we can describe translational motion in θ and ϕ, the angular coordinates of $\vec{r}$, in terms of the occupation of known orbital angular momentum states. With this knowledge, we can describe the collision in terms of two new coordinates: $\vec{x}$ which is $(\vec{r}_1, \theta, \phi)$ and r which is $|\vec{r}|$. Combining the internal and the orbital angular momentum states, we can form a complete set of channels, which are the eigenstates for the $\vec{x}$ motion of the collision system at very large r. In a similar description of the collision, we parameterize the $\vec{x}$ coordinate as $\vec{x}(r)$. At any value of r, with some effort, we can form a complete set of adiabatic channels, which are the eigenstates for the $\vec{x}$ motion of the collision system at r. No matter which approach is used, we can describe the motion of the collision system at any value of r in terms of the occupation of the channels or adiabatic channels. If the function to be determined by a global method is expanded in terms of channels or adiabatic channels, the single equation for the function is reduced to a coupled set of equations in r for the channel coefficients. Methods which solve the

coupled set of equations we call channel methods.[2] In principle, channel methods are more efficient than global methods. The $\vec{x} \times r$ solution-space of global methods is reduced to the $N \times r$ solution-space of channel methods where N is the number of channels in the channel expansion. N is always far less than the number of points needed to cover $\vec{x}$. This advantage is not offset by the difficulty of forming channels or adiabatic channels.[3]

In contrast to global methods, channel methods for nonreactive collisions are not applicable, without major modifications, to any other type of binary collision. The efficiency of channel methods rests upon the fact that in nonreactive collisions the internal and translational angular coordinates can be treated differently from the separation coordinate. During a reactive collision all the coordinates can evolve into one another to produce a new set of internal and translational angular coordinates and a new separation coordinate. There is a set of channels for the original coordinates $(\vec{x}, r)$ and a different set of channels for the new coordinates $(\vec{x}', r')$. Channel methods for reactive collisions must find ways of linking together expansion coefficients for the two sets of channels.[4] In dissociative collisions, new coordinates can evolve with the form $(\vec{x}', r', r'')$. At present there is no known way to formulate dissociative scattering in terms of channel expansions.[5] Global methods make no distinctions between $\vec{x}$ and r and hence can be applied without major modifications to both reactive and nonreactive collisions.[6] Because the presence of two separation coordinates in dissociative collisions

introduces a continuum, not all global methods can be applied to dissociative scattering.

II. TIME-INDEPENDENT AND TIME-DEPENDENT CHANNEL METHODS

In this section we compare the channel methods that derive from the time-independent and from the time-dependent Schroedinger equations. Most exact channel methods in current use are based on the time-independent Schroedinger equation which we will examine first.

All information on the nonreactive scattering of two partners colliding with a total system energy of E is contained in the wavefunction Ψ, a solution of the time-independent Schroedinger equation

$$[\mathcal{H} - E]\Psi = 0 \tag{1}$$

$$\text{where } \mathcal{H} = -\frac{\hbar^2}{2m} \nabla^2_{\vec{r}} + V(\vec{r}, \vec{r}_1) + \mathcal{H}(\vec{r}_1)$$

where $\mathcal{H}(\vec{r}_1)$ is the Hamiltonian for the internal motion of both partners, $V(\vec{r},\vec{r}_1)$ is the intermolecular potential, and $\nabla^2_{\vec{r}}$ has the form

$$-\frac{\hbar^2}{2m} \nabla^2_{\vec{r}} = -\frac{\hbar^2}{2m} \frac{1}{r^2} \left(r^2 \frac{\partial}{\partial r}\right) + \frac{\hat{L}^2}{2mr^2} \tag{2}$$

where $\hat{L}^2$ is the squared angular momentum operator and m is the reduced mass. If the initial internal states of both partners are characterized by $\xi_i(\vec{r}_1)$, the i^{th} eigenfunction of $\mathcal{H}(\vec{r}_1)$, then the two boundary conditions for Ψ_i are

$$\Psi_i \xrightarrow[r\to 0]{} 0 \tag{3}$$

$$\Psi_i \xrightarrow[r\to\infty]{} \xi_i(\vec{r}_1)\ell^{ik_i z} + \sum_j f_{ij}(\Omega)\xi_j(\vec{r}_1)\frac{\ell^{ik_j r}}{r} \tag{4}$$

where k_j is the wavenumber for the translational motion of the two collision partners in the j^{th} state, $f_{ij}(\Omega)$ an unknown function of the solid angle Ω, and z is r cos θ. The first boundary condition prevents the inner penetration of particles. The second boundary condition describes a system operating under steady state conditions. The Hamiltonian for motion in the coordinates $\vec{x}(r)$ is

$$\mathcal{H}_{\vec{x}(r)} = \frac{\hat{L}^2}{2mr^2} + V(\vec{r}, \vec{r}_1) + \mathcal{H}(\vec{r}_1). \tag{5}$$

The eigenfunctions of this Hamiltonian are the adiabatic channels. At large r, the intermolecular potential is zero. Therefore, the Hamiltonian whose eigenfunctions are channels is:

$$\mathcal{H}_{\vec{x}} = \frac{\hat{L}^2}{2mr^2} + \mathcal{H}(\vec{r}_1). \tag{6}$$

There are an infinite number of channels or adiabatic channels. However, the intermolecular potential couples the channels, in the proper representation,[7] into finite member sets; members of different sets are left uncoupled. Each set is an expansion set for a partial wavefunction. Each partial wavefunction is a solution to Schroedinger's equation and obeys the first boundary condition on Ψ_i and that part of the second boundary condition on Ψ_i which involves

the channels of its expansion set. Ψ_i is the sum of all the partial wavefunctions. Let a particular partial wavefunction be expanded as $\frac{1}{r}\vec{\chi}\vec{\phi}_i$ where the row vector $\vec{\chi}$ is the channel expansion set and the column vector $\vec{\phi}_i$ is the set of channel coefficients. Substitution in Eq. (1) followed by multiplication by each χ_i and integration over $\vec{x}$ gives

$$[-\underset{\sim}{\frac{\partial^2}{\partial r^2}} + \underset{\sim}{U}(r) - \underset{\sim}{\kappa^2}]\vec{\phi}_i = 0 \tag{7}$$

$$\text{where } \underset{\sim}{\frac{\partial^2}{\partial r^2}} = \frac{\partial^2}{\partial r^2}\underset{\sim}{I} \text{ and } \underset{\sim}{\kappa^2} = \kappa^2 \underset{\sim}{I}.$$

Here $\underset{\sim}{I}$ is the identity matrix, κ is the wavenumber for the total energy, and the (i, j) element of $\underset{\sim}{U}$ is

$$U_{ij} = \frac{2m}{\hbar^2}\langle \chi_i \mathcal{H}_{\vec{x}}(r)\, \chi_j \rangle \tag{8}$$

where the brackets denote integration over $\vec{x}$. One boundary condition on $\vec{\phi}_i$ is

$$\vec{\Phi}_i \xrightarrow[r\to 0]{} 0. \tag{9}$$

The other boundary condition follows from the asymptotic form of the partial wavefunction. $\vec{\phi}_i$ cannot be determined directly, because its second boundary condition specifies a form and not a value. Instead, Eq. (7) must be solved for all the independent solutions that obey the one value boundary condition on $\vec{\phi}_i$. We call these solutions primitive. If N is the number of channels in the expansion,

there are N independent primitive solutions. Let $\underset{\sim}{\psi}$ be the N × N matrix whose columns are these N solutions. Then any method which derives from the time-independent Schroedinger equation and involves an expansion in channels solves the equation:

$$[-\underset{\sim}{\frac{\partial^2}{\partial r^2}} + \underset{\sim}{U}(r) - \underset{\sim}{\kappa^2}]\underset{\sim}{\psi} = 0 \tag{10}$$

$$\text{where } \underset{\sim}{\psi} \xrightarrow[r\to\infty]{} 0$$

and where the second boundary condition on $\underset{\sim}{\psi}$ is arbitrary, provided it yields a linearly independent $\underset{\sim}{\psi}$. If the partial wavefunction is expanded in the set of adiabatic channels $\vec{\chi}(r)$, then the same analysis as above produces a different equation[8] for $\underset{\sim}{\psi}$:

$$[-\underset{\sim}{\frac{\partial^2}{\partial r^2}} - 2\,\underset{\sim}{A}\,\underset{\sim}{\frac{\partial}{\partial r}} - \underset{\sim}{B} + \frac{2m}{\hbar^2}\,\underset{\sim}{\mathcal{E}}(r) - \underset{\sim}{\kappa^2}]\underset{\sim}{\psi} = 0 \tag{11}$$

$$\text{where } A_{ij} = \langle \chi_i(r)\, \frac{\partial}{\partial r}\, \chi_j(r)\rangle$$

$$B_{ij} = \langle \chi_i(r)\, \frac{\partial^2}{\partial r^2}\, \chi_j(r)\rangle .$$

$\underset{\sim}{\mathcal{E}}(r)$ is the diagonal matrix of the eigenvalues of $\vec{\chi}(r)$. An expansion in adiabatic channels is preferable to an expansion in channels only when $\vec{\chi}(r)$ and $\underset{\sim}{\mathcal{E}}(r)$ are readily available, such as from the calculation of the potential curves of atoms and molecules in various electronic states. Although Eqs. (10) and (11) appear to be quite different, everything we will discuss about the solution of Eq. (10)

can be applied with minor alteration to the solution of Eq. (11). For this reason we will no longer discuss the adiabatic channel expansions that result in Eq. (11).

When the time-dependent Schroedinger equation is used,[9] the wavefunction, $\Psi_i(\vec{r}_1, \vec{r}, t)$, for the system before collision at $t = 0$ is a wavepacket:

$$\Psi_i(\vec{r}_1, \vec{r}, 0) = \xi_i(\vec{r}_1) \int_{-\infty}^{\infty} G(k) \ell^{ikz} dk. \tag{12}$$

The wavenumber distribution, G(k), is dependent on the experimental conditions which the calculation simulates. The time-dependent method cannot determine the scattering of the collision system at a precise total system energy of E because the initial wavepacket contains contributions from the spread of relative translational energies allowed by G(k). The calculated scattering is specific to the experimental conditions that determine G(k). The time-dependent Schroedinger equation governs how $\Psi_i(\vec{r}_1, \vec{r}, t)$ evolves in time from $\Psi_i(\vec{r}_1, \vec{r}, 0)$. Its formal solution is:

$$\Psi_i(\vec{r}_1, \vec{r}, t) = e^{-i(t/\hbar)\mathcal{H}} \Psi_i(\vec{r}_1, \vec{r}, 0) \tag{13}$$

where $e^{-i(t/\hbar)\mathcal{H}}$ is the time evolution operator. For a short increment in time, the time evolution operator can be approximated[9] by

$$e^{-i(\Delta t/\hbar)\mathcal{H}} \approx [1 + (i\Delta t/2\hbar)\mathcal{H}]^{-1}[1 - (i\Delta t/2\hbar)\mathcal{H}]. \tag{14}$$

This produces the equation:

$$[1 + i(\Delta t/2\hbar)\mathcal{H}]\Psi_i(\vec{r}_1, \vec{r}, \Delta t) = [1 - i(\Delta t/2\hbar)\mathcal{H}]\Psi(\vec{r}_1, \vec{r}, 0). \qquad (15)$$

Naturally, this same equation can be used to relate $\Psi_i(\vec{r}_1, \vec{r}, 2\Delta t)$ to $\Psi_i(\vec{r}_1, \vec{r}, \Delta t)$. In this way Ψ_i can be propagated over all space to a post-collision time when it can be analyzed for the scattering information it contains. As before in time-independent formalism, we can decompose Ψ_i into partial wavefunctions each of which can be expanded in a different set of channels. However, now the channel coefficients will be functions of r and t. The equation for $\vec{\phi_i}(r, t)$ analogous to Eq. (10) in the time-independent formalism is:

$$[-\underset{\sim}{\frac{\partial^2}{\partial r^2}} + \underset{\sim}{U}(r) - \frac{i\Delta t\hbar}{4m}\underset{\sim}{I}]\vec{\phi}_i(r, \Delta t)$$

$$= [-\underset{\sim}{\frac{\partial^2}{\partial r^2}} + \underset{\sim}{U}(r) + \frac{i\Delta t\hbar}{4m}\underset{\sim}{I}]\vec{\phi}_i(r, 0) \qquad (16)$$

Since $\vec{\phi}_i(r, 0)$ can be determined from the wavepacket, the right hand side of this equation is a known function of r. All channel methods that derive from the time-dependent Schroedinger equation solve this set of equations. The advantage of this formalism is that ϕ_i can be directly calculated without the calculation of primitive solutions. The disadvantages are that complex arithmetic must be used (time-independent channel methods can avoid this) and that Eq. (16) must be solved at each time increment. If N_t is the number of time increments that must be calculated, it is generally true that $N_t \gg N$. It is faster to solve Eq. (10) once

for N primitive solutions than to solve Eq. (16) N_t times for one solution. Therefore, time-dependent channel methods are not as efficient as time-independent channel methods.

III. PROPAGATION AND MATRIX METHODS

In the solution of Eq. (10) for $\underset{\sim}{\psi}$ we are free to choose one linearly independent boundary condition we want $\underset{\sim}{\psi}$ to obey. There are two types of boundary conditions we can select which give rise to two types of channel methods. We can specify the value of the derivative of $\underset{\sim}{\psi}$ at the same point at which the nonarbitrary boundary condition specifies the value of $\underset{\sim}{\psi}$:

$$\frac{\partial}{\partial r} \underset{\sim}{\psi} \xrightarrow[r \to 0]{} \underset{\approx}{A} \tag{17}$$

where $\underset{\approx}{A}$ is a linearly independent constant matrix. Since $\underset{\sim}{\psi}$ obeys a second-order differential equation, the value and slope of $\underset{\sim}{\psi}$ at one point are all that a variety of numerical techniques require to propagate $\underset{\sim}{\psi}$ step-by-step through r space. Methods based on the initial specification of the value and slope of $\underset{\sim}{\psi}$ at one point we call propagation methods.[10] In another approach we can specify the value of $\underset{\sim}{\psi}$ or its derivative at some other point besides $r \to 0$. The only reasonable choice is to specify $\underset{\sim}{\psi}$ at $\bar{r}$, some value of r in the asymptotic region:

$$\underset{\sim}{\psi}(\vec{r}) = \underset{\approx}{B} \tag{18}$$

where $\underset{\approx}{B}$ is a linearly independent constant matrix. There are a

variety of techniques whereby $\underset{\sim}{\psi}(r)$ may be related to $\underset{\sim}{\psi}(r')$ and $\underset{\sim}{\psi}(r'')$ where $r' < r < r''$. Since $\underset{\sim}{\psi}$ at $r \to 0$ and $r = \bar{r}$ is known, $\underset{\sim}{\psi}$ on a grid of points between 0 and $\bar{r}$ can be simultaneously determined by the inversion of a large matrix which expresses the relationships between the values of $\underset{\sim}{\psi}$ on different points of the grid. We call such methods matrix methods.[12] Any other choice for a boundary condition besides Eqs. (17) and (18) will require a hybrid matrix propagation method with no gain in efficiency.

In the classically forbidden region, $\underset{\sim}{\psi}$ and the intermolecular potential are changing very rapidly. Any instabilities in the numerical techniques of a method are most likely to become severe in this region. From this point of view it is important to discuss the meaning of a boundary condition at $r \to 0$. In practice, it is found[13] that whatever boundary conditions apply at $r \to 0$ can also be made to apply at r_0, that value of r where the intermolecular potential is ten or fifteen times the total energy of the system. In fact in the region around r_0 the primitive solutions calculated with the boundary conditions applied at r_0 will differ by many orders of magnitude from the primitive solutions calculated with the boundary conditions applied exactly at $r = 0$. However, in the region about r_0 both solutions are very small. For $r \gg r_0$ where both solutions are significant in size, their agreement is essentially perfect. This indicates that large relative errors in the calculation of $\underset{\sim}{\psi}$ can be tolerated as long as $\underset{\sim}{\psi}$ is very small in the classically forbidden region. Consequently choosing a starting point smaller than r_0 does not improve the accuracy of

$\underset{\sim}{\psi}$ but does improve the odds that numerical instability will destroy the solution.

We would like to evaluate the relative efficiency of matrix and propagation methods. Before we can do that we must discuss the difficulties introduced by closed channels (Section IV) and perturbation methods, the most efficient of matrix and propagation methods (Section V).

IV. CLOSED CHANNELS

Because many collision systems execute highly excited transient modes of internal motion during the time of closest approach of the collision partners, many channel expansions must include closed (energetically inaccessible) channels. Let N and N_0 be the total number of channels and the number of open channels respectively. Let $\underset{\sim}{\phi}$ be the N × N matrix whose L^{th} column, for L = 1, ..., N, is the set of channel coefficients for the wavefunction whose initial channel is the L^{th} one. $\vec{\phi}_i$ in Eq. (7) is the i^{th} column of $\underset{\sim}{\phi}$. There are N_0 open columns of $\underset{\sim}{\phi}$ whose $N - N_0$ closed elements go to zero as r becomes large. This is true because closed channels describe only transient excited internal motion that cannot persist after the collision is over, that is, when r is large. In fact, the more highly excited the motion described by the closed channel, the more rapidly its channel coefficient will go to zero as a function of r. In general, all closed channel coefficients assume their asymptotic form at values of r smaller than

those at which open channel coefficients assume their final form. There are $N - N_0$ closed columns of $\underset{\sim}{\phi}$ whose diagonal elements blow up as r grows large because of the negative translational energy associated with an initial closed channel. These columns of $\underset{\sim}{\phi}$ are completely unphysical. Because $\underset{\sim}{\psi}$ and $\underset{\sim}{\phi}$ are both a complete set of independent solutions to the same equations there exists a matrix $\underset{\sim}{C}$ with a well defined inverse such that:

$$\underset{\sim}{\psi} = \underset{\sim}{\phi}\underset{\sim}{C} \tag{19}$$

$$\underset{\sim}{\phi} = \underset{\sim}{\psi}\underset{\sim}{C}^{-1}. \tag{20}$$

Since the form of $\underset{\sim}{\phi}$ is specified in the asymptotic region of large r, once $\underset{\sim}{\psi}$ is known in the asymptotic region, $\underset{\sim}{C}^{-1}$ and hence $\underset{\sim}{\phi}$ can be readily determined.

With matrix methods, each column in $\underset{\sim}{\psi}$ is calculated separately. With the proper selection of $\underset{\sim}{B}$, the first N_0 columns can be open and independent. These N_0 columns span the space of open solutions. Therefore, any open solution of $\underset{\sim}{\phi}$ can be expressed as a linear combination of just these N_0 columns; $\underset{\sim}{C}^{-1}$ would not couple any other columns of $\underset{\sim}{\psi}$ into the first N_0 columns in the construction of any open column of $\underset{\sim}{\phi}$. While the other $(N - N_0)$ columns of $\underset{\sim}{\psi}$ could be generated, it would be pointless because these columns only give us information about the unphysical closed columns of $\underset{\sim}{\phi}$. The selection of $\underset{\sim}{B}$ which necessitaties the calculation of only N_0 columns of $\underset{\sim}{\psi}$ is straightforward. Each column in $\underset{\sim}{B}$ is used in calculating the corresponding column in $\underset{\sim}{\psi}$. If the

closed elements of the first N_0 columns of $\underset{\sim}{B}$ are zero but the columns are linearly independent, then the first N_0 columns of $\underset{\sim}{\psi}$ will have closed elements that are zero in the asymptotic region, i.e., the first N_0 columns of $\underset{\sim}{\psi}$ will be open.

It is often assumed that propagation methods must propagate the full $N \times N$ $\underset{\sim}{\psi}$ matrix into the asymptotic region. If this were true, then propagation methods would not handle closed channels as efficiently as matrix methods. However, the assumption is not true. To show this we must discuss the stabilization of $\underset{\sim}{\psi}$ and its implications.

If $\underset{\sim}{A}$ is linearly independent, $\underset{\sim}{\psi}$ at the start of its propagation will also be linearly independent. However, due to the unbounded growth of the closed columns of $\underset{\sim}{\phi}$, at large enough r the closed columns of $\underset{\sim}{\phi}$ will completely dominate $\underset{\sim}{\phi}\underset{\sim}{C}$. This means that during propagation each of $\underset{\sim}{\psi}$'s columns become, to all significant figures retained, the linear combination of only the closed columns of $\underset{\sim}{\phi}$. In other words, when closed channels are present, $\underset{\sim}{\psi}$ has an innate tendency to linear dependence. Any procedure which suppresses this tendency we will call stabilization. Although there are several stabilization procedures, their derivations are similar to the following simplified set of arguments. When $\underset{\sim}{\psi}$ has propagated to a large enough value of r to show signs of linear dependence, we wish to find a matrix $\underset{\sim}{T}$ which back multiplies $\underset{\sim}{\psi}$ so that $\underset{\sim}{\psi}\underset{\sim}{T}$ has a much reduced tendency to linear dependence. Then the propagation is continued with $\underset{\sim}{\psi}\underset{\sim}{T}$. The proper $\underset{\sim}{T}$ must remove most of the contribution of the L^{th} closed column of $\underset{\sim}{\phi}$ from all but the

L^{th} column of $\underset{\sim}{\psi}\,\underset{\sim}{T}$. If the closed elements of $\underset{\sim}{\phi}$ assumed their asymptotic form for all values of r, then all of the contribution of the L^{th} closed column of $\underset{\sim}{\phi}$ would be removed from all but the L^{th} column of $\underset{\sim}{\psi}\,\underset{\sim}{T}$ if

$$(\underset{\sim}{\psi}\,\underset{\sim}{T})_{LK} = 0 \quad \text{for } L \neq K \qquad (21)$$
$$= 1 \quad \text{for } L = K$$

for all K and for all $L > N_0$. This condition is sufficient to define $\underset{\sim}{T}$. Since $\underset{\sim}{\phi}$'s closed elements do not assume their asymptotic form for all values of r, $\underset{\sim}{T}$ defined by Eq. (21) will leave in each column of $\underset{\sim}{\psi}\,\underset{\sim}{T}$ residual contributions from the closed columns of $\underset{\sim}{\phi}$. At some larger value of r, linear dependence will again appear in $\underset{\sim}{\psi}\,\underset{\sim}{T}$ and the process must be repeated. However, each succeeding transformation leaves less and less residual contributions from the closed columns of $\underset{\sim}{\phi}$. In this way a linearly independent $\underset{\sim}{\psi}$ can be propagated into the asymptotic region.

Stabilization has two important implications. First, each succeeding transformation makes the first N_0 columns of $\underset{\sim}{\psi}$ look like just a linear combination of the open columns of $\underset{\sim}{\phi}$ and makes any other column of $\underset{\sim}{\psi}$ look like the corresponding column in $\underset{\sim}{\phi}$. Consequently, in the asymptotic region, to a high degree of accuracy only the first N_0 columns of $\underset{\sim}{\psi}$ are needed to determine any open column of $\underset{\sim}{\phi}$ by Eq. (20). The only reason for calculating the $N_0 + 1$ to N columns of $\underset{\sim}{\psi}$ is to permit stabilization; these columns are required in the determination of each $\underset{\sim}{T}$. The second implication of stabilization is as follows. Since each transformation

of $\underset{\sim}{\psi}$ increases the similarity of its closed rows to those of $\underset{\sim}{\phi}$, at large enough values of r, the nondiagonal elements of each closed row of $\underset{\sim}{\psi}$ can be set to its asymptotic form of zero with no appreciable effect on the other elements. In general, this will occur at values of r before the asymptotic region. If a value of r has been reached where the L^{th} closed row of $\underset{\sim}{\psi}$ can be set to zero except for ψ_{LL}, then there is no longer any reason to calculate the L^{th} column of $\underset{\sim}{\psi}$ for it is no longer needed to determine any subsequent $\underset{\sim}{T}$ matrix. In fact, the L^{th} row and column of $\underset{\sim}{\psi}$ can be dropped for the rest of the propagation. In practice the value of r where the L^{th} row and column can be dropped can be determined from tests like the ratio of $|U_{N_0L}\,\psi_{LN_0}|$ to $|(U_{N_0N_0} - E)\psi_{N_0N_0}|$. If this ratio is small, the L^{th} closed element in the $N_0{}^{th}$ column has little effect on the open elements of the column. Assuming all open columns are basically alike in this regard, when the ratio is small enough, the L^{th} row and column can be discarded.

With propagation methods, the full $N \times N$ $\underset{\sim}{\psi}$ matrix begins the propagation. However, the stabilizing transformations allow the dimensions of $\underset{\sim}{\psi}$ to be reduced to $N_0 \times N_0$ during the course of the propagation. In matrix methods, only N_0 columns are calculated but all N elements in each column are retained for the entire calculation. Both methods handle closed channels with about the same efficiency.

V. PERTURBATION METHODS

In the more straightforward matrix and propagation methods, the primitive solutions are calculated on a grid of points covering r space. The grid must be fine enough to permit the accurate determination of each oscillation that any element in the primitive solution may undergo. As a rule of thumb, a grid size should be about a tenth of a wavelength of the most rapidly oscillating channel coefficient. However, there is a more sophisticated approach, first fully developed by Gordon,[14] which calculates the primitive solutions by a perturbation scheme based upon an approximation to the intermolecular potential. These perturbation methods, both matrix and propagation, accurately determine the primitive solutions over intervals much larger than one tenth of a wavelength. For this reason, these methods are the most efficient methods that derive from the time-independent Schroedinger equation. In this section we develop the basic theory and several special features of perturbation propagation methods;[14, 15] reference will be made to matrix propagation methods[16] at the end.

The first step in a perturbation method is to approximate the potential matrix $\underset{\sim}{U}(r)$. Suppose we expand the partial wavefunction in the set of adiabatic channels, represented by the row vector $\vec{\chi}_{r_c}$, that are eigenfunctions of $\mathcal{H}_{\vec{x}}(r_c)$ [see Eq. (5)]. Let the potential matrix in this basis be $\underset{\sim}{U}(r_c, r)$ where the r_c emphasizes that the adiabatic channels are defined at $r = r_c$. From the

definition of $\underset{\sim}{U}(r)$ [Eq. (8)], $\underset{\sim}{U}(r_c, r_c)$ is diagonal. We can expand $\underset{\sim}{U}(r_c, r)$ about r_c:

$$\underset{\sim}{U}(r_c, r) = \underset{\sim}{U}(r_c, r_c) + (r - r_c)\underset{\sim}{U}'(r_c, r_c) + \tfrac{1}{2}(r - r_c)^2\underset{\sim}{U}''(r_c, r_c) + \ldots \tag{22}$$

where $\underset{\sim}{U}'(r_c, r_c)$, $\underset{\sim}{U}''(r_c, r_c)$, etc., are, in general, not diagonal. Over an interval centered about r_c, this expansion of $\underset{\sim}{U}(r_c, r)$ would converge with only a few terms. We could segment all r space into intervals over which the potential matrix, in the basis of adiabatic channels for the interval midpoint, would have its Taylor series expansion about the interval midpoint converge with only a few terms. To use this interval by interval approximation of the potential matrix, we have to be able to change the basis in which $\underset{\sim}{\psi}$ is expressed. For the n^{th} interval, let $\underset{\sim}{\psi}_n$ and r_n be the primitive solutions and the interval midpoint respectively. It is easy to show that if T_n is the unitary matrix defined by

$$\underset{\sim}{T}_n\underset{\sim}{U}(r_n)\underset{\sim}{T}_n^{-1} = \underset{\sim}{U}(r_n, r_n) \tag{23}$$

then at the boundary between the n^{th} and $(n + 1)^{th}$ interval

$$\underset{\sim}{\psi}_{n+1} = \underset{\sim}{T}_{n+1}^{-1}\underset{\sim}{T}_n\underset{\sim}{\psi}_n. \tag{24}$$

This relation allows us to change the basis of $\underset{\sim}{\psi}$ from interval to interval and thus use the expansion of $\underset{\sim}{U}(r)$ particular to each interval.

The second step in a perturbation propagation method is to devise an efficient way to propagate across an interval. We now drop the index n for the n^{th} interval. We would like to expand $\underset{\sim}{\psi}$ in a perturbation expansion:

$$\underset{\sim}{\psi} = \underset{\sim}{\psi}^0 + \underset{\sim}{\psi}^1 + \underset{\sim}{\psi}^2 + \ldots \tag{25}$$

where

$$[-\frac{\partial^2}{\partial \underset{\sim}{r}^2} + \underset{\sim}{U}_0(r_c, r) - \underset{\sim}{\kappa}^2]\underset{\sim}{\psi}^0 = 0. \tag{26}$$

For the perturbation expansion to be useful, $\underset{\sim}{\psi}^0$ must be readily determined. Practically, this demands that $\underset{\sim}{U}_0(r_c, r)$ be diagonal. $\underset{\sim}{U}_0(r_c, r)$ can be any number of terms in the Taylor series expansion of the diagonal of $\underset{\sim}{U}(r_c, r)$ about r_c. We propagate $\underset{\sim}{\psi}$ in the $\hat{\chi}_{r_c}$ basis over this interval because $\underset{\sim}{\psi}^0$ will be a good zeroth order estimate of $\underset{\sim}{\psi}$ since there are several choices of $\underset{\sim}{U}_0(r_c, r)$ that approximate $\underset{\sim}{U}(r_c, r)$ well over the interval. $\underset{\sim}{\psi}^0$ has the form

$$\underset{\sim}{\psi}^0 = \underset{\sim}{A}\,\underset{\sim}{a} + \underset{\sim}{B}\,\underset{\sim}{b} \tag{27}$$

where $\underset{\sim}{a}$ and $\underset{\sim}{b}$ are constant matrices and $\underset{\sim}{A}$ and $\underset{\sim}{B}$ are diagonal matrices whose i^{th} diagonal elements, A_i and B_i, are the two independent solutions to:

$$[-\frac{\partial^2}{\partial r^2} + U_{0\,ii}(r_c, r) - \kappa^2] \begin{Bmatrix} A_i \\ B_i \end{Bmatrix} = 0. \tag{28}$$

Substituting the expansion for $\underset{\sim}{\psi}$ in the equation for $\underset{\sim}{\psi}$ [Eq. (10)] and utilizing the definition of $\underset{\sim}{\psi}^0$, we get the equation for $\underset{\sim}{\psi}^i$ for

$i > 0$:

$$[-\underset{\sim}{\frac{\partial^2}{\partial r^2}} + \underset{\sim}{U}_0(r_c,r) - \underset{\sim}{\kappa}^2]\underset{\sim}{\psi}^i + [\underset{\sim}{U}(r_c,r) - \underset{\sim}{U}_0(r_c,r)]\underset{\sim}{\psi}^{i-1} = 0. \tag{29}$$

If r_s is the smaller interval boundary, the solution to $\underset{\sim}{\psi}^i$ is:

$$\underset{\sim}{\psi}^i = \underset{\sim}{W}^{-1} \int_{r_s}^{r} [-\underset{\sim}{A}(r)\underset{\sim}{B}(r') + \underset{\sim}{B}(r)\underset{\sim}{A}(r')][\underset{\sim}{U}(r_c,r') - \underset{\sim}{U}_0(r_c,r')]\underset{\sim}{\psi}^{i-1}(r')dr'$$

$$+ \underset{\sim}{A}\,\underset{\sim}{a}^i + \underset{\sim}{B}\,\underset{\sim}{b}^i \tag{30}$$

where

$$\underset{\sim}{W} = \underset{\sim}{B}'(r)\underset{\sim}{A}(r) - \underset{\sim}{B}(r)\underset{\sim}{A}'(r).$$

$\underset{\sim}{W}$, the wronskian matrix, is a constant matrix as are $\underset{\sim}{a}^i$ and $\underset{\sim}{b}^i$. The "$'$" denotes the derivative with respect to the distance coordinate. If $\underset{\sim}{a}$ and $\underset{\sim}{b}$ are chosen so that

$$\underset{\sim}{\psi}(r_s) = \underset{\sim}{\psi}^0(r_s) \text{ and } \underset{\sim}{\psi}'(r_s) = \underset{\sim}{\psi}^{0\prime}(r_s) \tag{31}$$

then $\underset{\sim}{a}^i$ and $\underset{\sim}{b}^i$ are zero for all values of i. Under these conditions, it is easy to show that the first nonzero derivative of $\underset{\sim}{\psi}^i$ evaluated at r_s is the $(i+1)^{th}$ derivative. This means that with propagation in r each higher order in the expansion of ψ changes more and more slowly from its value at r_s. This also means that the perturbation expansion can be made to converge to any order by choosing a small enough interval. This of course is

related to the fact that the Taylor series expansion of $\underset{\sim}{U}(r_c, r)$ converges to any order for a small enough interval about r_c.

The third and last step in a perturbation propagation method is to devise a procedure for determining the length of the interval. It is usually impractical to calculate any higher order than $\underset{\sim}{\psi}^1$. Therefore, the interval must be short enough so that $\underset{\sim}{\psi}^1$ is small relative to $\underset{\sim}{\psi}^0$, making $\underset{\sim}{\psi}^2$ negligibly small. Because of the matrix nature of $\underset{\sim}{\psi}^1$ and $\underset{\sim}{\psi}^0$, their relative comparison deserves some attention. What is important is that the largest element in each column of $\underset{\sim}{\psi}^1$ be small relative to the length of the corresponding column in $\underset{\sim}{\psi}^0$. In that way, the dominant scattering processes, which give rise to the largest channel coefficients, will be most accurately calculated; the lesser processes will be not so accurately calculated. Since experimental measurements also have this error pattern, there is no need to do the comparison any other way. Because $\underset{\sim}{\psi}^0$ and $\underset{\sim}{\psi}^1$ oscillate in the classically allowed region of r space, their relative comparison will also oscillate for reasons that do not reflect the convergence of the perturbation expansion. To remedy this difficulty, we proceed as follows. Over an interval in the classically allowed region, ψ^0_{ij} goes roughly as $\sin \vec{k}_i r$, where $\vec{k}_i$ is the average local wavenumber over the interval for the i^{th} channel. $\psi^{0\prime}_{ij}$ goes as $\vec{k}_i \cos \vec{k}_i r$. Because $|\sin \vec{k}_i r| + |\cos \vec{k}_i r|$ is an approximately constant function, $|\underset{\sim}{\psi}^0| + |\underset{\sim}{D}\,\underset{\sim}{\psi}^{0\prime}|$ is approximately constant over the interval if $\underset{\sim}{D}$ is a diagonal matrix whose i^{th} diagonal element is $\vec{k}_i^{-1}$. For the same interval, $|\underset{\sim}{\psi}^1| + |\underset{\sim}{D}\,\underset{\sim}{\psi}^{1\prime}|$ grows with propagation across the interval

and the comparison of $|\underset{\sim}{\psi}^1| + |\underset{\sim}{D}\,\underset{\sim}{\psi}^{1\prime}|$ to $|\underset{\sim}{\psi}^0| + |\underset{\sim}{D}\,\underset{\sim}{\psi}^{0\prime}|$ is non-oscillatory. Then in the classically allowed region, for $\underset{\sim}{\psi}^2$ to be negligibly small, ρ, the ratio of the largest element in $|\underset{\sim}{\psi}^1| + |\underset{\sim}{D}\,\underset{\sim}{\psi}^{1\prime}|$ to the length of the corresponding column in $|\underset{\sim}{\psi}^0| + |\underset{\sim}{D}\,\underset{\sim}{\psi}^{0\prime}|$, must be small at the end of the interval. In the interest of continuity we can apply this test, with $\underset{\sim}{D}$ suitably modified, to the classically forbidden region and the classical turning point regions of r space. We want to know how ρ goes with interval length h. We can determine how fast $|\underset{\sim}{\psi}^1| + |\underset{\sim}{D}\,\underset{\sim}{\psi}^{1\prime}|$ grows with interval length h by looking at the leading term in the Taylor series expansion of $\underset{\sim}{\psi}^1(r_s + h)$ about r_s:

$$\underset{\sim}{\psi}^1(r_s + h) = \underset{\sim}{\psi}^1(r_s) + h\psi^{1\prime}(r_s) + \tfrac{1}{2}h^2\psi^{1\prime\prime}(r_s) + \cdots$$

$$= 0 + h\cdot 0 + \tfrac{1}{2}h^2[\underset{\sim}{U}(r_c, r_s) - \underset{\sim}{U}_0(r_c, r_s)]\underset{\sim}{\psi}^0(r_s) + \cdots \quad (32)$$

Recalling the Taylor series expansion of $\underset{\sim}{U}(r_c, r)$ about r_c [Eq. (22)] and that $\underset{\sim}{U}_0(r_c, r)$ is diagonal, irrespective of the choice of $\underset{\sim}{U}_0(r_c, r)$, the lowest power of h in $\underset{\sim}{U}(r_c, r_s) - \underset{\sim}{U}_0(r_c, r_s)$ is

$$\underset{\sim}{U}(r_c, r_s) - \underset{\sim}{U}_0(r_c, r_s) = -\frac{h}{2}\,\underset{\sim}{U}'(r_c, r_c)_{od} + \cdots \quad (33)$$

where od means only the off diagonal elements of $\underset{\sim}{U}'(r_c, r_c)$. Hence for any perturbation method, the lead term in the expansion of $\underset{\sim}{\psi}^1(r_s + h)$ about r_s goes as the cube of the interval length. If we ignore the change in $|\underset{\sim}{\psi}^0| + |\underset{\sim}{D}\,\underset{\sim}{\psi}^{0\prime}|$ with h and presume that the lead term in the expansion of $|\psi^1(r_s + h)| + |\underset{\sim}{D}\,\psi^{1\prime}(r_s + h)|$ about

r_s dominates, then we can say ρ is proportional to h^3. If n and n + 1 label adjacent intervals, if δ is a given fraction for the maximum size of ρ, and if the proportionality constant between ρ and h^3 is about the same for adjacent intervals, then

$$h_{n+1} = \left(\frac{\delta}{\rho_n}\right)^{\frac{1}{3}} h_n. \tag{34}$$

Using this formula and an estimate for the first interval length, each successive interval can be estimated from the preceding one.

In the classically forbidden region, the interval predicting procedure can be modified. The length of the i^{th} column in $|\underset{\sim}{\psi}| + |D\underset{\sim}{\psi}'|$ grows exponentially in the classically forbidden region but reaches an approximate final value by the i^{th} classical turning point. In section III we pointed out that when the channel coefficients are very small in the classically forbidden region, large errors in their determination have negligible effect on the value of the coefficients in the classically allowed region. In practice, if the length of the i^{th} column of $|\underset{\sim}{\psi}| + |D\underset{\sim}{\psi}'|$ is approximately 1 by the i^{th} classical turning point, then in the region before that point only the absolute, not relative, size of the elements in the i^{th} column of $|\underset{\sim}{\psi}^1| + |D\underset{\sim}{\psi}^{1\prime}|$ need be considered in determining ρ. The result is smaller ρ's and larger h's, all consonant with the fact that larger relative errors in the wavefunction are tolerable when the wavefunction is small in the classically forbidden region. To choose the initial conditions such that the i^{th} column of $|\underset{\sim}{\psi}| + |D\underset{\sim}{\psi}'|$ will be approximately 1 by the i^{th} classical turning point,

we do the following. $\underset{\sim}{\psi}$ is very crudely approximated by $\underset{\sim}{\psi}^0+\underset{\sim}{\psi}^1$ over the one large interval from the origin of the calculation to the first classical turning point. At the origin,

$$\psi \approx \underset{\sim}{\psi}^0 = \underset{\sim}{A}\,\underset{\sim}{a} + \underset{\sim}{B}\,\underset{\sim}{b} \tag{35}$$

In this classically forbidden region either $\underset{\sim}{A}$ or $\underset{\sim}{B}$ is exponentially increasing with increasing r. Assume $\underset{\sim}{A}$ is increasing. Then $\underset{\sim}{B}$ is exponentially increasing with decreasing r and therefore $\underset{\sim}{b}$ must be zero or else $\underset{\sim}{\psi}$ will not go to zero at the origin. We are allowed to choose any value of $\underset{\sim}{a}$ as long as $\underset{\sim}{\psi}^0$, and therefore $\underset{\sim}{\psi}$, is linearly independent. The simplest choice for $\underset{\sim}{a}$ is

$$\underset{\sim}{a} = \bar{a}\,\underset{\sim}{I} \tag{36}$$

where $\bar{a}$ is just a constant. The constant is so adjusted that at the first classical turning point, the length of the first column of $|\underset{\sim}{\psi}^0 + \underset{\sim}{\psi}^1| + |\underset{\sim}{D}(\underset{\sim}{\psi}^{0\prime} + \underset{\sim}{\psi}^{1\prime})|$ is 1; to a much poorer approximation, this value of $\bar{a}$ will also make the length of the i^{th} column of $|\underset{\sim}{\psi}^0 + \underset{\sim}{\psi}^1| + |\underset{\sim}{D}(\underset{\sim}{\psi}^{0\prime} + \underset{\sim}{\psi}^{1\prime})|$ about 1 at the i^{th} classical turning point. Because the interval size is so large ρ for this propagation will always be much larger than δ. However, ρ can be used to estimate how long the first interval should be for an accurate propagation of $\underset{\sim}{\psi}$. This provides the estimate of the first interval size which we need before we can use the interval prediction formula Eq. (34).

There are three important implications of the perturbation propagation method outlined here. First, the intermolecular

potential and its derivatives have to be known only at the midpoint of each interval. For nonperturbation methods the potential has to be known at many more points. That means that relative to other methods the execution time of perturbation methods is not so potential-dependent and calculations with complicated potentials are correspondingly more practical. Second, most of the time taken up by perturbation methods is both in the determination of $\underset{\sim}{U}_0(r_c, r)$ and $\underset{\sim}{U}(r_c, r) - \underset{\sim}{U}_0(r_c, r)$ and in the transformation of $\underset{\sim}{\psi}$ from one adiabatic basis set to another. All this work is independent of κ^2. Therefore, if the scattering over an energy spectrum is to be performed, information from the calculation at one energy can be stored and then reused to drastically reduce the calculation time for other energies.[17] Third, perturbation matrix methods are not as efficient as similar propagation methods because the length of the interval cannot vary according to the dynamics of the collision. In matrix methods the channel coefficients at any one point cannot be known until the channel coefficients at all points are known. Hence, information about the channel coefficients, or the dynamics of the collision, cannot be used to determine interval lengths.

Time-independent perturbation methods, whether matrix or propagation, are the most efficient methods that derive from a differential formalism. While other methods must calculate $\underset{\sim}{\psi}$ on a fine grid of points over r space, perturbation methods need calculate only $\underset{\sim}{\psi}^0$ and $\underset{\sim}{\psi}^1$ at the end of a comparatively small number of intervals. Perturbation methods shrink the r dimension of solution space in somewhat the same way that the channel expansion shrinks

the $\vec{x}$ dimension of solution space. In addition, in their computational procedures these methods make more apparent the information we hope to obtain from the calculation, i.e., the relation of dynamics (channel coefficients) to structure (intermolecular potentials).

VI. INTEGRAL CHANNEL METHODS

It is well known that the Lipmann-Schwinger equation is an integral equation. When the wavefunction is expanded in channels, coupled integral equations result. Although there are standard techniques for solving such equations, there have been very few scattering calculations[18] employing integral channel methods and no calculations for nonreactive scattering. There are many different versions of the Lipmann-Schwinger equation. We will pick a particularly simple version and follow the development of Sams and Kouri.[19]

The Lipman-Schwinger equation for Ψ_i the wavefunction for the collision of two partners in initial internal states indexed by i with total system energy E, is

$$\Psi_i = \Psi_i^{in} + GV\Psi_i \tag{37}$$

where V is the intermolecular potential $V(\vec{r}, \vec{r}_1)$ and G is the Green's function operator

$$G = (E - H_0 + i\epsilon)^{-1} \tag{38}$$

where H_0 is the Hamiltonian with V set to zero. In an operational sense, there are many different Green's functions that are defined by Eq. (38). Each Green's function gives rise to a wavefunction which obeys a different asymptotic boundary condition. By G we mean the Green's function that obeys Eq. (38) and gives rise to a Ψ_i which obeys the boundary conditions Eq. (3) and (4). Ψ_i^{in} is the solution of

$$(H_0 - E)\Psi_i^{in} = 0 \tag{39}$$

obeying the same boundary conditions. Since there is no intermolecular potential in H_0, all the f_{ij}'s in Eq. (4) are zero and the asymptotic boundary condition reduces to

$$\Psi_i^{in} \xrightarrow[r\to\infty]{} \xi_i(\vec{r}_1)e^{ik_i z}. \tag{40}$$

Ψ_i can be expanded in the same partial wavefunctions of differential formalism. These partial wavefunctions obey the same boundary conditions but now satisfy Eq. (37). If we expand one partial wavefunction as $\frac{1}{r}\vec{\chi}\cdot\vec{\phi}_i$ and follow the same steps as we did in deriving the differential equation for $\vec{\phi}_i$ [Eq. (7)], we get for ϕ_{ni}, the n^{th} element of $\vec{\phi}_i$:

$$\begin{aligned}\phi_{ni} &= \delta_{ni}\phi_i^{in} + \int \chi_n(\vec{x})GV(\vec{x}, r) \sum_m \chi_m(\vec{x})\phi_{mi}(r)d\vec{x} \\ &= \delta_{ni}\phi_i^{in} + \int \chi_n(\vec{x})\Big[\int\int G(\vec{x}, r\,|\vec{x}', r')V(\vec{x}', r') \sum_m \chi_m(\vec{x}') \\ &\qquad \phi_m(r')d\vec{x}'\,dr'\Big]d\vec{x}\end{aligned} \tag{41}$$

where δ_{ni} is 1 when n = i but is 0 otherwise. ϕ_i^{in} is the only nonzero channel coefficient in the channel expansion if V is exactly zero; in general ϕ_i^{in} is closely related to a spherical Bessel function. $G(\vec{x}, r\,|\,\vec{x}', r')$ has the form

$$G(\vec{x}, r\,|\,\vec{x}', r') = \sum_j \chi_j(\vec{x})\chi_j(\vec{x}') \begin{cases} \phi_j^{out}(r)\phi_j^{in}(r) & r > r' \\ \phi_j^{in}(r)\phi_j^{out}(r) & r < r' \end{cases} \tag{42}$$

ϕ_j^{in} is ϕ_i^{in} for i = j. Although ϕ_j^{out} satisfies the same equation as ϕ_j^{in}, its asymptotic boundary condition is appropriate for a channel containing only scattered amplitude; in general ϕ_j^{out} is closely related to a spherical Hankel function. Substituting Eq. (42) into Eq. (41) and taking advantage of the orthonormality of $\vec{\chi}$, we obtain

$$\begin{aligned} \phi_{ni}(r) &= \delta_{ni}\phi_i^{in}(r) + \phi_n^{out}(r) \sum_m \int_0^r \phi_n^{in}(r')V_{nm}(r')\phi_{mi}(r')dr' \\ &\quad + \phi_n^{in}(r) \sum_m \int_r^\infty \phi_n^{out}(r')V_{nm}(r')\phi_{mi}(r')dr' \\ &= \delta_{ni}\phi_i^{in}(r) + \phi_n^{out}(r) \sum_m \int_0^r \phi_n^{in}(r')V_{nm}(r')\phi_{mi}(r')dr' \\ &\quad - \phi_n^{in}(r) \sum_m \int_0^r \phi_n^{out}(r')V_{nm}(r')\phi_{mi}(r')dr' \\ &\quad + \phi_n^{in}(r) \sum_m \int_0^\infty \phi_n^{in}(r')V_{nm}(r')\phi_{mi}(r')dr' \end{aligned} \tag{43}$$

where $V_{nm}(r') = \int \chi_n(\vec{x}')V(\vec{x}', r')\chi_m(\vec{x}')d\vec{x}'$.

For the matrix $\underset{\sim}{\phi}$ whose i^{th} column is $\vec{\phi}_i$, this equation straightforwardly becomes

$$\underset{\sim}{\phi} = \underset{\sim}{\phi}^{in} + \underset{\sim}{\phi}^{out} \int_0^r \underset{\sim}{\phi}^{in}(r')\underset{\sim}{V}(r')\underset{\sim}{\phi}(r')dr'$$

$$- \underset{\sim}{\phi}^{in} \int_0^r \underset{\sim}{\phi}^{out}(r')\underset{\sim}{V}(r')\underset{\sim}{\phi}(r')dr'$$

$$- \underset{\sim}{\phi}^{in} \int_0^\infty \underset{\sim}{\phi}^{out}(r')\underset{\sim}{V}(r')\underset{\sim}{\phi}(r')dr' \qquad (44)$$

where $\underset{\sim}{\phi}^{in}$ and $\underset{\sim}{\phi}^{out}$ are diagonal matrices whose i^{th} diagonal elements are ϕ_i^{in} and ϕ_i^{out} respectively. Sams and Kouri[19] point out that this equation can be considered an inhomogeneous integral equation with the last term being the inhomogeneity. To obtain $\underset{\sim}{\phi}$ we should seek a homogeneous solution $\underset{\sim}{\phi}^0$ and a particular solution $\underset{\sim}{\phi}^1$:

$$\underset{\sim}{\phi} = \underset{\sim}{\phi}^0 + \underset{\sim}{\phi}^1 \qquad (45)$$

where $\underset{\sim}{\phi}^0$ solves the homogeneous equation:

$$\underset{\sim}{\phi}^0 = \underset{\sim}{\phi}^{in} + \underset{\sim}{\phi}^{out} \int_0^r \underset{\sim}{\phi}^{in}(r')\underset{\sim}{V}(r')\underset{\sim}{\phi}^0(r')dr'$$

$$- \underset{\sim}{\phi}^{in} \int_0^r \underset{\sim}{\phi}^{out}(r')\underset{\sim}{V}(r')\underset{\sim}{\phi}^0(r')dr' . \qquad (46)$$

Substituting this equation into the equation for $\underset{\sim}{\phi}$ gives the equation for $\underset{\sim}{\phi}^1$:

$$\underset{\sim}{\phi}^1 = \underset{\sim}{\phi}^{out} \int_0^r \underset{\sim}{\phi}^{in}(r')\underset{\sim}{V}(r')\underset{\sim}{\phi}^1(r')dr'$$

$$- \underset{\sim}{\phi}^{in} \int_0^r \underset{\sim}{\phi}^{out}(r')\underset{\sim}{V}(r')\underset{\sim}{\phi}^0(r')dr'$$

$$+ \underset{\sim}{\phi}^{in} \int_0^\infty \underset{\sim}{\phi}^{out}(r')\underset{\sim}{V}(r')[\underset{\sim}{\phi}^0(r') + \underset{\sim}{\phi}^1(r')]dr'. \qquad (47)$$

This equation is solved by

$$\underset{\sim}{\phi}^1 = \underset{\sim}{\phi}^0 \underset{\sim}{C}$$

where $$\underset{\sim}{C} = \int_0^\infty \underset{\sim}{\phi}^{out}(r)\underset{\sim}{V}(r)[\underset{\sim}{\phi}^0(r) + \underset{\sim}{\phi}^1(r)]dr$$

or $$\underset{\sim}{C} = [\underset{\sim}{I} - \int_0^\infty \underset{\sim}{\phi}^{out}(r)\underset{\sim}{V}(r)\underset{\sim}{\phi}^0(r)dr]^{-1}$$

$$\times \int_0^\infty \underset{\sim}{\phi}^{out}(r)\underset{\sim}{V}(r)\underset{\sim}{\phi}^0(r)dr.$$

Therefore the final solution to $\underset{\sim}{\phi}$ is

$$\underset{\sim}{\phi} = \underset{\sim}{\phi}^0 + \underset{\sim}{\phi}^0 \underset{\sim}{C}. \qquad (49)$$

The coupled integral equation for $\underset{\sim}{\phi}^0$ can be solved noniteratively because the determination of ϕ^0 at r depends only on the knowledge of ϕ^0 over $r' < r$.

The formalism developed in this section exactly parallels the differential formalism developed in the previous sections. To get any column of $\underset{\sim}{\phi}$, N primitive independent solutions $\underset{\sim}{\phi}^0$ must be obtained. There are two general schemes applicable to solving the coupled integral equations for $\underset{\sim}{\phi}^0$. The integral can be replaced by a quadrature form[19] and $\underset{\sim}{\phi}^0$ can then be propagated from its initial zero value at $r \to 0$. $\underset{\sim}{\phi}^0$ can be expanded in a set of

basis functions[18] resulting in a large matrix equation for the coefficients. These two types of methods are analogous to the propagation and matrix methods of differential formalism. Although we will not carry out the necessary analysis to confirm this suspicion, we expect that the effects of closed channels and the implementation of perturbation schemes are very much the same in integral matrix and propagation methods as they are in differential matrix and propagation methods. This implies that the relative efficiency between integral methods and analogous differential methods are determined mainly by the technical aspects of each method.

VII. SUMMARY

Exact quantum methods for the calculation of the scattering of nonreactive collisions can be classified as follows. There are global methods and channel methods, the latter being more efficient. Channel methods can be derived from differential or integral formalism. Consider differential channel methods first. They can be divided into time-dependent and time-independent methods, the latter being more efficient. The time-independent methods can be further divided into matrix and propagation methods. Both divisions handle the difficulties caused by closed channels in equally efficient, but considerably different, ways. However, propagation methods can take full advantage of perturbation solution techniques while matrix methods cannot. Channel methods based on

integral formalism can be divided into matrix and propagation methods whose efficiency is essentially the same as analogous differential methods. In global methods the solution space can be thought of as $\vec{x} \times r$. In the most efficient methods, perturbation propagation channel methods, the solution space can be thought of as $N \times N_{int}$ where N is the number of channels and N_{int} is the number of intervals. Both the $\vec{x}$ and r dimensions of solution space have been reduced by expanding the motion in known or readily calculated basis functions. Since both dimensions of solution space have been reduced, it is doubtful that any more dramatic improvements in exact nonreactive quantum methods are possible. Of course improvements in the technical aspects of a method, not discussed in this article, can still result in important progress.

REFERENCES

[1]D. J. Diestler and V. McKoy, J. Chem. Phys. 48, 2941 (1968); 48, 2951 (1968).

[2]There are a large number of channel methods which we will reference after further classification of such methods.

[3]A good example of the superiority of channel over global methods is the comparison of the channel method FDM [V. P. Gutschick, V. McKoy, and D. J. Diestler, J. Chem. Phys. 52, 4807 (1970)] to the analogous global method of Ref. 1. Executions times for FDM are at least an order of magnitude faster.

[4]C. C. Ranken and J. C. Light, J. Chem. Phys. 51, 1701 (1969).

[5]The only progress so far made along these lines is by L. M. Delves, Nucl. Phys. 9, 391 (1958).

[6]D. J. Diestler and V. McKoy, J. Chem. Phys. 48, 2951 (1968).

[7]The angular momentum information in a channel expansion can be represented in a number of ways. For a general discussion of this, see N. F. Mott and H. S. W. Massey, The Theory of Atomic Collisions (Oxford University Press, New York, 1965), 3rd ed., p. 392. Two common representations are partial orbital angular momentum waves and partial total angular momentum waves [see A. M. Arthurs and A. Dalgarno, Proc. Roy. Soc. (London) A256, 540 (1960)].

[8]Methods that solve this equation are often called Perturbed Stationary State methods. For a review of early work done with these methods see D. R. Bates, Atomic and Molecular Processes (Academic Press, New York, 1962), p. 597. A later but approximate use of these methods is by R. A. Suplinskas and J. Rose, J. Chem. Phys. 47, 321 (1967).

[9]The most recent development of time dependent scattering for chemically interesting systems is by R. E. Wyatt and E. A. McCullough, Jr., J. Chem. Phys. 54, 3578 (1971). They developed a global method for reactive scattering.

[10]For examples, see D. Secrest and B. R. Johnson, J. Chem. Phys. 45, 4556 (1966) and M. E. Riley, Energy Transfer in Molecular Collisions (unpublished thesis, California Institute of Technology, 1968). Perturbation propagation methods will be referenced later.

[12]See Gutschick, et al., in Ref. 3. A perturbation matrix method will be referenced later.

[13]M. E. Riley, Ref. 10, pp. 49 and 149.

[14]R. Gordon, J. Chem. Phys. 51, 14 (1969).

[15]S. Chan, J. Light, and J. Lin, J. Chem. Phys. 49, 86 (1968). This method is not based on the use of adiabatic channels as is Gordon's method (whose development we generalize). The formalism is far more complicated and less easily generalized precisely because the special features of adiabatic channels are not used.

[16]A. S. Cheung and D. J. Wilson, J. Chem. Phys. 51, 4733 (1969); 51, 3449 (1969).

[17]A. C. Allison, J. of Comp. Phys. 6, 378-391 (1970).

[18]M. Baer and D. J. Kouri, Phys. Rev. A, 4, 1924 (1971); W. N. Sams and D. J. Kouri, J. Chem. Phys. 51, 4809 (1969).

[19]W. N. Sams and D. J. Kouri, J. Chem. Phys. 51, 4815 (1969).

Part 2: Quantum Mechanical Calculations of Rotational-Vibrational Scattering in Homonuclear Diatom-Atom Collisions

I. INTRODUCTION

The study of intermolecular forces is a major motivation for many experiments in nonreactive, vibrationally inelastic diatom-atom collisions.[1] In these collisions, the most detailed observation possible has the form $O^{\alpha \ell_1 m_1}_{\bar{\alpha}\bar{\ell}_1\bar{m}_1}$. This designates an observation of the scattering from initial diatomic state $|\bar{\alpha}\bar{\ell}_1\bar{m}_1\rangle$ to final state $|\alpha\ell_1 m_1\rangle$. Here and elsewhere α and ℓ_1 are the diatom's vibrational and rotational quantum numbers and m_1 is the diatom's angular momentum projection quantum number along the initial direction of the atom. A bar over a quantum number shows that it indexes the precollision system. In most experiments the diatom is not prepared in a specific rotational state and is randomly oriented. Also, the diatom's rotational state and orientation after scattering is not resolved. In such experiments, the only observation possible has the form $O^{\alpha}_{\bar{\alpha}}$, designating an observation of the scattering from one diatom vibrational state to another.

An intermolecular potential (IP) can be quantitatively determined only when experimental measurements can be reproduced by a calculation with an assumed IP. Therefore, one needs to calculate at least $O^{\alpha}_{\bar{\alpha}}$. $O^{\alpha}_{\bar{\alpha}}$ can not be directly calculated, because it obeys the relation

$$O^{\alpha}_{\bar{\alpha}} = \sum_{\bar{\ell}_1} P_{\bar{\alpha}}(\bar{\ell}_1)\, O^{\alpha}_{\bar{\alpha}\bar{\ell}_1} \tag{1}$$

where $P_{\bar{\alpha}}(\bar{\ell}_1)$ is the experimentally controlled probability that the

diatom with quantum number $\bar{\alpha}$ will also have quantum number $\bar{\ell}_1$. $O^{\alpha}_{\bar{\alpha}\bar{\ell}_1}$, which can be calculated, is an observation of the scattering of a randomly oriented diatom in the vibrational rotational state of $\bar{\alpha}$ and $\bar{\ell}_1$ into all states with quantum number α. Ideally, the calculation should be quantum mechanical and the assumed IP should be angularly asymmetric so as to cause both rotational and vibrational scattering. However all exact, and most approximate, quantum mechanical calculations[2] of $O^{\alpha}_{\bar{\alpha}\bar{\ell}_1}$ use an angularly symmetric IP. Such an approximate IP treats the diatom as a breathing sphere and hence there can be no rotational scattering. There are two reasons for the breathing sphere approximation (BSA). First, $O^{\alpha}_{\bar{\alpha}\bar{\ell}_1}$ is mainly a measure of vibrational scattering and so should be sensitive primarily to the symmetric part of the real IP. Second, the wavefunction for a symmetric IP has only enough detail to determine $O^{\alpha}_{\bar{\alpha}\bar{\ell}_1}$; but the wavefunction for a realistic IP should determine all $O^{\alpha\ell_1 m_1}_{\bar{\alpha}\bar{\ell}_1\bar{m}_1}$ from which $O^{\alpha}_{\bar{\alpha}\bar{\ell}_1}$ can be obtained:

$$O^{\alpha}_{\bar{\alpha}\bar{\ell}_1} = \frac{1}{(2\bar{\ell}_1+1)} \sum_{\bar{m}_1=-\bar{\ell}_1}^{\bar{\ell}_1} \sum_{m_1=-\ell_1}^{\ell_1} O^{\alpha\ell_1 m_1}_{\bar{\alpha}\bar{\ell}_1\bar{m}_1} . \qquad (2)$$

Since each vibrational quantum number indexes tens to hundreds of diatomic states, such information is basically too difficult and expensive to obtain. The approximate quantum mechanical calculations not using the BSA have used instead dynamical approximations that are hard to evaluate. This can be said of most semiclassical

and classical calculations[2] not using the BSA. However, a two-dimensional classical calculation by Benson and Berend[3] indicates that the BSA is accurate for the calculation of vibrational relaxation times of O_2-A, while a three dimensional classical calculation by Razner[4] implies that the BSA is inaccurate for the calculation of energy transfer in very energetic Br_2-A collisions.

We have been able to determine the degree of error in a BSA calculation of $O^{\alpha}_{\bar{\alpha}\bar{\ell}_1}$ for the simplest class of collisions exhibiting vibrational inelasticity--the collision of an atom with a homonuclear diatom at energies low enough to involve only two vibrational states. This is done by comparing two quantum mechanical calculations, one using the BSA and the other an angularly asymmetric IP with restricted rotational scattering. In the next section, we define our coordinate system, units, and the three representative homonuclear diatom-atom collision systems studied: H_2-A, O_2-He, and I_2-He. In the third section, we derive the theory for model restricted rotational scattering by a realistic IP. In the fourth section, we discuss the numerical and analytical methods used to solve Schroedinger's equation for the collision system wavefunction. In the fifth section, we study in detail the BSA induced inaccuracies in the partial, and partial differential, cross-sections of H_2-A. In the sixth section, we study the BSA induced inaccuracies in the partial cross sections of O_2-He and I_2-He. We then summarize our results.

II. SYSTEM DESCRIPTIONS

Figure 1 shows our coordinate system. Vector $\vec{r}_1$ (r_1, θ_1, ϕ_1) is the distance of one end of the diatom from its center of mass and vector $\vec{r}_2$ (r_2, θ_2, ϕ_2) is the distance of the colliding atom from the diatom's center of mass. γ is the angle between these two vectors, while the z axis, from which θ_1 and θ_2 are measured, points in the initial direction of the atom.

We represent the diatom as a rigidly rotating harmonic oscillator, an approximation which is valid at our low collision energies. For an IP, we choose

$$V(r_1, r_2, \gamma) = V_0(r_1, r_2) + V_2(r_1, r_2)P_2(\cos\gamma) \tag{3}$$

where

$$V_0(r_1, r_2) = 4\epsilon \left[\left(\frac{\sigma}{r_2 - r_1}\right)^{12} - \left(\frac{\sigma}{r_2 - r_1}\right)^{6}\right]$$

$$V_2(r_1, r_2) = 4\epsilon \left[\left(\frac{\sigma}{r_2 - r_1}\right)^{12} a_{SR} - \left(\frac{\sigma}{r_2 - r_1}\right)^{6} a_{LR}\right]$$

where $P_2(\cos\gamma)$ is the second Legendre polynomial. Both V_0 and V_2 are of a Lennard-Jones type with V_2 modified by a short and long range $P_2(\cos\gamma)$ asymmetry defined by a_{SR} and a_{LR}. Real IP's are known[5] to have a long range attractive and a short range repulsive part, with each part having its own angular asymmetry; our parametrized IP contains these features.

The Hamiltonian $\mathcal{H}$ for the collision of A striking B_2 is[6]

$$\mathcal{H} = -\frac{1}{2M}\nabla_2^2 + \left\{-\tfrac{1}{2}\frac{\partial^2}{\partial y^2} + \frac{y^2}{2} + B_0\hat{L}_1^2\right\} + V(r_1, r_2, \gamma) \qquad (4)$$

where

$$M = \frac{m_A}{m_A + 2m_B} .$$

Here m_A and m_B are the masses of A and B. The units of energy and length are $\hbar\omega$ and one-half the classical ground state vibrational amplitude, respectively. $\hat{L}_1^2$ is the rotational angular momentum operator, B_0 the rotational constant, and y is the diatom's bond displacement from equilibrium. To specify $\mathcal{H}$ for a collision system we need M, B_0, σ, ϵ, a_{SR}, and a_{LR}.

We considered three systems: H_2-A, O_2-He, and I_2-He. The parameters for these three systems are listed in Table I. The IP for H_2-A is approximately correct while that for O_2-He is only qualitatively correct. The IP for I_2-He is just a guess, since it is based on results or estimates for a variety of systems. However, for most homonuclear diatom-atom systems realistic values for the six Hamiltonian parameters fall within the range of the values chosen for our three systems. For reasons of economy, each system is studied at one total energy E and one initial rotational state indexed by $\bar{\ell}_1$. However, each system has different values for these two parameters. E and $\bar{\ell}_1$ are listed in Table I along with T, the temperature equivalent, assuming a Boltzmann

distribution, of the relative translational energy of the atom when the total energy is E and the diatom is initially in the $\overline{\ell}_1$ rotational state of the first excited vibrational state. Shock tube experiments on H_2-A[7] and O_2-He[8] have been conducted at these temperatures. The value of $\overline{\ell}_1$ for H_2-A and O_2-He is not unreasonable for these experiments. At least one experiment on I_2-He[9] has preselected the diatom in our initial rotational state.

III. THEORY

A. Formalism

To determine $O^{\alpha}_{\bar{\alpha}\bar{\ell}_1}$ for any α we need to know the wavefunction $\psi^{E}_{\bar{\alpha}\bar{\ell}_1\bar{m}_1}$ for all $\bar{m}_1$ and the relevant range of E, where

$$\mathcal{H}\psi^{E}_{\bar{\alpha}\bar{\ell}_1\bar{m}_1} = E\psi^{E}_{\bar{\alpha}\bar{\ell}_1\bar{m}_1}, \text{ and} \tag{5}$$

$$\psi^{E}_{\bar{\alpha}\bar{\ell}_1\bar{m}_1} \xrightarrow[r_2 \to \infty]{} |\bar{\alpha}\bar{\ell}_1\bar{m}_1\rangle e^{i\bar{k}z} + \sum_{\alpha\ell_1 m_1} f^{\alpha\ell_1 m_1}_{\bar{\alpha}\bar{\ell}_1\bar{m}_1}(E, \Omega_2) \frac{e^{ikr_2}}{r_2} |\alpha\ell_1 m_1\rangle$$

where $\bar{k}$ and k are the initial and final wavenumbers of the relative motion, $f^{\alpha\ell_1 m_1}_{\bar{\alpha}\bar{\ell}_1\bar{m}_1}(E, \Omega_2)$ is the amplitude at total energy E for $|\bar{\alpha}\bar{\ell}_1\bar{m}_1\rangle$ to be excited to $|\alpha\ell_1 m_1\rangle$ while scattering the atom into solid angle Ω_2 specified by θ_2 and ϕ_2 . $O^{\alpha}_{\bar{\alpha}\bar{\ell}_1}$ can be determined from all these amplitudes. The usual first step in obtaining $\psi_{\bar{\alpha}\bar{\ell}_1\bar{m}_1}$ (we will suppress the index E) is its expansion[10] in a set of functions complete in r_1, θ_1, ϕ_1, θ_2, and ϕ_2 space. The spherical harmonics are complete in θ_2 and ϕ_2 space. Furthermore each spherical harmonic describes an orbital angular momentum state of the atom. In the total angular momentum representation the product of the diatomic states, complete in r_1, θ_1, and ϕ_1 space, and the spherical harmonics is the most convenient set of functions to

expand $\psi_{\bar{\alpha}\bar{\ell}_1\bar{m}_1}$. We call a member of that set a channel designated by $^J|\alpha\ell_1\ell_2\rangle$ where ℓ_2 is the orbital quantum number which couples with ℓ_1 to form J, the total angular momentum quantum number. In general, a channel's z component of J should be specified, but atom-diatom scattering is independent of this momentum. A channel is open if its diatomic state factor has an energy less than E; otherwise it is closed.

The boundary condition on $\psi_{\bar{\alpha}\bar{\ell}_1\bar{m}_1}$ is:

$$\psi_{\bar{\alpha}\bar{\ell}_1\bar{m}_1} \xrightarrow[r_2 \to \infty]{} \sum_{\bar{\ell}_2=0} \sum_{J=|\bar{\ell}_1-\bar{\ell}_2|}^{\bar{\ell}_1+\bar{\ell}_2} C^{\bar{\alpha}\bar{\ell}_1\bar{m}_1}_{\bar{\ell}_2 J} \times$$

$$\left\{ \frac{e^{-i(\bar{k}r_2 - \bar{\ell}_2\pi/2)}}{\sqrt{\bar{k}}\, r_2} \; {}^J|\bar{\alpha}\bar{\ell}_1\bar{\ell}_2\rangle \right.$$

$$\left. - \sum_{\alpha\ell_1\ell_2} {}^J S^{\alpha\ell_1\ell_2}_{\bar{\alpha}\bar{\ell}_1\bar{\ell}_2} \frac{e^{i(kr_2 - \ell_2\pi/2)}}{\sqrt{k}\, r_2} \; {}^J|\alpha\ell_1\ell_2\rangle \right\} \qquad (6)$$

where each $C^{\bar{\alpha}\bar{\ell}_1\bar{m}_1}_{\bar{\ell}_2 J}$ is a known constant[10] and ${}^J S^{\alpha\ell_1\ell_2}_{\bar{\alpha}\bar{\ell}_1\bar{\ell}_2}$ is an element of what we call a solution vector, $\overrightarrow{{}^J S_{\bar{\alpha}\bar{\ell}_1\bar{\ell}_2}}$, in which $O^{\alpha}_{\bar{\alpha}\bar{\ell}_1}$ can be directly expressed [see Eqs. (7) and (10)]. Let us call the solution to the Schroedinger equation which obeys the boundary condition enclosed in brackets above a partial wavefunction (pwfn) designated $\psi^{\bar{\alpha}\bar{\ell}_1}_{\bar{\ell}_2 J}$. $\psi^{\bar{\alpha}\bar{\ell}_1}_{\bar{\ell}_2 J}$ is the wavefunction for that part of the collision system initially described by unit amplitude in $^J|\bar{\alpha}\bar{\ell}_1\bar{\ell}_2\rangle$ with unit

incoming current in the r_2 direction. The square of ${}^{J}S^{\alpha\ell_1\ell_2}_{\bar{\alpha}\bar{\ell}_1\bar{\ell}_2}$ is the probability that the collision will scatter ${}^{J}|\bar{\alpha}\bar{\ell}_1\bar{\ell}_2\rangle$ into ${}^{J}|\alpha\ell_1\ell_2\rangle$. To obtain $\psi^{\bar{\alpha}\bar{\ell}_1}_{\bar{\ell}_2 J}$, we expand it in channels and generate a coupled set of differential equations in r_2 for the channel coefficients. The channel coefficients at large r_2 contain the pwfn's solution vector. Describing the collision in terms of the scattering of each initial channel into other channels is more convenient than describing it in terms of the scattering of the initial diatomic state into other states and of the atom into different directions.

B. The Influence of the IP

The expense and difficulty of determining $O^{\alpha}_{\alpha\bar{\ell}_1}$ lie almost entirely in solving the coupled set of differential equations for the channel coefficients of each pwfn. The calculation time for each set is roughly proportional to the number of channel coefficients cubed. The importance of the IP is that a pwfn's channel set is effectively complete if it includes only those channels which the IP significantly couples to the initial channel in some region of r_2. The form of the IP limits a pwfn's channel set in two ways. First, all meaningful IP's must conserve total angular momentum as well as reflect the symmetry of a homonuclear diatom. Therefore, $\psi^{\bar{\alpha}\bar{\ell}_1}_{\bar{\ell}_2 J}$ will need only those channels with total angular momentum J and rotational and orbital angular momenta of the same parity (even or odd) as $\bar{\ell}_1$ and $\bar{\ell}_2$. Second, if an IP is angularly symmetric, $\psi^{\bar{\alpha}\bar{\ell}_1}_{\bar{\ell}_2 J}$ will need only those channels with rotational and orbital angular momenta $\bar{\ell}_1$ and $\bar{\ell}_2$. Beyond these two general statements, a pwfn's channel set depends on the strength, not the form, of the IP.

The differences between a BSA and an exact determination of $O^{\alpha}_{\alpha\bar{\ell}_1}$ stem from the differences between the scattering of each initial channel by an angularly symmetric or asymmetric IP. In Figs. 2 and 3 we schematically illustrate the scattering of one initial channel by both IP's. In each figure, a channel is represented by a square whose position specifies the channel's vibrational, rotational, and orbital quantum numbers. Only channels strongly coupled to the initial channel are shown; these channels

must have the same J and the same parity in ℓ_1 and ℓ_2 as the initial channel. Arrows of a thickness proportional to the excitation probability connect final and initial channels. For clarity, pure elastic scattering is not shown in either figure and some arrows are left out of Fig. 3. Vibrationally elastic scattering takes place within the initial channel's plane of channels while all other scattering is vibrationally inelastic. Only two channels are coupled in Fig. 2 by the symmetric IP while 50 channels are coupled in Fig. 3 by the asymmetric IP. The ratio of BSA to exact calculation time for the pwfn is therefore $2^3/50^3$ or about 1/16, 000. We refer to the scattering between channels alike in ℓ_1 and ℓ_2 as vertical and all other channel scattering as lateral. The symmetric IP causes only vertical scattering, while the asymmetric IP causes both vertical and lateral scattering. The vibrational scattering produced by an elastic or inelastic lateral process is different in at least three ways from that produced by the analogous vertical process. First, the two processes differ in the vibrational coupling between initial and final channels. Second, the energy of rotational and orbital motion during the collision is different; this affects the amount of energy directly available to force vibrational scattering. Third, because the final channels of the two processes differ in ℓ_1 and ℓ_2, they describe an atom-diatom system separating at different speeds in different directions. The greater the change in ℓ_1 and ℓ_2 from $\bar{\ell}_1$ and $\bar{\ell}_2$, the more a lateral process will differ from the analogous vertical one. A pwfn's contribution to $O^{\alpha}_{\bar{\alpha}\bar{\ell}_1}$ involves a sum over

all the vibrationally elastic or inelastic scattering of its initial channel. If, in the exact calculation, the difference between each elastic or inelastic lateral process and the analogous vertical process does not sum to zero for enough initial channels, then the BSA determination of $O^{\alpha}_{\overline{\alpha\ell}_1}$ will be in error.

C. Model Rotational Scattering

Suppose we obtain $\psi_{\overline{\alpha \ell_1 m_1}}$ for an asymmetric IP by expanding each pwfn $\psi^{\overline{\alpha \ell_1}}_{\ell_2 J}$ in a channel set composed only of channels with ℓ_2 equal to $\overline{\ell}_2$. This very incomplete channel set does not permit $\psi^{\overline{\alpha \ell_1}}_{\overline{\ell}_2 J}$ to obey its boundary condition unless we assume ${}^{J}S^{\alpha \ell_1 \ell_2}_{\overline{\alpha \ell_1 \ell_2}}$ equals zero if ℓ_2 is not equal to $\overline{\ell}_2$. The channel scattering for the same initial channel of Figs. 2 and 3 is represented in Fig. 4. This calculation takes only 125 times longer than a BSA calculation versus the factor of 16000 we previously estimated for the exact calculation. However, each lateral scattering process in Fig. 4 is probably more intense than the same process calculated with a complete channel set (Fig. 3) because the initial channel's amplitude is being forced into fewer final channels. This feature implies that differences between lateral and vertical scattering will be larger in the approximate than in the exact calculation. The implication is that the difference between the approximate and the BSA determined $O^{\alpha}_{\overline{\alpha \ell_1}}$ will tend to be larger than the difference between the exact and the BSA determined $O^{\alpha}_{\alpha \overline{\ell}_1}$. Let us define a model calculation of $O^{\alpha}_{\overline{\alpha \ell_1}}$ as one in which each pwfn is expanded in a channel set made incomplete by the same artificial set of restrictions. The degree of error in a BSA $O^{\alpha}_{\overline{\alpha \ell_1}}$ can be semiquantitatively defined by its comparison to $O^{\alpha}_{\alpha \overline{\ell}_1}$ from feasible calculations for models whose restrictions emphasize lateral processes with large changes in ℓ_1 or ℓ_2.

We have studied four different models. We will now define each model's set of restrictions and, as an example, apply these to the pwfn $\psi^{0,9}_{5,5}$.

Each model restricts a pwfn's channel set, one plane at a time (see Figs. 2, 3, and 4), starting from the initial channel or the channel in the plane vertically connected to the initial channel. We will look at just one channel plane for $\psi^{0,9}_{5,5}$, where we will presume that all channels with ℓ_1 equal to 1 to 13 are needed for completeness. The plane is shown in Figs. 5A and 5B. The four sets of restrictions are:

Model 1: Include those channels whose ℓ_2 equals $\overline{\ell}_2$. These channels are marked by lines slanted to the right in Fig. 5A.

Model 2: Consider all the channels with the same value for ℓ_1 to be in a row. Starting from the initial channel, advance from row to row, choosing the one channel in each row which, first, is one of the nearest neighbors to the included channel of the previous row and, second, has a value of ℓ_2 nearest without exceeding the row's average value of ℓ_2. These channels are marked by lines slanted to the left in Fig. 5A.

Model 3: As in Model 1 with "ℓ_1 equals $\overline{\ell}_1$" replacing "ℓ_2 equals $\overline{\ell}_2$" and the results shown in Fig. 5B.

Model 4: As in Model 2 with the roles of ℓ_1 and ℓ_2 interchanged and the results shown in Fig. 5B.

Models 1 and 2 emphasize scattering in ℓ_1, while models 3 and 4 emphasize scattering in ℓ_2. As in model 2's description, let us divide each plane of channels into rows indexed by ℓ_1. In a complete channel set calculation, the initial channel may scatter into final channels similar to itself; then the most probable final channel in each row is indexed by ℓ_2 equal to $\bar{\ell}_2$. Under this assumption, model 1's channel set is an average of the complete channel set over ℓ_2. Another assumption is that the quantum numbers of the initial channel would be "forgotten" during a scattering process in which changes in the quantum numbers are large. Then each row's most probable final channel depends on the size of ℓ_1-$\bar{\ell}_1$. The final channel's ℓ_2 goes from $\bar{\ell}_2$, when ℓ_1-$\bar{\ell}_1$ is small, to the row's average when ℓ_1-$\bar{\ell}_1$ is large. Under this assumption, model 2's channel set is an average of the complete channel set over ℓ_2. Models 3 and 4 are similarly motivated.

For a realistic IP, the complete channel set of $\psi^{\bar{\alpha}\bar{\ell}_1}_{\ell_2 J}$ is usually considered to be at least all the open channels indexed by J and by ℓ_1 and ℓ_2 whose parities are those of $\bar{\ell}_1$ and $\bar{\ell}_2$. Should any of our models be applied to the thousands of open channels in the I_2-He system, hundreds of channels would still be left in the incomplete channel sets. However, only channels that the IP couples significantly to a pwfn's initial channel are required in a complete set and this number is always much less than all the open channels. These significant channels can be determined from exploratory calculations and experimental results. For each

collision system, we will define the channel sets to which the models are applied.

IV. METHODS

We used two methods to solve the coupled set of equations for the channel coefficients and solution vector of each pwfn. The first method is the propagation method of Gordon[11] with one major modification. This modification is the complete elimination of closed channel coefficients from the calculation at intermediate values of r_2 as the channel coefficients propagate from $r_2 = 0$ to the asymptotic region. This modification is a direct outgrowth of what Gordon refers to as stabilization and is a general feature of all propagation methods. This modification tends to make the computation time proportional to the cube of the number of open channels rather than the number of open and closed channels. See Part I, Section IV for details. Using the propagation method, we obtained approximately three place accuracy in any probability (squared amplitude of a solution vector element) greater than 10^{-6}. We tested the accuracy of our solution vectors in two ways. First, a vector's probabilities should sum to 1; our sum values were always 1 to four decimal places. Second, if P_{mn} is the probability that the initial channel m will scatter into final channel n, then $\frac{P_{mn} - P_{nm}}{P_{mn}}$ should be zero by time reversal. Our values were always less than 0.05 and usually less than 0.01 for all $P_{mn} > 10^{-6}$. In model calculations on the I_2-He system, this accuracy could not be obtained when closed channels were included in a model channel set with twenty or more open channels. For unknown

reasons the stabilization procedure described by Gordon failed to prevent the closed channel coefficients from exponentially blowing up as they propagate. We did not pursue this difficulty because of expense and because, as we will later prove, BSA induced errors in $O^{\alpha}_{\alpha\bar{\ell}_1}$ for the I_2-He system can be determined by model and BSA calculations that exclude closed channels.

The second method is analytic and approximate but valid when $\bar{\ell}_2$ is very large. In such cases, the initial channel's scattering is essentially elastic. The scattering is that of potential scattering where the potential is the initial channel's expectation value of the IP. The unknown is the phase shift which is one half the phase of the only non-zero element in the solution vector. The channel expectation value of our IP is a Lennard-Jones potential. For Lennard-Jones potential scattering when $\bar{\ell}_2$ is large, a valid analytic formula exists.[12] Solution vectors calculated by this analytic method pass smoothly, as a function of $\bar{\ell}_2$, into those calculated by the propagation method.

V. THE H_2-A SYSTEM

For this system, we calculate both the partial cross sections $\sigma^0_{0,3}$, $\sigma^1_{1,3}$, $\sigma^1_{0,3}$, and $\sigma^0_{1,3}$ using all four models and the BSA, and the partial differential cross sections $d\sigma^0_{0,3}(\theta_2)$, $d\sigma^1_{1,3}(\theta_2)$, $d\sigma^1_{0,3}(\theta_2)$, and $d\sigma^0_{1,3}(\theta_2)$ using models 1 and 3 and the BSA. To review our notation, $\sigma^{\alpha}_{\bar{\alpha}\bar{\ell}_1}$ and $d\sigma^{\alpha}_{\bar{\alpha}\bar{\ell}_1}(\theta_2)$ are the cross section and differential cross section respectively for the scattering of a randomly oriented diatom in the vibrational rotational state of $\bar{\alpha}$ and $\bar{\ell}_1$ into all states with quantum number α. We solve for pwfns $\psi^{0,3}_{\bar{\ell}_2 J}$ and $\psi^{1,3}_{\bar{\ell}_2 J}$ for all J and for $\bar{\ell}_2$ ranging from 9 to 199. The propagation method was used for $\bar{\ell}_2$ between 0 and 80 and the analytic method for $\bar{\ell}_2$ between 81 and 199. The models restrict the complete channel sets of $\psi^{0,3}_{\bar{\ell}_2 J}$ and $\psi^{1,3}_{\bar{\ell}_2 J}$. The range of values that the α, ℓ_1, and ℓ_2 indices of a channel can assume specifies a pwfn's complete channel set. This range may vary with all four indices of the pwfn, but we let it vary only with $\bar{\ell}_2$. In Table II, the range of α and ℓ_1 as a function of $\bar{\ell}_2$ are listed for the H_2-A system. For $\bar{\ell}_2 > 80$ the channel scattering is essentially elastic and the pwfn's complete channel set is just its initial channel. For each pwfn, ℓ_2 ranges over all values allowed by the pwfn's value of J. Not all open channels are included, but we estimate that use of this channel set would incorrectly determine only vibrationally elastic and inelastic lateral processes of probabilities less than 10^{-4} and 10^{-7} respectively. $O^{\alpha}_{\bar{\alpha}\bar{\ell}_1}$ would probably not be altered by an exact calculation with a pwfn channel sets larger than those of Table II.

A. Model 1, Model 3, and the BSA

The full expression[13] for the partial cross section $\sigma_{\alpha\ell_1}^{\alpha}$ is

$$\sigma_{\alpha\ell_1}^{\alpha} = \lambda\!\!\!^{-2}\pi \frac{1}{(2\bar{\ell}_1+1)} \sum_{\bar{\ell}_2=0}^{\infty} \sum_{J=|\bar{\ell}_2-\bar{\ell}_1|}^{\bar{\ell}_2+\bar{\ell}_1} (2J+1) \sum_{\ell_1} \sum_{\ell_2=|J-\ell_1|}^{J+\ell_1} \left| \delta_{\alpha\ell_1\ell_2}^{\alpha\ell_1\ell_2} - {}^{J}S_{\alpha\ell_1\ell_2}^{\alpha\ell_1\ell_2} \right|^2 \tag{7}$$

where $\lambda\!\!\!^{-}$ is the wavelength for the initial translational motion divided by 2π. The sum over ℓ_1 includes all values with the same parity as that of $\bar{\ell}_1$; δ_i^j is 1 when i equals j and zero otherwise. For each model calculation, the solution vector elements indexing final channels left out of the channel set equal zero in the expression. For a BSA calculation, all vector elements not of the form ${}^{J}S_{\alpha\bar{\ell}_1\bar{\ell}_2}^{\alpha\bar{\ell}_1\bar{\ell}_2}$ can be set to zero. Furthermore a BSA solution vector is independent of J. Let us represent ${}^{J}S_{\alpha\bar{\ell}_1\bar{\ell}_2}^{\alpha\bar{\ell}_1\bar{\ell}_2}$ by ${}^{\bar{\ell}_1\bar{\ell}_2}S_{\bar{\alpha}}^{\alpha}$ for the BSA calculation. Since

$$\frac{1}{(2\bar{\ell}_1+1)} \sum_{J=|\bar{\ell}_2-\bar{\ell}_1|}^{\bar{\ell}_2+\bar{\ell}_1} (2J+1) = (2\bar{\ell}_2+1), \tag{8}$$

the expression for $\sigma_{\alpha\ell_1}^{\alpha}$ can be simplified for the BSA calculation:

$$\sigma_{\alpha\ell_1}^{\alpha} = \lambda\!\!\!^{-2}\pi \sum_{\bar{\ell}_2=0}^{\infty} (2\bar{\ell}_2+1) \left| \delta_{\bar{\alpha}}^{\alpha} - {}^{\bar{\ell}_1\bar{\ell}_2}S_{\bar{\alpha}}^{\alpha} \right|^2. \tag{9}$$

The partial cross sections for models 1 and 3 are in Table III. Table III also shows the results of five BSA calculations indexed from zero to four. Each one uses different values for σ and ϵ in its IP. Only BSA0 uses the values of σ and ϵ used by models 1 and 3. Table III lists σ and ϵ for each calculation. We want to use Table III to estimate the error due to the BSA in the partial cross sections of the H_2-A system. From the five BSA calculations, we can give those errors in terms of the errors in the values of σ and ϵ determined by the BSA calculations that reproduce the cross sections of both models. If there were no errors, BSA0 would reproduce the results of each model. From the results of Table III, models 1 and 3 estimate that BSA induced errors for the H_2-A system are less than 1% in σ and 10% in ϵ for elastic cross sections and less than 1 or 2% in σ for inelastic cross sections. Also, the BSA results show that inelastic cross sections are extremely insensitive to the value of ϵ.

Partial differential cross sections can also be determined from these seven calculations. The full expression[13] for $d\sigma^{\alpha}_{\bar{\alpha}\bar{\ell}_1}(\theta_2)$ is

$$d\sigma^{\alpha}_{\bar{\alpha}\bar{\ell}_1}(\theta_2) = \frac{1}{2\pi}\int_0^{2\pi} \lambda\!\!\!^{-2}\,\frac{\pi}{(2\bar{\ell}_1+1)}\sum_{\bar{m}_1=-\bar{\ell}_1}^{\bar{\ell}_1}\sum_{\ell_1}\sum_{m_1=-\ell_1}^{\ell_1}$$

$$\Big|\sum_{\bar{\ell}_2=0}^{\infty}(2\bar{\ell}_2+1)^{\frac{1}{2}}\, i^{\bar{\ell}_2}\sum_{J=|\bar{\ell}_2-\bar{\ell}_1|}^{\bar{\ell}_2+\bar{\ell}_1}\sum_{M=-J}^{J}\times$$

$$\sum_{\ell_2=|J-\ell_1|}^{J+\ell_1}\sum_{m_2=-\ell_2}^{\ell_2} i^{-\ell_2}(\bar{\ell}_2\bar{\ell}_1 0\,\bar{m}_1\,|\,\bar{\ell}_2\bar{\ell}_1\,JM)\Big[\delta^{\alpha\ell_1\ell_1}_{\bar{\alpha}\bar{\ell}_1\bar{\ell}_2}$$

$$- {}^{J}S^{\alpha\ell_1\ell_2}_{\bar{\alpha}\bar{\ell}_1\bar{\ell}_2}\Big](\ell_2\ell_1 m_2 m_1\,|\,\ell_2\ell_1 JM)\,Y_{\ell_2 m_2}(\theta_2,\phi_2)\Big|^2 d\phi_2 \qquad (10)$$

where (ijkl | ijmn) is a Clebsch-Gordan coefficient and $Y_{\ell_2 m_2}(\theta_2, \phi_2)$ is a spherical harmonic. Notice our partial cross section is averaged over ϕ_2 space. $\sigma^{\alpha}_{\bar{\alpha}\bar{\ell}_1}$ and $d\sigma^{\alpha}_{\bar{\alpha}\bar{\ell}_1}(\theta_2)$ are related by

$$\sigma^{\alpha}_{\bar{\alpha}\bar{\ell}_1} = 2\pi \int_0^{\pi} d\sigma^{\alpha}_{\bar{\alpha}\bar{\ell}_1}(\theta_2) \sin\theta_2 d\theta_2 . \tag{11}$$

The properties of Clebsch-Gordan coefficients allow $d\sigma^{\alpha}_{\bar{\alpha}\bar{\ell}_1}$ to be simplified for a BSA calculation:

$$d\sigma^{\alpha}_{\bar{\alpha}\bar{\ell}_1} = \lambda^2 \tfrac{1}{4} \Big| \sum_{\bar{\ell}_2 = 0}^{\infty} (2\bar{\ell}_2 + 1)[\delta^{\alpha}_{\bar{\alpha}} - \bar{\ell}_1\bar{\ell}_2 S^{\alpha}_{\bar{\alpha}}] P_{\bar{\ell}_2}(\cos\theta_2) \Big|^2 . \tag{12}$$

In Figs. 6, 7, 8, and 9, we plot $d\sigma^0_{0,3}(\theta_2)$, $d\sigma^1_{1,3}(\theta_2)$, $d\sigma^1_{0,3}(\theta_2)$, and $d\sigma^0_{1,3}(\theta_2)$ respectively for model 1, model 3, and BSA0. In Figs. 10 and 11, we plot $d\sigma^1_{1,3}(\theta_2)$ and $d\sigma^1_{0,3}(\theta_2)$ respectively for BSA1, BSA2, BSA3, and BSA4. In each figure, unless θ_2 is very small, $d\sigma^{\alpha}_{\bar{\alpha}\bar{\ell}_1}(\theta_2)$ is plotted over those values of θ_2 for which the cross section is large. At very small angles, differential cross sections cannot be measured because of experimental difficulties. Figs. 6 through 11 show two features. First, models 1 and 3 estimate the BSA induced errors for the H_2-A system to be about 1 or 2% in σ for the inelastic partial differential cross sections. Second, the inelastic partial differential cross sections are not sensitive to ϵ and the elastic partial differential cross sections are not sensitive to either ϵ or σ. All the potential sensitivity in elastic differential cross sections is concentrated in the experimentally inaccessible

region of very small angles. We confirm this in Table IV, where the values of $d\sigma^0_{0,3}(\theta_2)$ for θ_2 equal to 0° through 4° are listed for all five BSA calculations. The difference in potential sensitivity of elastic cross sections and elastic differential cross sections are due to experimental limitations. However, the lack of sensitivity to ϵ-like parameters in inelastic cross sections and inelastic differential cross sections are due to the nature of the collision system.

B. Interpolation for Partial Cross Sections

Because models 2 and 4 allow more lateral scattering than models 1 and 3, the former are less likely to underestimate errors due to the BSA. They are also much more expensive to use. To circumvent this difficulty, we have devised a way of interpolating, with respect to $\bar{\ell}_2$, the solution vectors of either a model or a BSA calculation. The interpolated vectors are good only for the construction of approximate partial cross sections. However the difference between an approximate cross section of a model and that of a BSA calculation is almost exactly the same as the difference between analogous uninterpolated cross sections. Therefore, the interpolation scheme can be used without destroying the ability of model calculations to determine BSA induced errors in partial cross sections.

The comparison of Eqs. (7) and (9) shows that both the full and BSA expression for $\sigma^{\alpha}_{\bar{\alpha}\bar{\ell}_1}$ depends on a sum over $\bar{\ell}_2$. Each term in the $\bar{\ell}_2$ sum of the BSA expression can be constructed from the solution vector $\overrightarrow{\bar{\ell}_1\bar{\ell}_2 S_{\bar{\alpha}}}$. The amplitude squared and the phase of each element in this solution vector is a relatively smooth function of $\bar{\ell}_2$. Each term in the $\bar{\ell}_2$ sum of the full expression can be constructed from solution vectors $\overrightarrow{{}^{J}S_{\bar{\alpha}\bar{\ell}_1\bar{\ell}_2}}$ for all J. The amplitude squared and phase of each element in these vectors is not a smooth function of $\bar{\ell}_2$. Let us rearrange the full expression for $\sigma^{\alpha}_{\bar{\alpha}\bar{\ell}_1}$ into

$$\sigma_{\overline{\alpha}\overline{\ell}_1}^{\alpha} = \lambda^2\pi \sum_{\overline{\ell}_2=0}^{\infty} (2\overline{\ell}_2 + 1)\{|\delta_{\overline{\alpha}}^{\alpha} - {}^{V\overline{\ell}_1\overline{\ell}_2}S_{\overline{\alpha}}^{\alpha}|^2 + |{}^{L\overline{\ell}_1\overline{\ell}_2}S_{\overline{\alpha}}^{\alpha}|^2\}. \quad (13)$$

We call $\overrightarrow{{}^{V\overline{\ell}_1\overline{\ell}_2}S_{\overline{\alpha}}}$ and $\overrightarrow{{}^{L\overline{\ell}_1\overline{\ell}_2}S_{\overline{\alpha}}}$ vertical and lateral pseudo vectors respectively. To form a term in $\sigma_{\overline{\alpha}\overline{\ell}_1}^{\alpha}$ for any α we need to know the amplitude squared of each element of both pseudo vectors as well as the phase of the elastic element of the vertical pseudo vector ; these quantities are defined in order as

$$|{}^{V\overline{\ell}_1\overline{\ell}_2}S_{\overline{\alpha}}^{\alpha}|^2 \equiv \frac{1}{(2\overline{\ell}_2+1)(2\overline{\ell}_1+1)} \sum_J (2J+1)|{}^{J}S_{\overline{\alpha}\overline{\ell}_1\overline{\ell}_2}^{\alpha}|^2 \quad (14)$$

$$|{}^{L\overline{\ell}_1\overline{\ell}_2}S_{\overline{\alpha}}^{\alpha}|^2 \equiv \frac{1}{(2\overline{\ell}_2+1)(2\overline{\ell}_1+1)} \sum_J (2J+1) \sum_{\substack{\ell_1 \\ (\ell_1,\ell_2)\neq(\overline{\ell}_1,\overline{\ell}_2)}} \sum_{\ell_2} |{}^{J}S_{\overline{\alpha}\overline{\ell}_1\overline{\ell}_2}^{\alpha\ell_1\ell_2}|^2 \quad (15)$$

$${}^{V\ell_1\ell_2}\phi_{\overline{\alpha}}^{\overline{\alpha}} \equiv \arccos\left[\frac{\frac{1}{(2\overline{\ell}_2+1)(2\overline{\ell}_1+1)} \sum_J (2J+1)|{}^{J}S_{\overline{\alpha}\overline{\ell}_1\overline{\ell}_2}^{\overline{\alpha}\overline{\ell}_1\overline{\ell}_2}|\cos {}^{J}\phi_{\overline{\alpha}\overline{\ell}_1\overline{\ell}_2}^{\overline{\alpha}\overline{\ell}_1\overline{\ell}_2}}{\sqrt{|{}^{V\ell_1\ell_2}S_{\overline{\alpha}}^{\overline{\alpha}}|^2}}\right] \quad (16)$$

where ${}^{\ell}\phi_m^n$ is the phase of vector element ${}^{\ell}S_m^n$. These quantities are all relatively smooth functions of $\overline{\ell}_2$. To compare BSA and model determined cross sections, we can calculate BSA solution vectors and model pseudo vectors for the same grid of $\overline{\ell}_2$ values, then interpolate with respect to $\overline{\ell}_2$ the remaining vectors and pseudo vectors to form the cross sections. If the grid of $\overline{\ell}_2$ values is

fine enough to produce approximately correct cross sections, then the differences between these BSA and model cross sections will be nearly exact. Since it is trivial to generate solution vectors or pseudo vectors by the analytical method, the interpolation need only be carried out in the region of $\overline{\ell}_2$ where the propagation method applies. Because any phase is undetermined within an integral multiple of 2π, the interpolation of the elastic phases of the solution or pseudo vectors is not straightforward; this minor complication is fully discussed in the Appendix.

C. Model 2, Model 4, and the BSA

For the H_2-A system, we use our interpolation scheme to determine the partial cross sections for models 2 and 4 and to redetermine the cross sections for models 1 and 3 and the five BSA calculations. For $\overline{\ell}_2$ equals 0 to 80, we solve for the solution and pseudo vectors for every tenth value of $\overline{\ell}_2$, starting from 0, and interpolate the remaining vectors. The results are in Table V. The comparison of Table V to Table III confirms our assertion that the interpolation scheme can produce partial cross sections whose absolute values are approximate, but whose relative values are exact. The results of Table V show that the BSA induced errors in partial cross sections are the same for all four models.

All our calculations on the H_2-A system support two conclusions:

(1) The BSA can be used to determine accurately the symmetric part of the IP from measurements sensitive to potential parameters.

(2) The inelastic partial cross sections are insensitive to ϵ-like parameters while the entire potential sensitivity of the elastic partial differential cross sections is concentrated in the very small angle region.

VI. THE O_2-He AND I_2-He SYSTEMS

A. Interpolation for Pseudo Vectors

The construction of $\overrightarrow{V\bar{\ell}_1\bar{\ell}_2 S_{\bar{\alpha}}}$ and $\overrightarrow{L\bar{\ell}_1\bar{\ell}_2 S_{\bar{\alpha}}}$ requires $\overrightarrow{{}^J S_{\bar{\alpha}\bar{\ell}_1\bar{\ell}_2}}$ for all J. If $\bar{\ell}_2 \geq \bar{\ell}_1$, the number of values for J is $(2\bar{\ell}_1 + 1)$. For H_2-A, $(2\bar{\ell}_1 + 1)$ is only 7; but for O_2-He and I_2-He, it is 27 and 65, respectively. For model calculations on the O_2-He and I_2-He systems, the number of solution vectors which must be calculated for each pair of pseudo vectors is so large that the determination of partial cross sections by the interpolation of pseudo vectors is impractical. To overcome this difficulty, we again turn to interpolation. From one solution vector, three quantities are used in the construction of the parts of the two pseudo vectors that are used in the expression for the partial cross section. From Eqs. (14), (15), and (16), the three quantities are: $\left|{}^J S_{\bar{\alpha}\bar{\ell}_1\bar{\ell}_2}^{\alpha\bar{\ell}_1\bar{\ell}_2}\right|^2$ for all α, $\sum_{\ell_1}\sum_{\ell_2}{}_{(\ell_1,\ell_2)\neq(\bar{\ell}_1,\bar{\ell}_2)} \left|{}^J S_{\bar{\alpha}\bar{\ell}_1\bar{\ell}_2}^{\alpha\ell_1\ell_2}\right|^2$ for all α, and ${}^J\phi_{\bar{\alpha}\bar{\ell}_1\bar{\ell}_2}^{\bar{\alpha}\bar{\ell}_1\bar{\ell}_2}$. These quantities are not smooth functions of J but are relatively smooth functions of ${}^J\langle\bar{\alpha}\bar{\ell}_1\bar{\ell}_2|P_2(\cos\gamma)|\bar{\alpha}\bar{\ell}_1\bar{\ell}_2\rangle$ designating the expectation value of $P_2(\cos\gamma)$ with respect to the initial channel ${}^J|\bar{\alpha}\bar{\ell}_1\bar{\ell}_2\rangle$. This expectation value contains the entire J dependence of the initial channel's expectation value of our asymmetric IP [see Eq. (3)]. Let us index a model calculation by nJ when each calculated pair of pseudo vectors was constructed from n solution vectors from the

propagation method and the remaining solution vectors from interpolation of the above three quantities with respect to ${}^{J}\langle\bar{\alpha}\bar{\ell}_1\bar{\ell}_2|P_2(\cos\gamma)|\bar{\alpha}\bar{\ell}_1\bar{\ell}_2\rangle$. These calculated pairs of pseudo vectors are used to interpolate other pseudo vectors, with respect to $\bar{\ell}_2$, to form partial cross sections. For a fixed interpolation of pseudo vectors with respect to $\bar{\ell}_2$, the interpolation of solution vectors with respect to ${}^{J}\langle\bar{\alpha}\bar{\ell}_1\bar{\ell}_2|P_2(\cos\gamma)|\bar{\alpha}\bar{\ell}_1\bar{\ell}_2\rangle$ is accurate for that value n such that there is a negligible difference in partial cross sections between the nJ and the (n - 1)J model calculation. Let us call ALL-J a model calculation where all solution vectors used in the construction of pseudo vectors were calculated; the model calculations for the H_2-A system were ALL-J calculations. In Table VI we compare the partial cross sections for the H_2-A system determined by 2J, 3J, and ALL-J calculations of models 2 and 4. Any of the three calculations for both models would have estimated the same degree of BSA induced error in partial cross sections. This indicates that our interpolation scheme drastically reduces the number of solution vectors that must be calculated for each pair of pseudo vectors.

B. Results for the O_2-He System

For this system, we calculate $\sigma^0_{0,13}$, $\sigma^1_{1,13}$, $\sigma^1_{0,13}$, and $\sigma^0_{1,13}$ for only model 2 and the BSA. We solve for pwfns $\psi^{0,13}_{\bar{\ell}_2 J}$ and $\psi^{1,13}_{\bar{\ell}_2 J}$ for $\bar{\ell}_2$ ranging from 0 to 130. The propagation method is used for $\bar{\ell}_2$ = 0, 9, 18, 27, 36, 48, 60, 70, and 80; interpolation with respect to $\bar{\ell}_2$ supplies the missing pseudo vectors for $\bar{\ell}_2$ = 0 to 80. The analytic method is used for $\bar{\ell}_2$ = 81 to 130. The complete channel sets of $\psi^{0,13}_{\bar{\ell}_2 J}$ and $\psi^{1,13}_{\bar{\ell}_2 J}$ are defined in Table VII where, as a function of $\bar{\ell}_2$, the ranges of α and ℓ_1 are listed. A channel set's range of ℓ_2 has all values allowed by the value of J of the set's pwfn. Not all open channels are included in each pwfn's channel set, but we estimate that a calculation with this set would incorrectly determine only vibrationally elastic and inelastic lateral processes of probabilities less than 10^{-4} and 10^{-7} respectively.

Table VIII lists the partial cross sections for a 2J and a 3J model 2 calculation and for five BSA calculations. Each BSA calculation uses different values for σ and ϵ, which are also listed in Table VIII. From the results of Table VIII, the 2J and 3J calculations of model 2 are nearly the same and indicate that BSA induced errors for the O_2-He system are less than 1% in σ and about 5% in ϵ for elastic cross sections and about 1% in σ for inelastic cross sections. The BSA calculations also show that inelastic cross sections are very insensitive to the value of ϵ. Because all four models estimate the same BSA induced errors in the H_2-A system, we doubt that other model calculations on O_2-He would

radically alter our conclusions. If we assume that the BSA is as good for differential cross sections as for cross sections, then we can use the BSA to investigate the potential sensitivity of differential cross sections. The five BSA calculations were redone with each solution vector explicitly calculated. In Figs. 12 and 13 we plot $d\sigma^{1}_{1,13}(\theta_2)$ and $d\sigma^{1}_{0,13}(\theta_2)$ respectively for the five redone BSA calculations. The two figures show that, for O_2-He as for H_2-A, the potential sensitivity of the elastic differential cross sections is concentrated in the very small angle region, while the inelastic differential cross sections have the same potential sensitivity as inelastic cross sections.

C. Results for the I_2-He System

For this system, we calculate $\sigma^0_{0,34}$, $\sigma^1_{1,34}$, $\sigma^1_{0,34}$, and $\sigma^0_{1,34}$ for only model 2 and the BSA. We solve for pwfns $\psi^{0,34}_{\bar{\ell}_2 J}$ and $\psi^{1,34}_{\bar{\ell}_2 J}$ for $\bar{\ell}_2$ ranging from 0 to 100. The propagation method is used for every eighth value of $\bar{\ell}_2$ from 0 to 64; interpolation with respect to $\bar{\ell}_2$ supplies the missing pseudo vectors for $\bar{\ell}_2$ = 0 to 64. The analytic method is used for $\bar{\ell}_2$ = 65 to 100. The complete channel sets of $\psi^{0,13}_{\bar{\ell}_2 J}$ and $\psi^{1,13}_{\bar{\ell}_2 J}$ are defined in Table IX where, as a function of $\bar{\ell}_2$, the ranges of α and ℓ_1 are listed. A channel set's range of ℓ_2 has all values allowed by the value of J of the set's pwfn. Due to the technical difficulties discussed in Section IV, the channel sets defined by Table IX have no closed channels. We will discuss the effect of their absence on partial cross sections. We estimate that the absence of some open channels from the channel sets of Table IX will affect only vibrationally elastic and inelastic lateral processes of probabilities less than 10^{-4} and 10^{-5} respectively.

Table X lists the partial cross sections for a 2J and a 3J model 2 calculation and for five BSA calculations for five different values of σ and ϵ. From the results of Table X, the 2J and 3J calculations of model 2 are nearly the same and indicate that BSA induced errors for the I_2-He system are less than 1% in σ and 5% in ϵ for the elastic cross sections and less than 5% in ϵ for the inelastic cross sections. The BSA calculations also show that inelastic cross sections are insensitive to the value of σ. To

determine the effect on partial cross sections of the absence of closed channels from all channel sets, we redid the five BSA calculations including two closed channels in each pwfn's channel set. The resulting partial cross sections are listed in Table XI. The elastic cross sections are unchanged; the inelastic cross sections are all changed by the same small amount, leaving their relative values unchanged. We believe model cross sections will undergo the same alternations if closed channels are used in the calculation. By assuming the BSA is equally good for cross sections and differential cross sections, we redid once again the five BSA calculations to investigate the potential sensitivity of differential cross sections. In this new set of calculations, closed channels were used and each solution vector was explicitly calculated. In Fig. 14 we plot $d\sigma^1_{1,34}(\theta_2)$ for three BSA calculations and in Fig. 15 we plot $d\sigma^1_{0,34}(\theta_2)$ for all five BSA calculations. The two figures show that the elastic and inelastic differential cross sections of I_2-He have size and structure over a far wider range of angles than the differential cross sections of H_2-A and O_2-He. The large values of σ and ϵ make the collision of He with I_2 much "stickier" than the collision of A with H_2 or of He with O_2. Large angle scattering is significant with the consequence that both the inelastic and elastic <u>differential</u> cross sections of I_2-He show the same potential sensitivity as the corresponding cross sections.

VII. CONCLUSIONS

Two conclusions about low energy vibrational scattering in homonuclear diatom-atom collisions can be drawn from our results for the H_2-A, O_2-He, and I_2-He systems. First, the breathing sphere approximation can be used to analyze accurately experimental measurements for the potential parameters to which the measurements are sensitive. Second, the measurements most sensitive to potential parameters are, first, elastic cross sections, and, second, inelastic cross sections and inelastic differential cross sections. Elastic differential cross sections are as sensitive as elastic cross sections if the intermolecular potential is soft and the collision is "sticky" with large angle scattering (like I_2-He). Otherwise the entire potential sensitivity of elastic differential cross sections will be concentrated in the experimentally difficult region of very small angle scattering.

The approach used in this work can be applied to the study of the orientation effect of strong dipole forces present in most heteronuclear diatom-atom vibrational scattering. The intermolecular potential used in a breathing-sphere-approximation calculation cannot align the atom and diatom during collision, whereas the intermolecular potential used in a model calculation can. A significant difference between BSA and model observables would indicate the aligning power of dipole forces significantly affects vibrational scattering.

APPENDIX

The elastic phases of solution or pseudo vectors are undetermined within an integral multiple of 2π. The propagation method internally adds or subtracts 2π units to its phases to bring them within $\pm\pi$. Fig. 16 is the plot of the phase, as both a smooth function of $\bar{\ell}_2$ and as produced by the propagation method. Because the phase as a smooth function of $\bar{\ell}_2$ passes outside the range of $\pm\pi$, the phases produced by the propagation method are not suitable for interpolation with respect to $\bar{\ell}_2$. For BSA calculations this difficulty can be avoided by using the JWKB method to determine the elastic phase of each solution vector under the gross approximation that the initial channel experiences only potential scattering. The JWKB phases are smooth functions of $\bar{\ell}_2$. We use these phases to determine the number of 2π units the exact elastic phase of the propagation method must be displaced, by demanding the displaced phase be as close as possible to the JWKB phase. The displaced elastic phases are smooth functions of $\bar{\ell}_2$ and are suitable for interpolation. For the pseudo elastic phases of a model calculation, we use the same displacements determined for the BSA calculation whose IP is the symmetric part of the model's IP. In all cases where this procedure was used, the difference between an exact undisplaced and a JWKB phase was, within 1 or 2%, an exact multiple of 2π.

REFERENCES

[1]For a survey of such experiments, see R. G. Gordon, W. Klemperer, and J. I. Steinfeld, Ann. Rev. Phys. Chem. 19, 215 (1968).

[2]For review of theoretical calculations of $O\frac{\alpha}{\alpha\ell_1}$, see Ref. 1; J. L. Stretton, Transfer and Storage of Energy by Molecules (John Wiley and Sons Ltd., New York, 1969), Vol. 2, Chap. 2, p. 58; D. Rapp and T. Kassal, Chem. Rev. 69, 61 (1969).

[3]S. W. Benson and G. C. Berend, J. Chem. Phys. 44, 4247 (1966).

[4]R. Razner, J. Chem. Phys. 51, 5602 (1969).

[5]For example, see the calculated Li^+-H_2 IP of W. A. Lester, Jr., J. Chem. Phys. 54, 3171 (1971).

[6]D. Secrest and B. R. Johnson, J. Chem. Phys. 45, 4556 (1966).

[7]J. H. Kiefer and R. W. Lutz, J. Chem. Phys. 44, 668 (1966) and 45, 3888 (1966).

[8]D. R. White and R. C. Millikan, J. Chem. Phys. 39, 1807 (1963).

[9]J. I. Steinfeld and W. Klemperer, J. Chem. Phys. 42, 3475 (1965).

[10]A. M. Arthurs and A. Dalgarno, Proc. Roy. Soc. (London) A256, 540 (1960).

[11]R. G. Gordon, J. Chem. Phys. 51, 14 (1969).

[12]N. F. Mott and H. S. W. Massey, The Theory of Atomic Collisions (Oxford University Press, New York, 1965), 3rd ed., p. 89.

[13]J. M. Blatt and L. C. Biedenharn, Rev. Mod. Phys. 24, 258 (1952).

[14]For examples, see V. P. Gutschick, V. McKoy, and D. J. Diestler, J. Chem. Phys. 52, 4807 (1970); A. S. Cheung and D. J. Wilson, J. Chem. Phys. 51, 4733 (1969) and 51, 3449 (1969).

[15]For examples, see Ref. 11 and Ref. 6.

TABLE I. System parameters in reduced units.

Parameter	H_2-A	O_2-He	I_2-He
M	0.952	0.111	0.0155
B_0	0.0138[a]	0.000918[a]	0.000228[a]
σ	48.14[b]	115.5[c]	128.3[d]
ϵ	0.01158[b]	0.01593[c]	0.4073[d]
α_{SR}	0.25[e]	0.45[f]	0.55[g]
α_{LR}	0.128[h]	0.229[h]	0.10[i]
E	2.140	2.195	2.464
ℓ_1	3	13	34
T(°K)	2000°	800°	85°

[a]G. Herzberg, Spectra of Diatomic Molecules (D. Van Norstrand Company, Inc., Princeton, 1950), 2nd ed.

[b]R. Helbing, W. Gaide, and H. Pauly, Z. Physik 208, 215 (1968).

[c]Derived from the combining laws and the He-He parameters of J. O. Hirschfelder, C. F. Curtiss, and R. B. Bird, Molecular Theory of Gases and Liquids (John Wiley and Sons, Inc., New York, 1964), 2nd corrected printing, pp. 168, 1110; and the O_2-O_2 parameters of C. J. G. Raw and C. P. Ellis, J. Chem. Phys. 28, 1198 (1958).

[d]J. I. Steinfeld and W. Klemperer, J. Chem. Phys. 48, 3475 (1965); J. I. Steinfeld, J. Phys. Chem. 64, 14 (1968); parameters

TABLE I. Continued.

are for the B $^3\Pi_{ou+}$ electronic state of I_2.

[e]From the H_2-He potential surface calculated by M. D. Gordon and D. Secrest, J. Chem. Phys. 52, 120 (1970).

[f]Estimated from the O_2-O_2 atom centered Lennard Jones potential of J. R. Sweet and W. A. Steele, J. Chem. Phys. 47, 3029 (1967).

[g]Estimated from the Br_2-A atom centered Lennard Jones potential of R. Razner, J. Chem. Phys. 51, 5602 (1969).

[h]Derived from the polarization experiments of N. J. Bridge and A. D. Buckingham, Proc. Roy. Soc. (London) A295, 334 (1966).

[i]From the value for Br_2-Li^7 measured by R. K. B. Helbing and E. W. Rothe, J. Chem. Phys. 48, 3945 (1968).

TABLE II. Range of ℓ_1 as a function of α and $\mathcal{L}_2$ for the complete channel sets of H_2-A.

$\mathcal{L}_2$ \ α	0	1	2
0 – 40	1, 3, 5	1, 3, 5	1, 3, 5
41 – 80	1, 3, 5	1, 3, 5	

TABLE III. Partial cross sections in $\mathring{A}^2$ for H_2-A.

Type	σ	ϵ	$\sigma^0_{0,3}$	$\sigma^1_{1,3}$	$\sigma^1_{0,3}$	$\sigma^0_{1,3}$
Model 1	48.14	0.01158	51.94	65.29	0.000706	0.00225
Model 3	48.14	0.01158	51.94	65.05	0.000725	0.00226
BSA0	48.14	0.01158	51.97	64.94	0.000687	0.00214
BSA1	47.66	0.01158	50.77	63.33	0.000752	0.00234
BSA2	48.62	0.01158	53.18	66.57	0.000628	0.00195
BSA3	48.14	0.01043	50.48	61.24	0.000699	0.00218
BSA4	48.14	0.01273	53.53	68.82	0.000680	0.00211

TABLE IV. $d\sigma^{0}_{0,3}(\theta_2)$ in $\mathring{A}^2$ for very small angles for H_2-A.

Type	0°	1°	2°	3°	4°
BSA0	18420.	7479.	1639.	2.26	262.
BSA1	17510.	7248.	1635.	1.09	253.
BSA2	19370.	7711.	1637.	5.39	270.
BSA3	16430.	7177.	1604.	1.04	254.
BSA4	20600.	7801.	1675.	4.87	271.

TABLE V. Partial cross sections in $\mathring{A}^2$ for H_2-A. Cross sections constructed by interpolation.

Type	σ	ϵ	$\sigma^0_{0,3}$	$\sigma^1_{1,3}$	$\sigma^1_{0,3}$	$\sigma^0_{1,3}$
Model 1	48.14	0.01158	52.63	61.45	0.000737	0.00235
Model 2	48.14	0.01158	52.66	61.03	0.000822	0.00237
Model 3	48.14	0.01158	52.64	61.25	0.000727	0.00249
Model 4	48.14	0.01158	52.65	61.14	0.000699	0.00252
BSA0	48.14	0.01158	52.65	61.29	0.000712	0.00222
BSA1	47.66	0.01158	51.83	59.37	0.000785	0.00244
BSA2	48.62	0.01158	53.61	63.28	0.000649	0.00202
BSA3	48.14	0.01043	51.43	57.98	0.000732	0.00228
BSA4	48.14	0.01273	54.02	64.44	0.000708	0.00220

TABLE VI. Partial cross sections in $\mathring{A}^2$ for H_2-A from the 2J, 3J, and ALL-J calculations of models 2 and 4. Cross sections constructed by interpolation.

Type	$\sigma^0_{0,3}$	$\sigma^1_{1,3}$	$\sigma^1_{0,3}$	$\sigma^0_{1,3}$
Model 2 (2J)	52.56	61.05	0.000884	0.00242
Model 2 (3J)	52.65	61.03	0.000869	0.00240
Model 2 (ALL-J)	52.66	61.03	0.000822	0.00237
Model 4 (2J)	52.65	61.16	0.000707	0.00256
Model 4 (3J)	52.65	61.14	0.000695	0.00261
Model 4 (ALL-J)	52.65	61.14	0.000699	0.00252

TABLE VII. Range of ℓ_1 as a function of α and $\mathcal{L}_2$ for the complete channel sets of O_2-He.

$\mathcal{L}_2$ \ α	0	1	2
0 - 36	5, 7, . . . , 21	5, 7, . . . , 21	7, 9, . . . , 19
37 - 80	5, 7, . . . , 21	5, 7, . . . , 21	

TABLE VIII. Partial cross sections in $\mathring{A}^2$ for O_2-He. Cross sections constructed by interpolation.

Type	σ	ϵ	$\sigma^0_{0,13}$	$\sigma^1_{1,13}$	$\sigma^1_{0,13}$	$\sigma^0_{1,13}$
Model 2 (2J)	115.5	0.01593	52.87	61.45	0.00326	0.00927
Model 2 (3J)	115.5	0.01593	52.85	61.47	0.00320	0.00920
BSA0	115.5	0.01593	52.75	60.98	0.00339	0.00980
BSA1	114.3	0.01593	52.53	60.77	0.00363	0.01050
BSA2	116.7	0.01593	53.26	61.60	0.00316	0.00915
BSA3	115.5	0.01433	51.66	58.39	0.00338	0.00978
BSA4	115.5	0.01753	54.02	63.99	0.00340	0.00984

TABLE IX. Range of ℓ_1 as a function of α and $\bar{\ell}_2$ for the complete channel sets of I_2-He.

$\bar{\ell}_2$ \ α	0	1
0 - 16	22, 24, . . . , 46	22, 24, . . . , 46
17 - 24	24, 26, . . . , 46	26, 28, . . . , 44
25 - 32	26, 28, . . . , 42	26, 28, . . . , 42
33 - 64	26, 28, . . . , 38	26, 28, . . . , 38

TABLE X. Partial cross sections in $\mathring{A}^2$ for I_2-He. Cross sections constructed by interpolation. No closed channels used in calculations.

Type	σ	ϵ	$\sigma^0_{0,34}$	$\sigma^1_{1,34}$	$\sigma^1_{0,34}$	$\sigma^0_{1,34}$
Model 2 (2J)	128.3	0.4073	424.4	440.2	1.058	2.627
Model 2 (3J)	128.3	0.4073	424.0	440.7	1.054	2.618
BSA0	128.3	0.4073	424.1	431.2	1.063	2.598
BSA1	125.7	0.4073	412.8	385.7	1.058	2.587
BSA2	130.9	0.4073	430.3	480.7	1.065	2.603
BSA3	128.3	0.3870	428.8	416.4	1.001	2.446
BSA4	128.3	0.4275	418.3	457.4	1.126	2.752

TABLE XI. Partial cross sections in $\mathring{A}^2$ for I_2-He. Cross sections constructed by interpolation. Closed channels used in calculations.

Type	$\sigma^0_{0,34}$	$\sigma^1_{1,34}$	$\sigma^1_{0,34}$	$\sigma^0_{1,34}$
BSA0	424.0	431.1	1.091	2.666
BSA1	412.8	385.0	1.087	2.658
BSA2	430.3	480.3	1.091	2.667
BSA3	428.8	410.9	1.026	2.509
BSA4	418.0	457.7	1.156	2.825

FIGURE CAPTIONS

Fig. 1. Coordinates for the collision of atom A with diatom B_2.

Fig. 2. Channel scattering with an angularly symmetric IP.

Fig. 3. Channel scattering with an angularly asymmetric IP.

Fig. 4. Channel scattering with an asymmetric IP and an incomplete channel set.

Fig. 5A. Model 1 (///) and model 2 (\\\) applied to a plane of channels in the set for $\psi_{5,5}^{0,9}$.

Fig. 5B. Model 3 (///) and model 4 (\\\) applied to a plane of channels in the set for $\psi_{5,5}^{0,9}$.

Fig. 6. $d\sigma_{0,3}^{0}(\theta_2)$ for H_2-A. Each curve is generated from a calculated value at every degree.

Fig. 7. $d\sigma_{1,3}^{1}(\theta_2)$ for H_2-A. Each curve is generated from a calculated value at every degree.

Fig. 8. $d\sigma_{0,3}^{1}(\theta_2)$ for H_2-A. Each curve is generated from a calculated value at every other degree.

Fig. 9. $d\sigma_{1,3}^{0}(\theta_2)$ for H_2-A. Each curve is generated from a calculated value at every other degree.

Fig. 10. $d\sigma_{1,3}^{1}(\theta_2)$ for H_2-A. Each curve is generated from a calculated value at every degree.

Fig. 11. $d\sigma^{1}_{0,3}(\theta_2)$ for H_2-A. Each curve is generated from a calculated value at every other degree.

Fig. 12. $d\sigma^{1}_{1,13}(\theta_2)$ for O_2-He. Each curve is generated from a calculated value at every degree.

Fig. 13. $d\sigma^{1}_{0,13}(\theta_2)$ for O_2-He. Each curve is generated from a calculated value at every other degree.

Fig. 14. $d\sigma^{1}_{1,34}(\theta_2)$ for I_2-He. Each curve is generated from a calculated value at every degree.

Fig. 15. $d\sigma^{1}_{0,34}(\theta_2)$ for I_2-He. Each curve is generated from a calculated value at every other degree.

Fig. 16. Elastic phase as a function of $\bar{\ell}_2$. Phase generated by propagation method (Δ); phase as a smooth function (O).

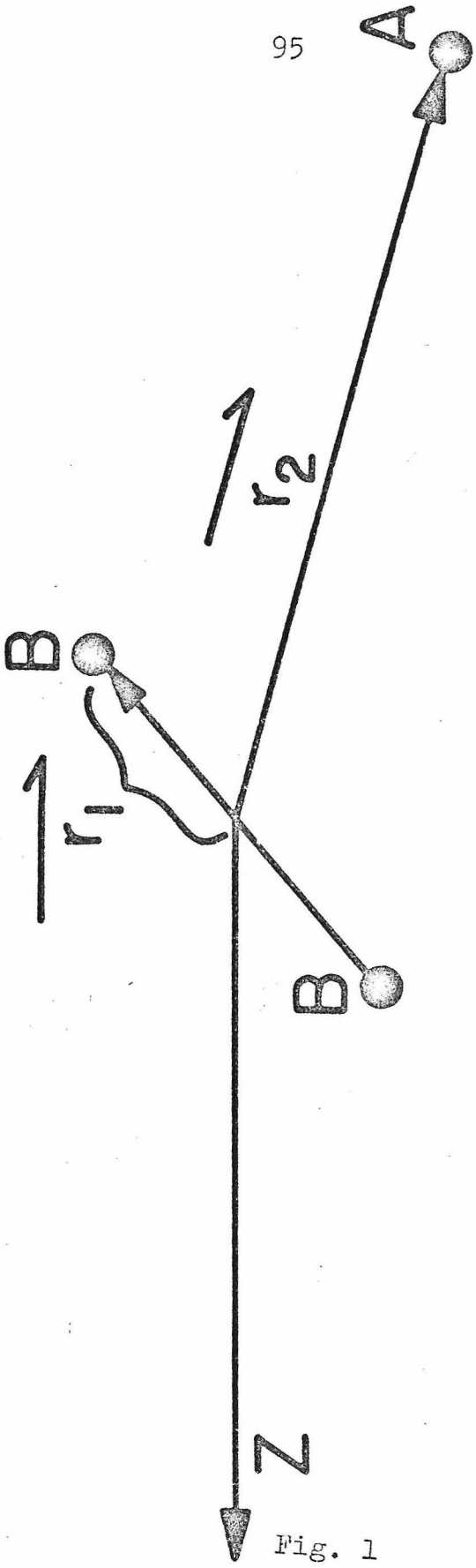

Fig. 1

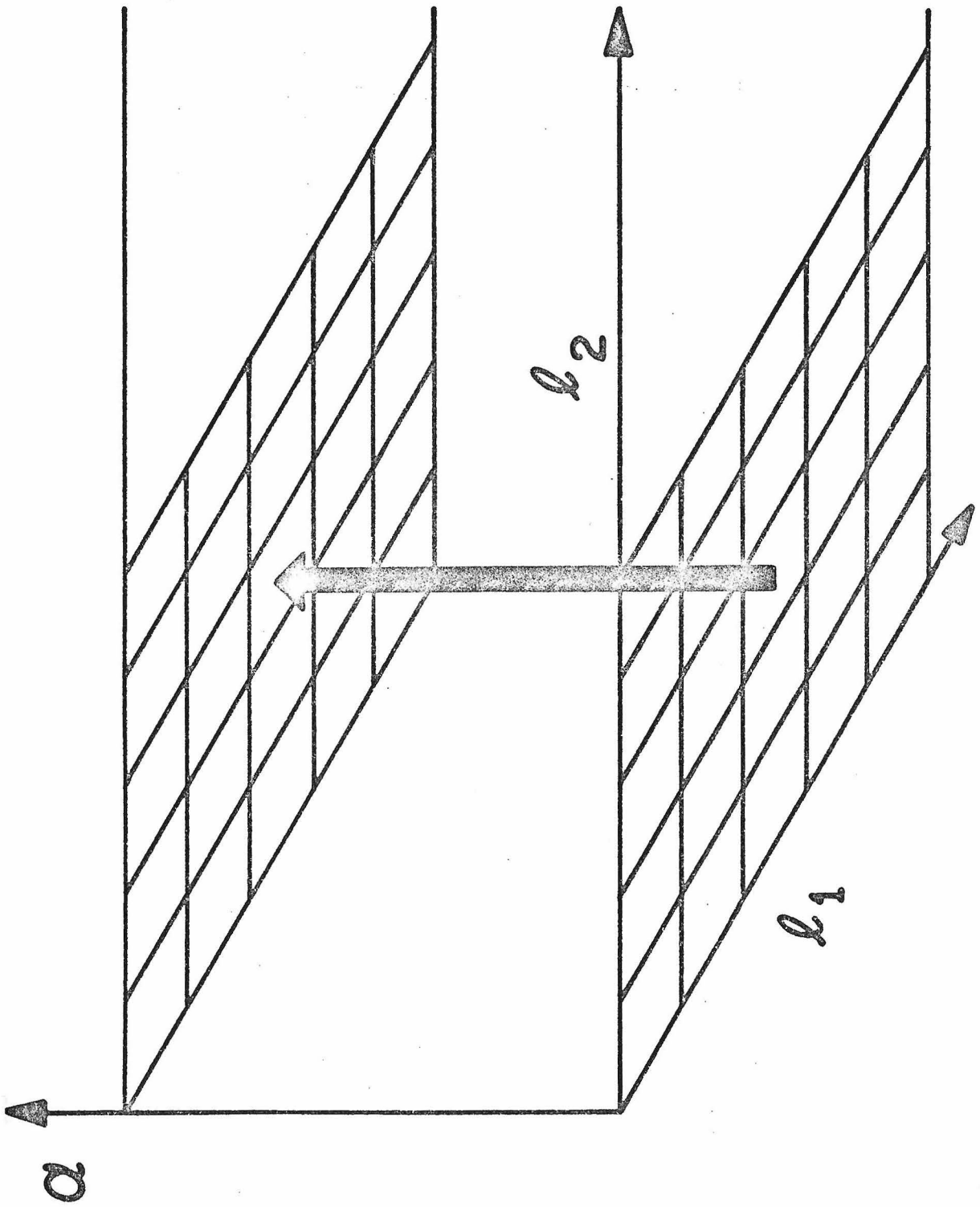

Fig. 2

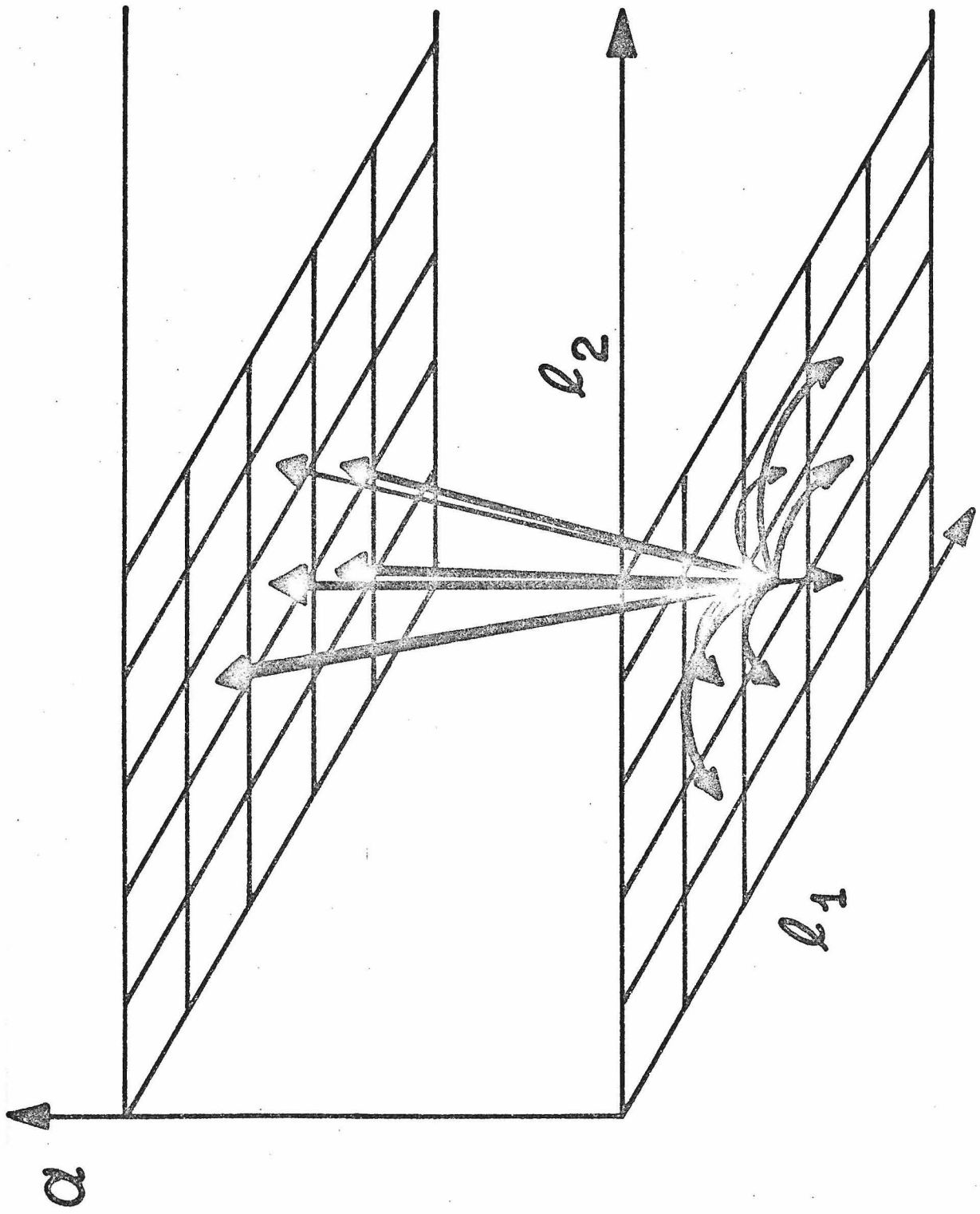

Fig. 3

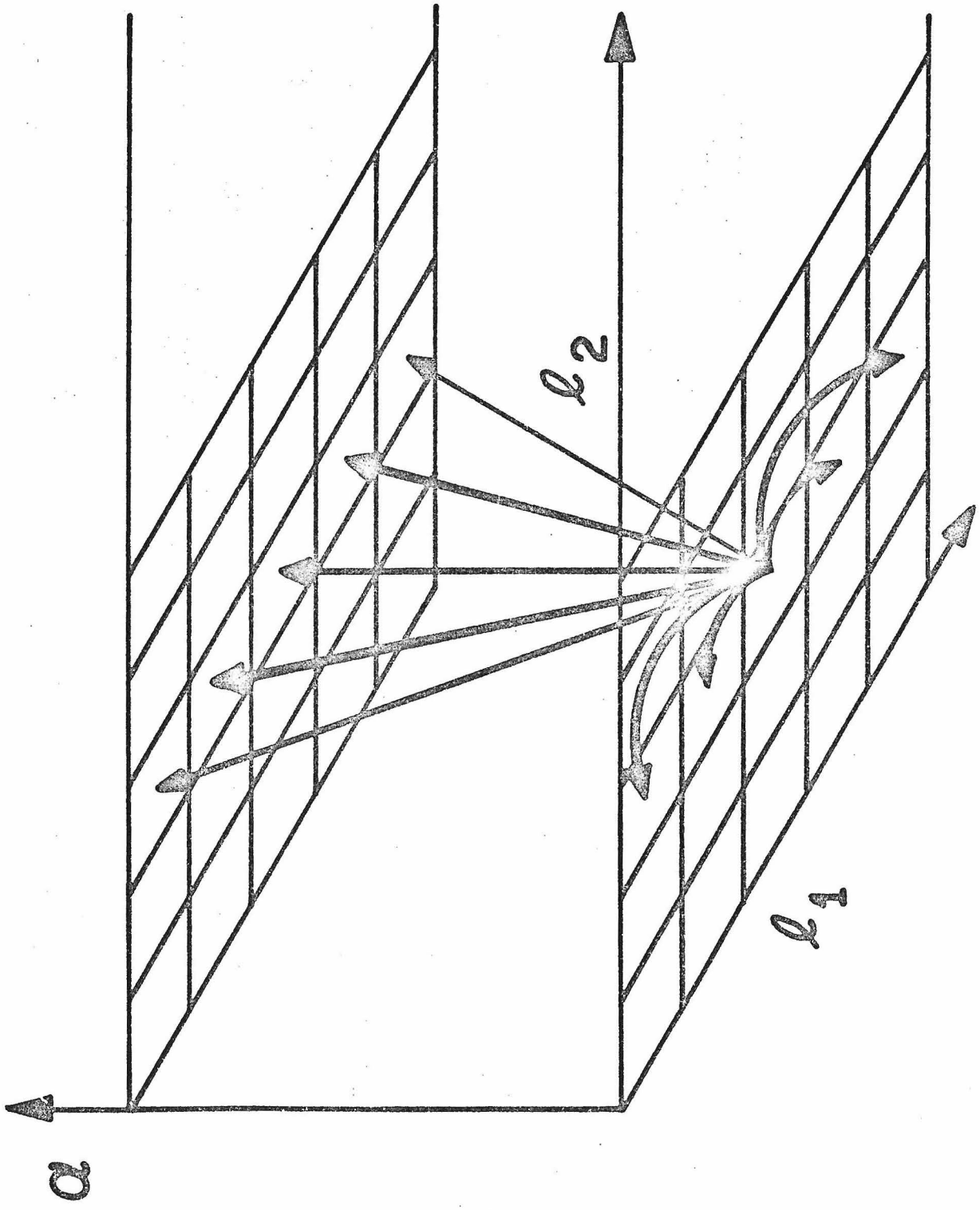

Fig. 4

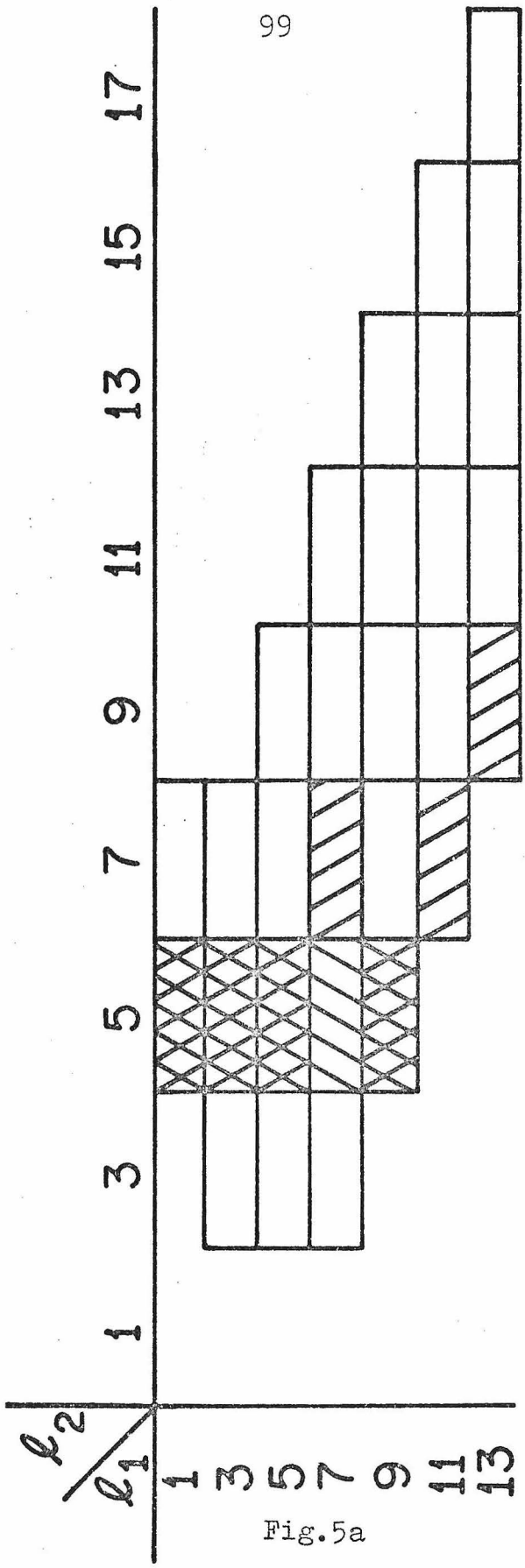

Fig.5a

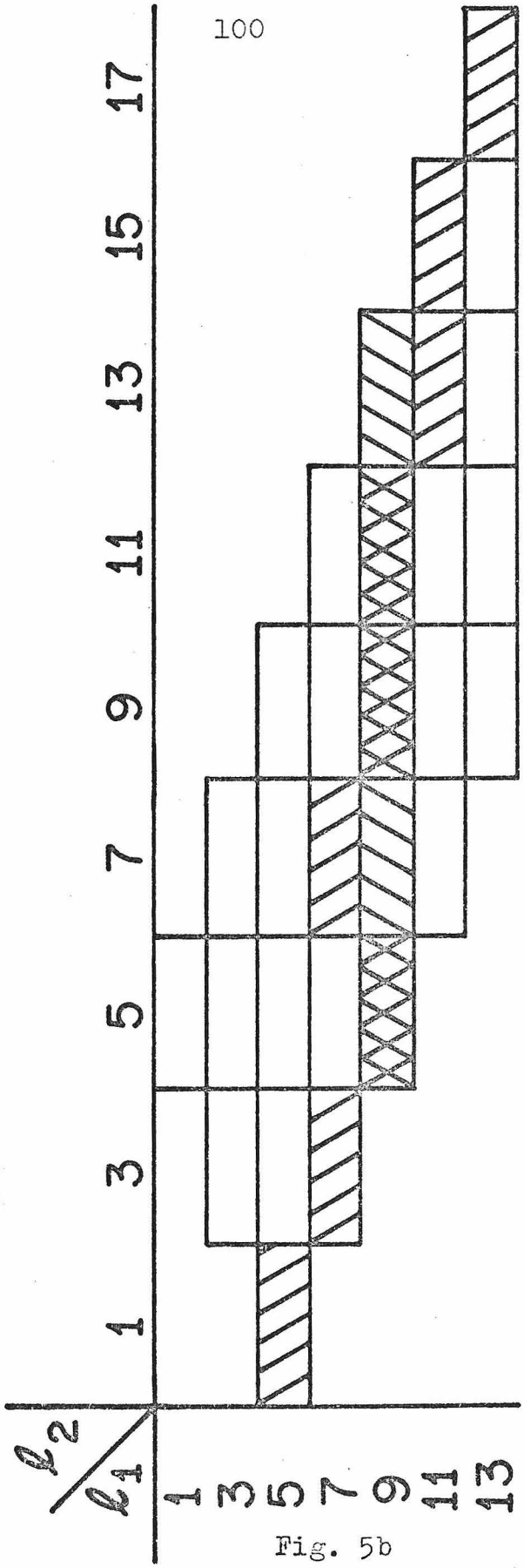

Fig. 5b

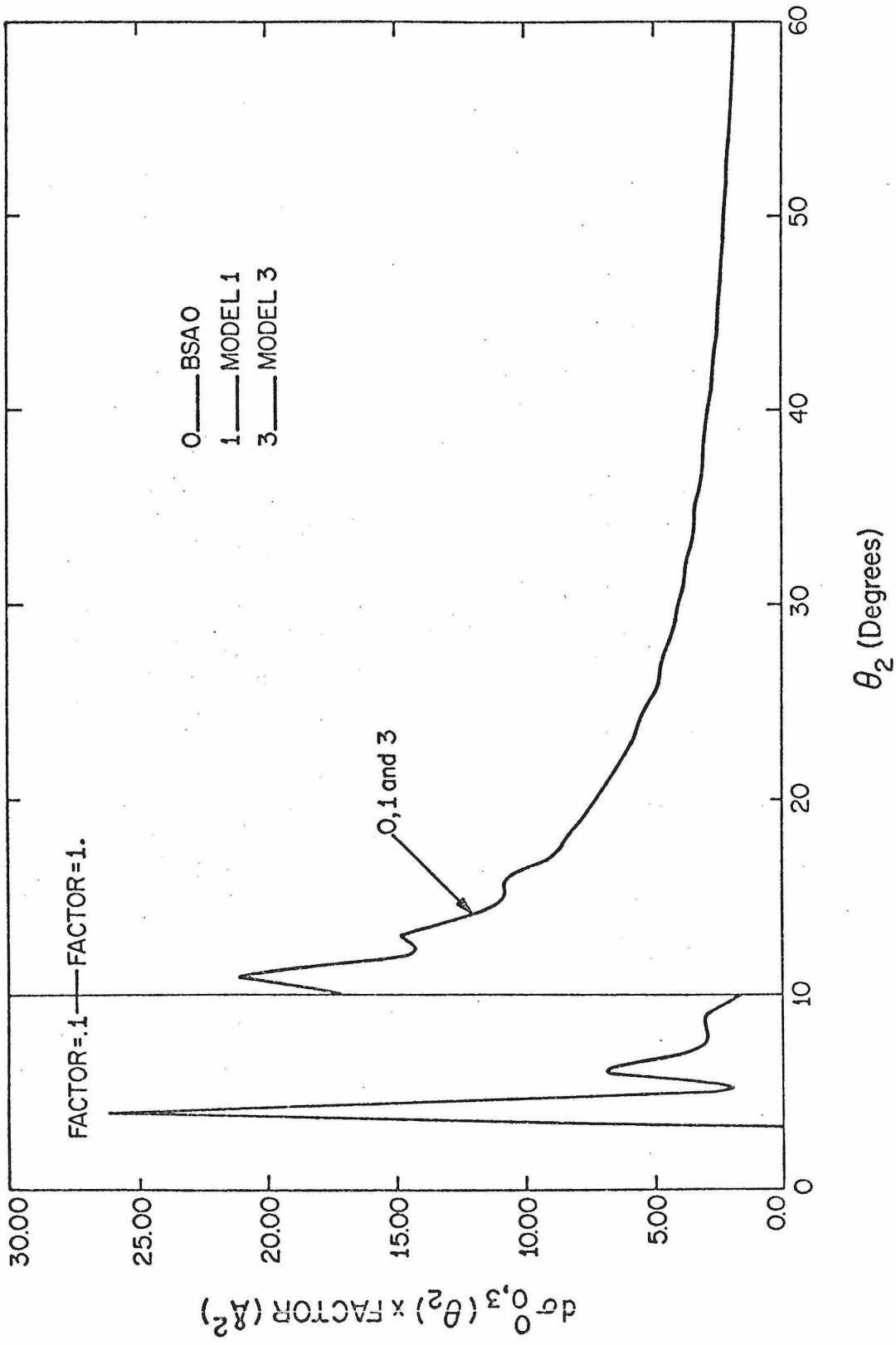
0 BSA 0
1 MODEL 1
3 MODEL 3
0,1 and 3
FACTOR=.1
FACTOR=1.
$d\sigma^{0}_{0,3}(\theta_2) \times \text{FACTOR}\ (\text{Å}^2)$
30.00
25.00
20.00
15.00
10.00
5.00
0.0
0
10
20
30
40
50
60
θ_2 (Degrees)

Fig. 6

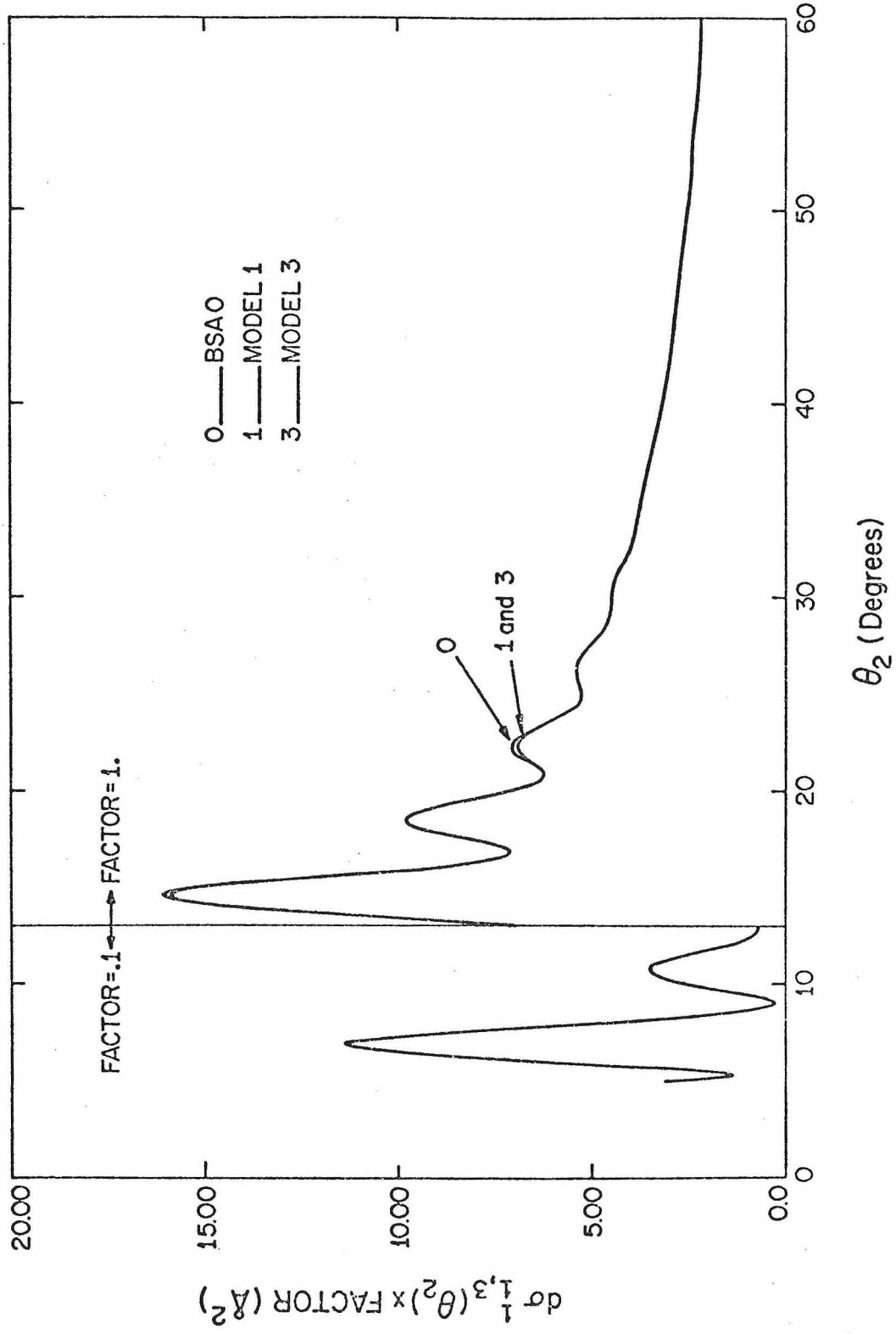
0 BSA 0
1 MODEL 1
3 MODEL 3
0
1 and 3
FACTOR=.1
FACTOR=1.
$d\sigma^{1}_{1,3}(\theta_2) \times$ FACTOR (A^2)
θ_2 (Degrees)
20.00
15.00
10.00
5.00
0.0
0
10
20
30
40
50
60

Fig.7

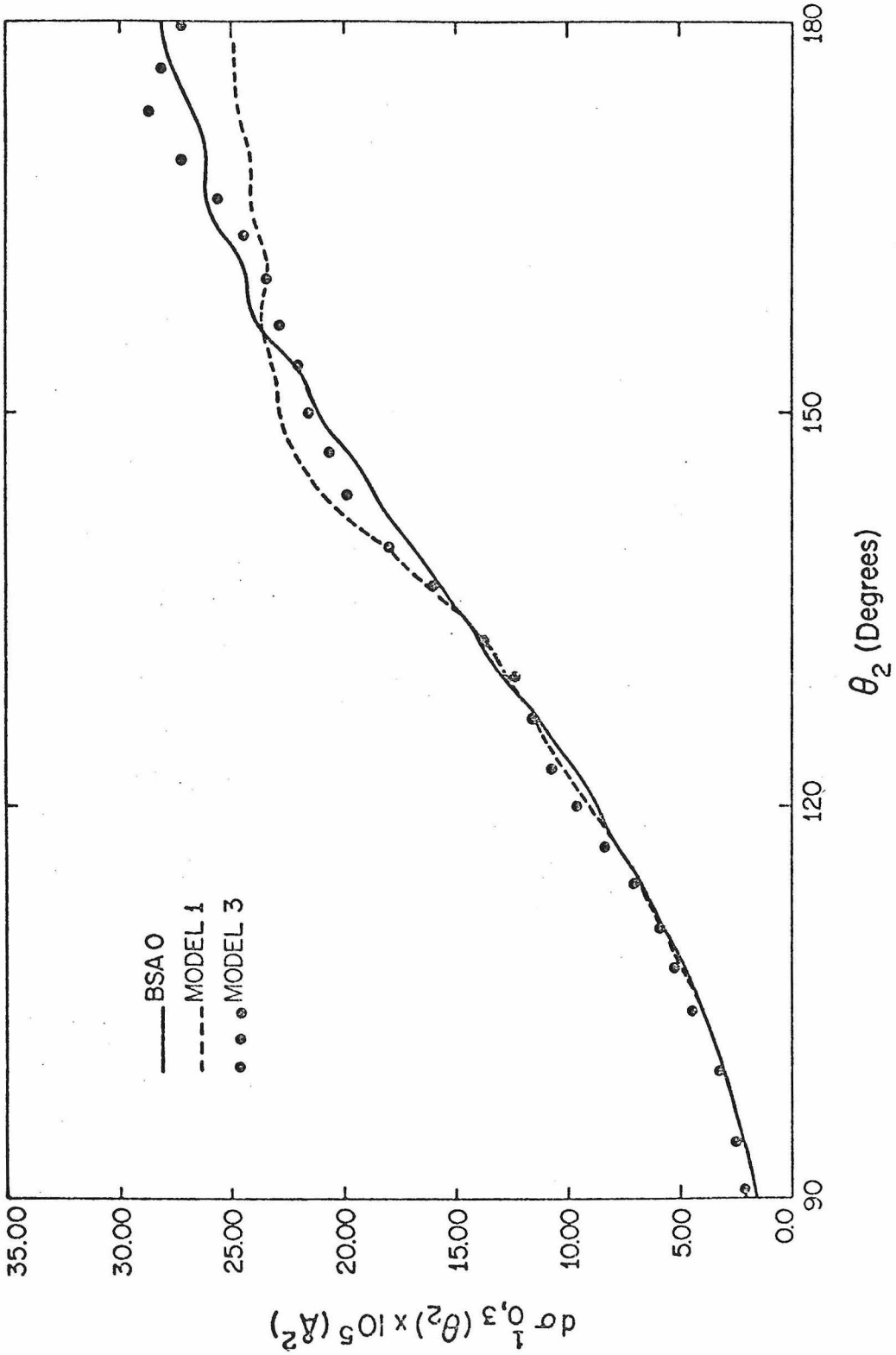
BSA 0
MODEL 1
MODEL 3
35.00
30.00
25.00
20.00
15.00
10.00
5.00
0.0
90
120
150
180
θ_2 (Degrees)
$d\sigma^{1}_{0,3}(\theta_2) \times 10^5$ (Å^2)

Fig.8

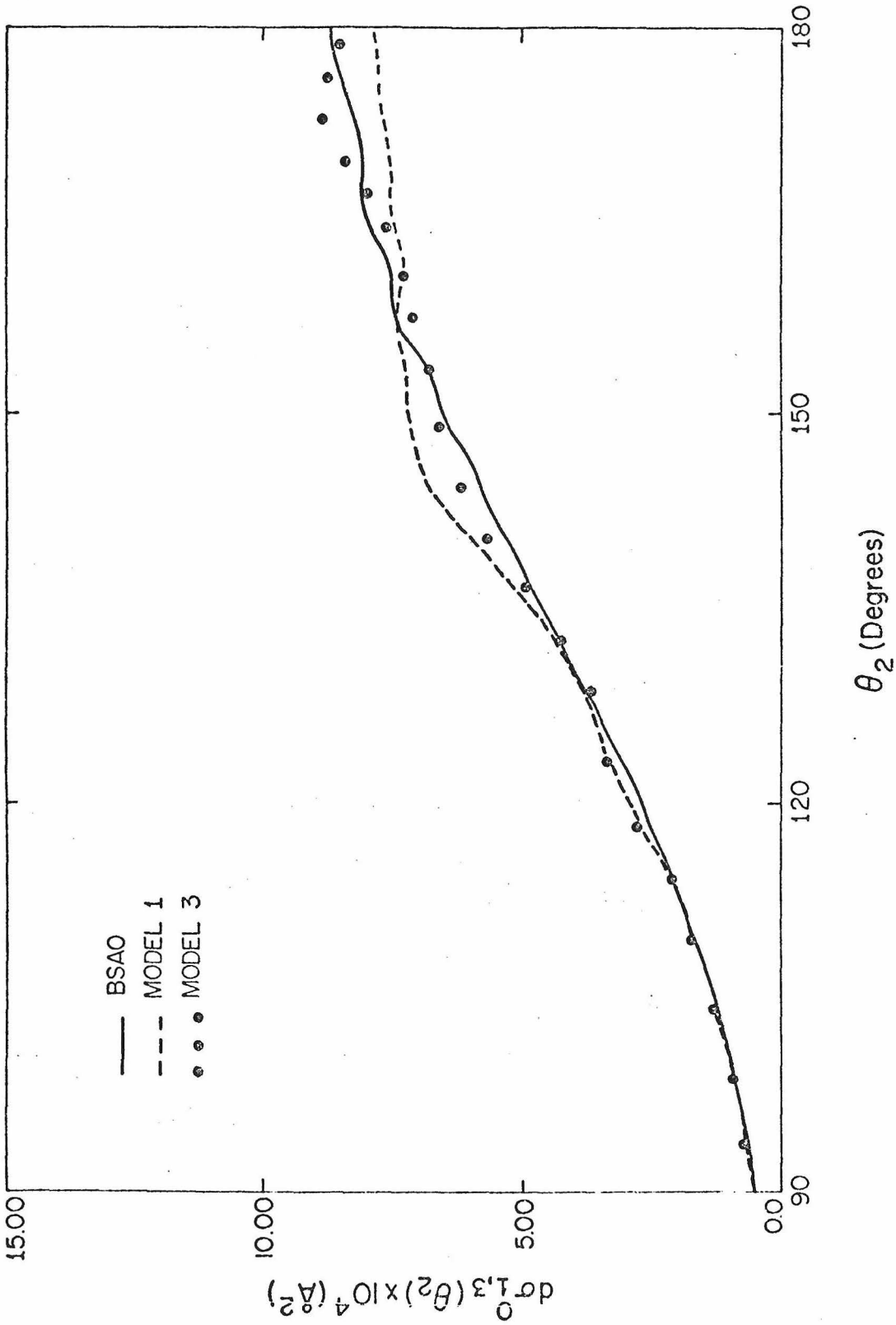
BSAO
MODEL 1
MODEL 3
15.00
10.00
5.00
0.0
90
120
150
180
θ_2 (Degrees)
$d\sigma^0_{1,3}(\theta_2) \times 10^4$ ($\mathring{A}^2$)

Fig.9

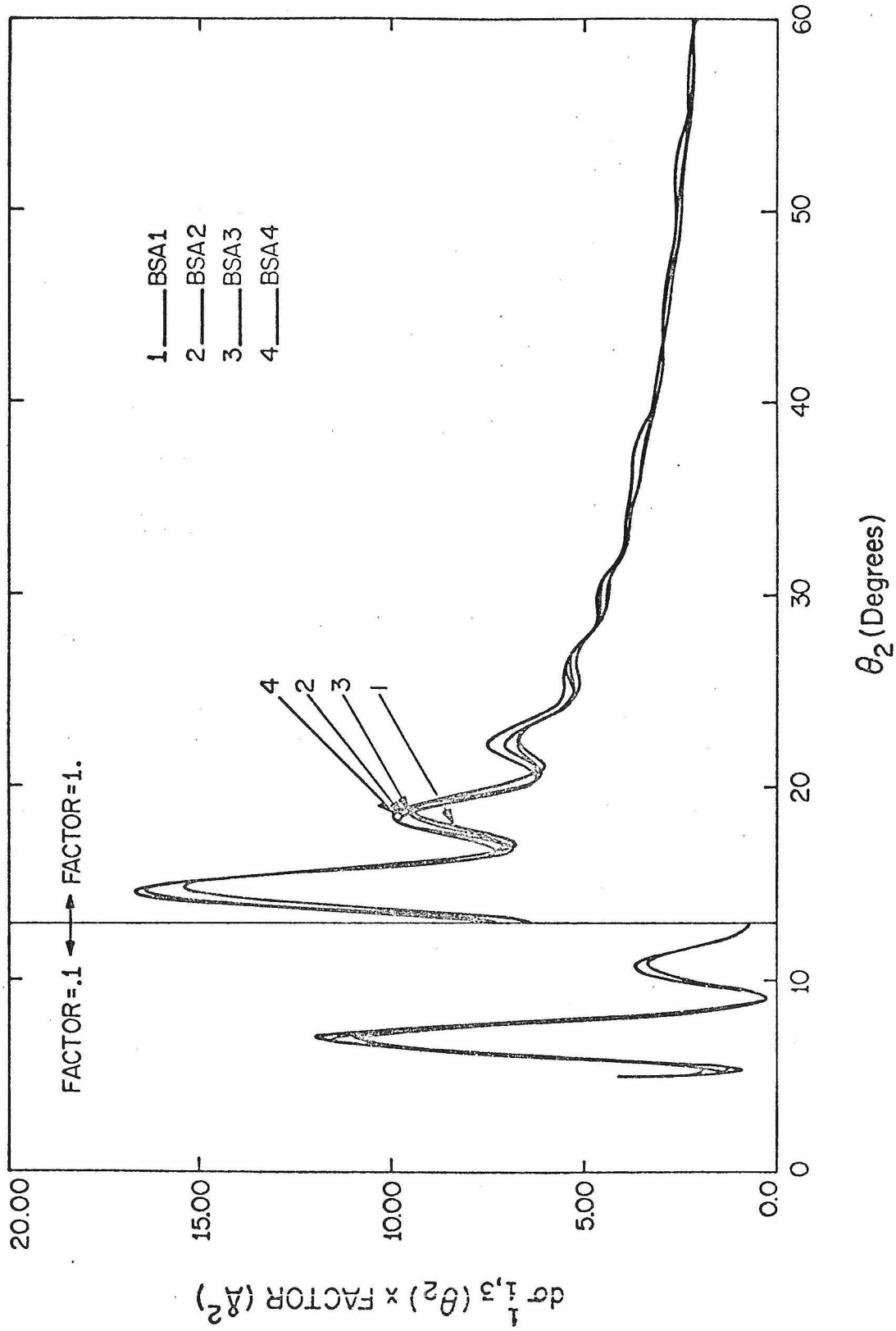
1 BSA1
2 BSA2
3 BSA3
4 BSA4
FACTOR=.1
FACTOR=1.
4
2
3
1
20.00
15.00
10.00
5.00
0.0
0
10
20
30
40
50
60
θ_2 (Degrees)
$d\sigma^1_{i,3}(\theta_2) \times \text{FACTOR}\ (A^2)$

Fig. 10

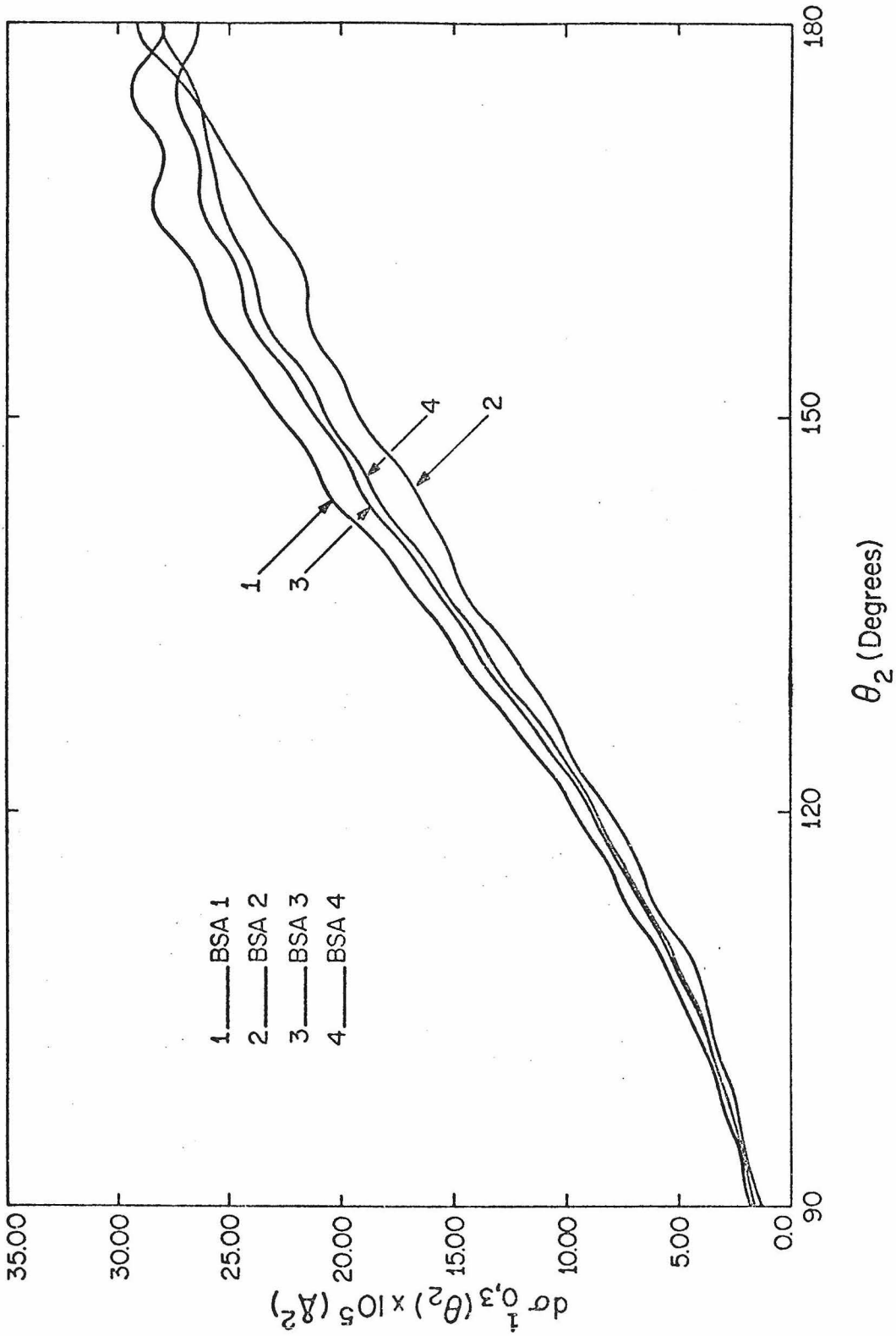
35.00
30.00
25.00
20.00
15.00
10.00
5.00
0.0
90
120
150
180
θ_2 (Degrees)
$d\sigma^{1}_{0,3}(\theta_2) \times 10^5$ (A^2)
1 BSA 1
2 BSA 2
3 BSA 3
4 BSA 4
1
2
3
4

Fig. 11

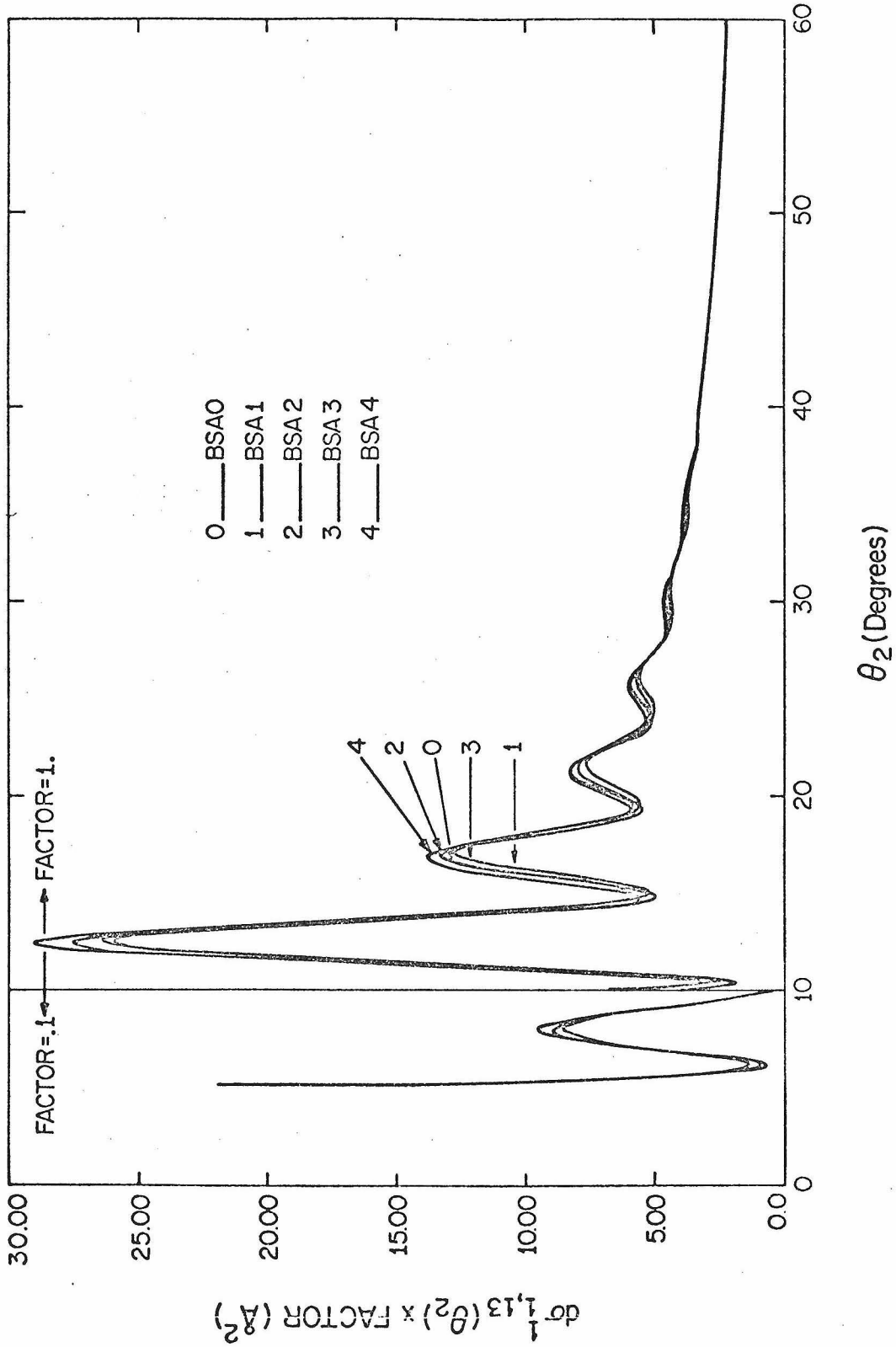
30.00
25.00
20.00
15.00
10.00
5.00
0.0
0
10
20
30
40
50
60
θ_2 (Degrees)
$d\sigma^1_{i,13}(\theta_2) \times$ FACTOR (A^2_1)
FACTOR=.1
FACTOR=1.
0 BSA0
1 BSA1
2 BSA2
3 BSA3
4 BSA4
4
2
0
3
1

Fig. 12

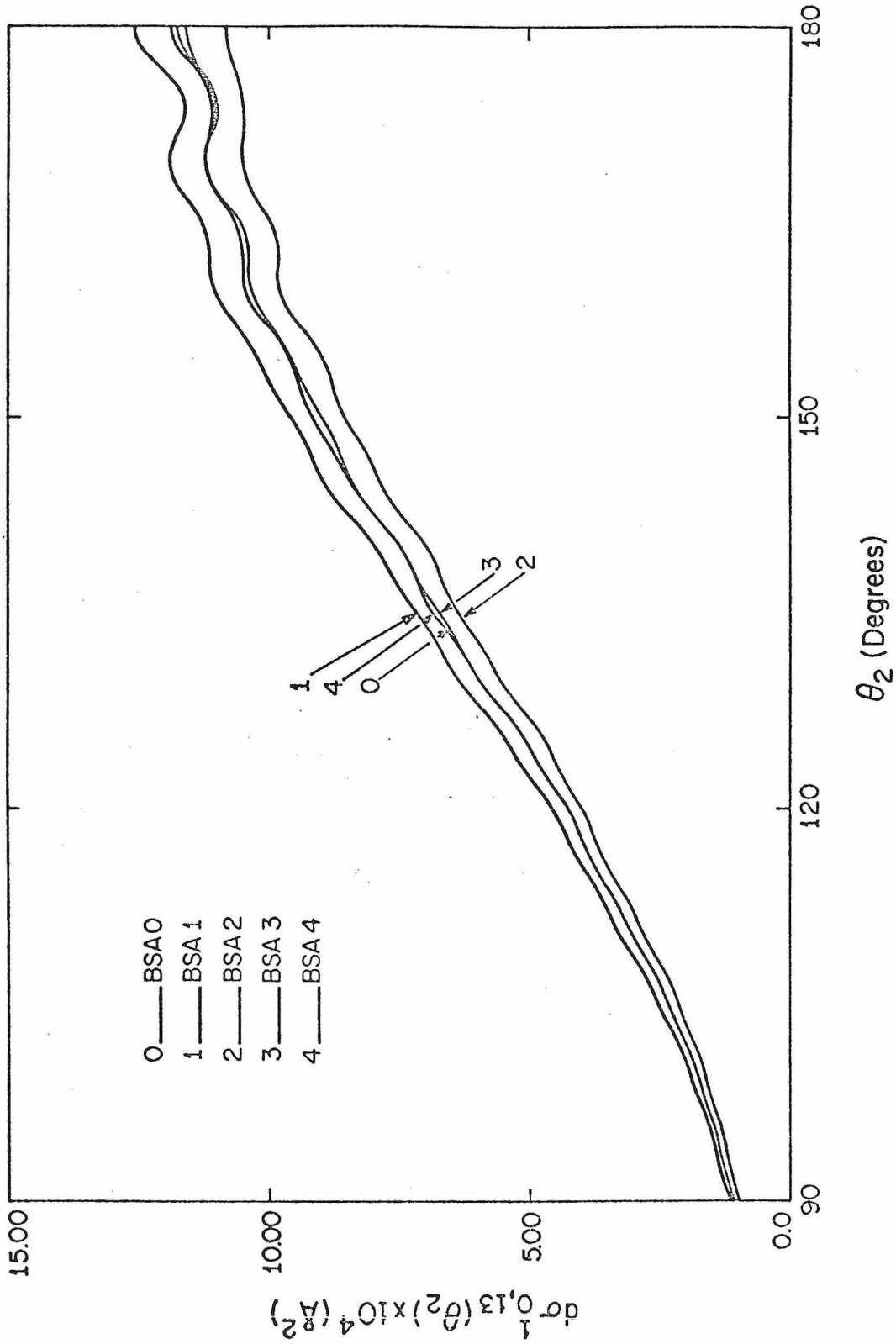
15.00
10.00
5.00
0.0
90
120
150
180
θ_2 (Degrees)
$d\sigma_{0,13}(\theta_2)\times10^4$ (A^2)
0—BSA 0
1—BSA 1
2—BSA 2
3—BSA 3
4—BSA 4
1
4
0
3
2

Fig. 13

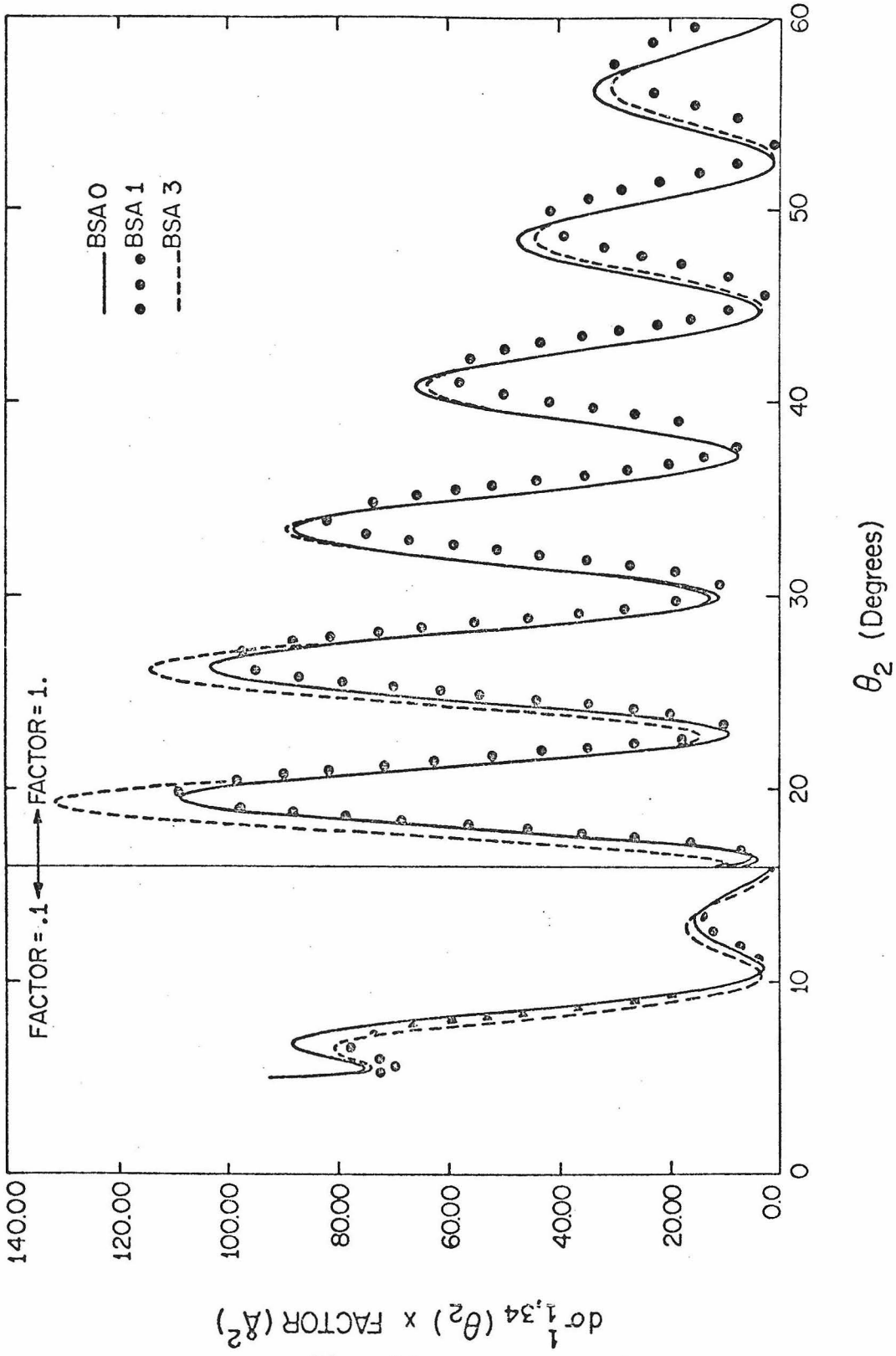
BSA 0
BSA 1
BSA 3
FACTOR = .1
FACTOR = 1.
140.00
120.00
100.00
80.00
60.00
40.00
20.00
0.0
0
10
20
30
40
50
60
θ_2 (Degrees)
$d\sigma^1_{1,34}(\theta_2) \times \text{FACTOR}\ (A^2)$

Fig. 14

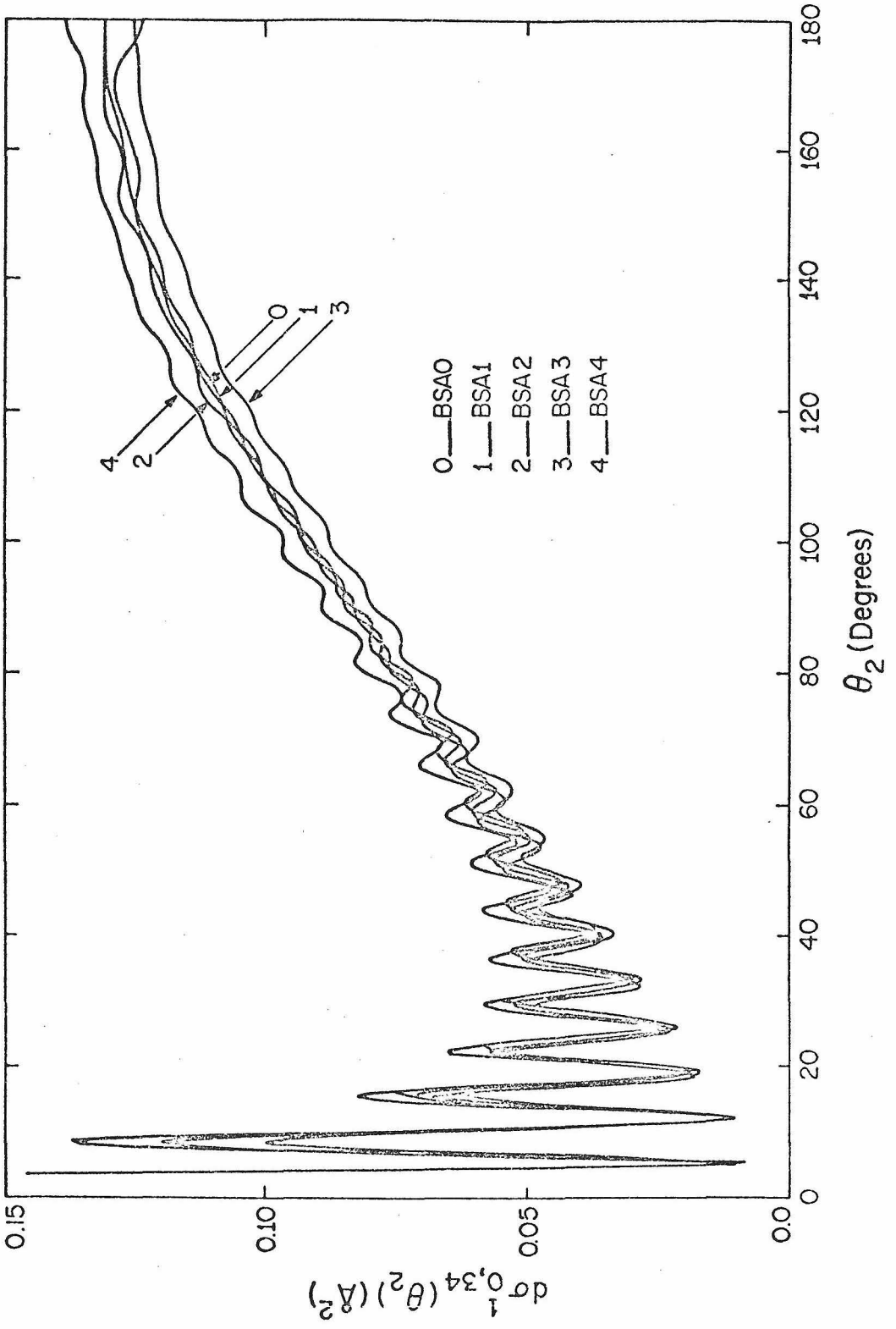
0—BSA0
1—BSA1
2—BSA2
3—BSA3
4—BSA4
0
1
2
3
4
0.0
0.05
0.10
0.15
0
20
40
60
80
100
120
140
160
180
θ_2 (Degrees)
$d\sigma^1_{0,34}(\theta_2)(\text{Å}^2)$

Fig. 15

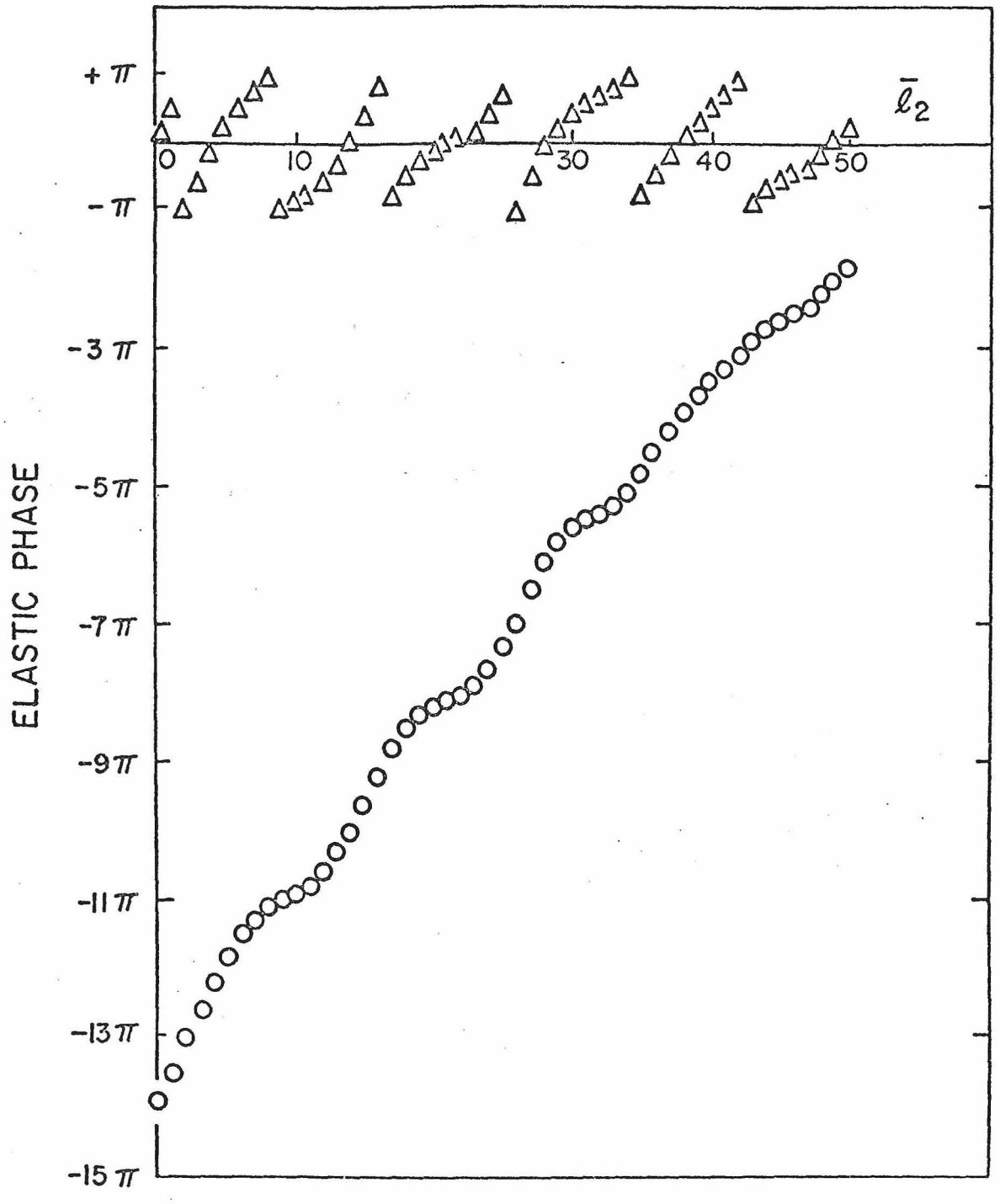

Fig. 16

Part 3: The Effect of the Potential Well on Vibrational Scattering and the Validity of SSH Theory

INTRODUCTION

Most collisions between neutral atoms and molecules are governed by attractive forces at large separations and repulsive forces at short separations. Hence the potential for the collision has an attractive well. For vibrational inelastic collisions of molecules with themselves or with atoms, the potential well is often assumed[1] only to increase the relative translational energy of the collision by an amount equal to the well depth. This acceleration approximation is basic to SSH theory,[1] which is widely used in analyzing the results of vibrational relaxation experiments. There have been several studies[1,2] of the accuracy of the acceleration approximation and of SSH theory, but they have employed approximate methods to obtain the necessary probabilities and crossections. In this article we have analyzed through exact quantum mechanical calculations the effects of the Lennard-Jones well on models of three different inelastic vibrational collision systems: O_2—O_2, Cl_2—Cl_2, and Br_2—Br_2. We have also evaluated the accuracy of SSH theory both in predicting and analyzing experiments on these systems. Wilson[3] has used exact quantum mechanical calculations to study the effects of the well on vibrational excitation. However, the collision systems he studied are quite unlike ours. Also, he did not evaluate the accuracy of SSH theory for his collision systems. This article is divided as follows. In section I, we discuss our choice of collision systems and the method of modeling the collisions and in section II, we describe the methods used to carry out the calculations. In section III, we examine the probability of deexcitation, by head-on

collision, from the first excited to the ground vibrational state, P_{10}, as a function of initial translational energy, E. Calculations are done on all three systems for a Lennard-Jones intermolecular potential and for two other "well-less" potentials suggested by SSH theory. For the Cl_2—Cl_2 system, we examine the crossection for deexcitation, σ_{10}, as a function of E for the same three potentials. In section IV we examine for all three systems P_{10} as a function of E for the Lennard-Jones potential and for a modified "well-less" Lennard-Jones potential. This comparison best isolates the effects of the well. In section V, we examine the accuracy of SSH theory for our three collision systems by comparing its predictions to those derived from the calculations in section III. Section IV summarizes our results.

I. SYSTEM MODELING

The three collision systems O_2—O_2, Cl_2—Cl_2, and Br_2—Br_2 have increasing well depths in units of $\hbar\omega$, the vibrational gap of the diatom. Taken as a set, the three well depths cover the range of depths usually found in diatom-diatom or diatom-atom collisions. Collision systems with hard interactions, such as H_2—H_2, are not well represented by our set of systems. However, systems with hard interactions usually have small well depths, due to the tight binding of electrons about their molecular centers and their resulting low polarizability. We exclude hard collision systems from our study under the assumption that their well effects would be small. Wilson[3] studied hard collision systems with large well depths. His study differs somewhat from ours and would not accurately model most collisions of simple molecules.

For the three systems of interest we wish to calculate the rotationally averaged crossection for deexcitation from the first excited to the ground vibrational state, σ_{10}, as a function of E. The angular asymmetry of the actual intermolecular potential produces rotational as well as vibrational scattering. To obtain σ_{10}, we must sum over the properly weighted crossections for each vibrational-rotational transition consistent with a $1 \rightarrow 0$ vibrational deexcitation. The spherically symmetric part of the intermolecular potential can produce only vibrational scattering. This potential is the result of rotationally averaging the full potential. It is frequently assumed that the vibrational cross-sections obtained directly from the rotationally averaged potential accurately approximate the rotationally averaged vibrational-rotational

crossections obtained from the full potential. This has been shown[4] to be true for low energy homonuclear diatom-atom collisions. We assume this is true here and use only spherically symmetric potentials. To further simplify our calculations, we will freeze one diatom's vibrational motion and approximate the other by a harmonic oscillator. The loss of half of the vibrational degrees of freedom and all of the anharmonicity of the actual collision system make our model quantitatively inaccurate. However, calculations[5] on the H_2—H_2 collision system indicate that these last two approximations create no qualitative discrepancies for head-on collisions, where such discrepancies are most likely to occur. Also, most of our results will be based on the relative comparison of P_{10} or σ_{10} for different but related intermolecular potentials, so some of the quantitative inaccuracies must cancel out. Finally, since SSH theory is based on the same modeling described here, our calculations can then be used to test the accuracy of the theory.

Figure 1 shows our coordinate system. The initial direction of the frozen diatom, particle A, is the z axis. The ball and spring picture for diatom B—B actually represents the breathing sphere responsible for our spherically symmetric intermolecular potential. r_1 is the distance of one atom in B—B from the molecular center of mass (or the distance between the surface of the breathing sphere and its center). θ and r_2 describe the position of particle A relative to the center of mass of B—B. Since the potential is spherically symmetric, there is no out-of-plane scattering and consequently no need for an azimuthal angle to describe the position of A. Since A is a frozen

B—B, its mass, m_A, is twice m_B, the mass of B. In reduced units[6], the hamiltonian $\mathcal{H}$ for the ℓ^{th} partial wave is

$$\mathcal{H} = -\frac{1}{2M}\frac{\partial^2}{\partial r_2^2} + \frac{\ell(\ell+1)}{2M r_2^2} - \frac{1}{2}\frac{\partial^2}{\partial y^2} + \frac{y^2}{2} + V(r_2-r_1) \qquad (1)$$

$$\text{where } M = \frac{m_A}{m_A + 2m_B} = .5$$

The units of energy and length are $\hbar\omega$ and one-half the classical ground state vibrational amplitude. The diatom's displacement from equilibrium is y, while $V(r_2-r_1)$ is the intermolecular potential. We select the Lennard-Jones intermolecular potential for $V(r_2-r_1)$:

$$V(r_2-r_1) = 4\epsilon\left(\left(\frac{\sigma}{r_2-r_1}\right)^{12} - \left(\frac{\sigma}{r_2-r_1}\right)^{6}\right) \qquad (2)$$

This potential is qualitatively correct, is most frequently used by experimentalists, and is the potential assumed by SSH theory. In Table I we list ϵ, σ, and the reduced units of energy and length for our systems. The values are those of Herzfeld et al.[1] These parameters are typical of nonhydrogenic collision systems.

The potential well should influence head-on collisions more strongly than glancing ones. Consequently, the effect of the well should be more pronounced in P_{10} than in σ_{10}. For this reason and for reasons of economy, we calculated P_{10} as a function of E for all three systems, while calculating σ_{10} as a function of E for only the Cl_2—Cl_2 system. The range of E for all calculations was from 0 to 12 reduced units (E will always be given in reduced units).

II. CALCULATIONAL METHODS

We use the propagation method of Gordon[7] to solve for $\underset{\sim}{S}^{\ell}$, the S matrix for the ℓ^{th} partial wave. P_{10} and σ_{10} are related to $\underset{\sim}{S}^{\ell}$, by

$$P_{10} = |{}^{0}S_{10}|^2 \tag{3}$$

$$\sigma_{10} = \frac{\pi}{K^2} \sum_{\ell} (2\ell + 1) |{}^{\ell}S_{10}|^2 \tag{4}$$

where the wavenumber K is $\sqrt{2ME}$. For our purposes, only the ${}^{\ell}S_{10}$ element in $\underset{\sim}{S}^{\ell}$ has to be accurate. In order to obtain an accurate ${}^{\ell}S_{10}$ for our systems, considerably fewer than the total number of open channels need be included in the channel expansion at higher energies. This is due to the fact that at higher energies the excited motion described by the higher open channels is not actually executed by the system during deexcitation from the first excited to the ground state. In Table II, we compare the total number of open channels for all three collision systems to the number of channels which must be retained in the expansion to obtain $|{}^{\ell}S_{10}|^2$ accurate to 3 or 4 digits in the third place. Since the calculation time increases as the cube of the number of channels in the expansion, a significant savings can be achieved by using less than the number of open channels at higher energies. It is generally true that calculations requiring only a part of the S matrix need use only a channel set restricted about the scattering processes of interest and that such a channel set will often be smaller than the total number of open channels.

For the Cl_2--Cl_2 system, σ_{10} must be calculated. At higher energies, σ_{10} may require $|{}^{\ell}S_{10}|^2$ for ℓ ranging from 0 to over 500. However, since $|{}^{\ell}S_{10}|^2$ is a smooth function of ℓ, it can be readily interpolated. At each energy we calculate $|{}^{\ell}S_{10}|^2$ for 4 to 8 values

of ℓ spanning the range of ℓ over which $|{}^{\ell}S_{10}|^2$ is important. We concentrate the calculated values of $|{}^{\ell}S_{10}|^2$ in regions where $|{}^{\ell}S_{10}|^2$ is changing rapidly with ℓ. These calculated elements are used to obtain the other values by interpolation. We actually interpolated $\log_{10}|{}^{\ell}S_{10}|^2$ since this is a smoother function of ℓ than $|{}^{\ell}S_{10}|^2$. The error in σ_{10} due to interpolation with this coarse grid of calculated points is less than 5% except in the very low energy region, where the error could be as much as 10%. Using an IBM 370/155 computer and the procedures described in this section, we can calculate, for the Cl_2—Cl_2 system, σ_{10} from $E \approx 0$ to $E = 12$ in roughly 10 minutes for one set of potential parameters. With procedures described elsewhere,[4] elastic crossections and elastic and inelastic differential crossections as a function of E can also be obtained with a negligible increase in computer time. Approximate theories such as SSH theory are very useful, but they are no longer the only practical way to analyze or predict experimental results.

III. LENNARD-JONES AND SSH INTERMOLECULAR POTENTIALS

All results obtained with the Lennard-Jones intermolecular potential are indicated by LJ. Fig. 2 shows $\log_{10}(P_{10}^{LJ})$ as a function of E for all three systems. The three P_{10}^{LJ} curves are featureless and very similar to each other. In general, P_{10}^{LJ} is an oscillatory function of E. For our systems, the oscillations set in at $E > 12$. For hydrogenic collisions,[3,5] oscillations are evident by $E \approx 4$.

If the well serves only to accelerate the colliding species to an additional translational energy equal to its depth ϵ, LJ should be replaceable by a potential whose value at large separations is $-\epsilon$. Such a potential boosts the incoming energy by ϵ. The short range part of the potential should duplicate as much as possible the repulsive wall of LJ. The replacement potential suggested by SSH theory has the form

$$V(r_2 - r_1) = He^{-\alpha(r_2 - r_1)} - \epsilon \quad . \tag{5}$$

Here H and α are functions of E, allowing a fit to LJ most appropriate for each value of E. There are two methods, A and B, for determining H and α; we designate the two intermolecular potentials EXPA and EXPB and so label any results obtained with them.

In Figs. 3 and 4, we plot $\log_{10}(P_{10}^{EXPA}/P_{10}^{LJ})$ and $\log_{10}(P_{10}^{EXPB}/P_{10}^{LJ})$ respectively (for all three systems). At energies less than or comparable to ϵ, P_{10}^{EXPA} differs from P_{10}^{LJ} by as much as an order of magnitude. At high energies P_{10}^{EXPA} is in close agreement with P_{10}^{LJ}. However, at these high energies the well has little influence on the colliding particles, because they are moving too fast to notice the well.

Consequently, the possibility of the well being represented by a potential whose asymptotic value is $-\epsilon$ cannot be determined accurately at high energies. The good agreement of P_{10}^{EXPA} and P_{10}^{LJ} in this region indicates only that the repulsive walls of the two potentials match closely. Similarly, the substantial disagreement of P_{10}^{EXPB} with P_{10}^{LJ} even at high energies implies that EXPB fails to duplicate the repulsive wall of LJ for our systems. For this reason, no further calculations were done with EXPB.

In Fig. 5 we plot $\log_{10}(\sigma_{10}^{LJ})$ as a function of E for the Cl_2—Cl_2 system; σ_{10}^{LJ} is in Å^2. Over this energy range, σ_{10}^{LJ} is very similar to P_{10}^{LJ} but roughly about an order of magnitude larger. In Fig. 6 we plot $\log_{10}(\sigma_{10}^{EXPA}/\sigma_{10}^{LJ})$ for the Cl_2—Cl_2 system and replot $\log_{10}(P_{10}^{EXPA}/P_{10}^{LJ})$ as a function of E. As expected, over the entire energy range σ_{10}^{EXPA} and σ_{10}^{LJ} are in better agreement than P_{10}^{EXPA} and P_{10}^{LJ}, because the well influences head-on collisions more strongly than glancing ones. Note that for E greater than 2 or 3, the crossection for either LJ or EXPA is overestimated only by a factor of 3 or 4 by the relatively crude approximation:

$$\sigma_{10} = \pi r_c^2 P_{10} \tag{6}$$

where r_c is the classical turning point. The physical interpretation of this approximation is that the hard sphere crossection, πr_c^2, is the cross section for all scattering processes while P_{10} is the probability that a scattering process leads to deexcitation.

IV. THE "LENNARD-JONES CUTOFF" POTENTIAL

Since EXPA approximates both the repulsive wall and the well of LJ, the low energy disagreement of P_{10}^{EXPA} with P_{10}^{LJ} may be due to both the limitations of fitting an exponentially repulsive potential to an inverse powers potential and the failure of representing the well entirely as an acceleration effect. The potential that is exactly LJ at small intermolecular separations and $-\epsilon$ at large separations would, in comparison with LJ, isolate the effects of only the well. Such a potential we call the Lennard-Jones cutoff potential (LJC), whose form is:

$$V(r_2 - r_1) = \begin{cases} 4\epsilon \left(\left(\frac{\sigma}{r_2 - r_1} \right)^{12} - \left(\frac{\sigma}{r_2 - r_1} \right)^{6} \right) & r_2 - r_1 < 2^{1/6}\sigma \\ -\epsilon & r_2 - r_1 \geq 2^{1/6}\sigma \end{cases} \tag{7}$$

where the minimum of LJ occurs at $2^{1/6}\sigma$. In Fig. 7, we plot $\log_{10}(P_{10}^{LJC})$ as a function of E for all three systems. The curves in Fig. 7 are quite unlike analogous curves for LJ, EXPA and EXPB in that at low energies, P_{10}^{LJC} has structure for all three systems. Such structure could in general, come from two sources: the effects of several non-initial open or nearly open channels competing for the initial channel's amplitude or the interference effects of the wavefunction scattering off of several different parts of the potential. The first source may be considered responsible for subexcitation resonances and for the strong oscillations of all probability curves at high enough energy. The second source usually accounts for structure in only elastic scattering observables. However, Wilson[3, 8] has done vibrational scattering calculations

with several potentials which have produced excitation probabilities with structure similar to ours over energy regions in which competitive effects seem unlikely. When we restrict the channel expansion of the wavefunction to only two channels at all energies and recalculate the curves shown in Fig. 7, the structure at low energies is modified, but in no way removed. This seems to indicate that competitive effects are not as important as interference effects from several different regions of LJC. This is surprising because the potential with the most apparent structure is LJ, yet it has no structure in its probability curves. An explanation for the structure in P_{10}^{LJC} could be as follows. For all potentials, the region about the classical turning point is important in determining the scattering. For a monotonic repulsive potential, the tail of the potential would not usually be important in the scattering. We would suspect this to be true for EXPA. Suppose that for LJC the tail can effectively scatter. At low energies, tail scattering would dominate, while at high energies classical turning point scattering would dominate. In the intermediate region there would be interference. In LJ, the effects of the tail of LJC are washed out by the climb out of the well the scattering wavefunction must undergo. The well makes LJ a long range, more adiabatic potential and allows the system to get used to and to get over the effects of the tail in LJC. To test this explanation, we can add on to LJC an exponential potential tail at $r_2 - r_1 = r_0$ where $\sigma \leq r_0 \leq 2^{1/6}\sigma$. The value and slope of the exponential potential can be made to match LJC at r_0. If the exponential tail is ineffective at scattering and if the explanation of the structure of P_{10}^{LJC} is correct, the probabilities of this composite potential, P_{10}^{C}, should be dominated

by classical turning point scattering and show no structure. For the O_2-O_2 and Cl_2-Cl_2 systems, we set r_0 equal to σ; for the $Br_2—Br_2$ system, we set r_0 equal to the position where LJC has a value - $\epsilon/2$. In Fig. 8 we plot $\log_{10}(P_{10}^{C})$ as a function of low energies for all three systems. Since there is no structure in P_{10}^{C}, our explanation seems to be reasonable. In Fig. 9, we plot for all three systems $\log_{10}(P_{10}^{LJC}/P_{10}^{LJ})$ as a function of E. The curves are dominated by the structure in P_{10}^{LJC}. However, outside this region of structure, the results in Fig. 9 indicate that increasing E by the well depth overestimates the effect of the well. This conclusion and our explanation for the structure in P_{10}^{LJC} emphasize that potentials with wells have a longer range and therefore are more adiabatic than "well-less" potentials and any structure in the probabilities for "well-less" potentials is washed out.

V. COMPARISONS WITH SSH THEORY

SSH theory provides analytical expressions to determine the collision number Z_{10}, the average number of collisions a molecule undergoes before relaxing from the first excited to the ground state. If τ_{10} is the relaxation time and τ_c is the time between collisions, then

$$Z_{10} = \frac{\tau_{10}}{\tau_c} \tag{8}$$

If the system's relaxation is dominated by relaxation from the first to the ground state, then

$$\tau_{10} = (k_{10} - k_{01})^{-1} = k_{10}^{-1} (1 - e^{-\hbar\omega/kT})^{-1} \tag{9}$$

where k_{10} is the rate constant. If k_c is the total rate at which scattering events take place per target molecule, then

$$\tau_c^{-1} = k_c \tag{10}$$

For a one-dimensional system in translational equilibrium, k_{10} has the following form

$$\begin{aligned} k_{10} &= \int_0^\infty p_{10}(E) \sqrt{\frac{2}{M}} E \, dn(E) \, dE \\ \text{where } dn(E) &= \rho \left(\frac{M}{2\pi kT}\right)^{\frac{1}{2}} e^{-E/kT} \frac{1}{\sqrt{2M}} E^{-\frac{1}{2}} \end{aligned} \tag{11}$$

Here ρ is the number of particles per unit length and dn(E) is the Maxwell distribution of particles per unit length between energies E and E + dE. For a one dimensional system, the probability that every encounter produces some scattering is 1, for the encounters are all head-on.

Therefore,

$$k_c = \int_0^\infty \sqrt{\frac{2}{M}E}\, dn(E)\, dE$$
$$= \rho \left(\frac{M}{2\pi kT}\right)^{\frac{1}{2}} \frac{kT}{M} \tag{12}$$

then the collision number for a one dimensional system is

$${}^1Z_{10} = (1 - e^{-\hbar\omega/kT})^{-1}\left[\frac{1}{kT}\int_0^\infty P_{10}(E)\, e^{-E/kT}\, dE\right]^{-1} \tag{13}$$

The superscript 1 on ${}^1Z_{10}$ indicates a one-dimensional system. For a three-dimensional system in translational equilibrium, k_{10} has the form

$$k_{10} = \int_0^\infty \sigma_{10}(E) \sqrt{\frac{2}{M}E}\, dn(E)\, dE \tag{14}$$
$$\text{where } dn(E) = \rho 2\pi \left(\frac{1}{\pi kT}\right)^{3/2} E^{\frac{1}{2}}\, e^{-\frac{E}{kT}}\, dE$$

Here ρ is the number of particles per unit volume and $dn(E)$ is the Maxwell distribution of particles per unit volume between energies E and E + dE. To determine k_c we need an expression for the total crossection. Herzfeld et al.[1] implicitly write k_c as

$$k_0 = \int_0^\infty (\text{total crossection}) \sqrt{\frac{2}{M}E}\, dn(E)\, dE$$
$$\approx \sigma_c \int_0^\infty \sqrt{\frac{2}{M}E}\, dn(E)\, dE \tag{15}$$
$$= \sigma_c \rho \frac{8\pi}{M^2} \left(\frac{M}{2\pi kT}\right)^{3/2} (kT)^2$$

Here σ_c is an effective crossection which is temperature-dependent. Since we will look at only ratios of collision numbers, the exact value

of σ_c is unimportant. The collision number for a three-dimensional system is

$$Z_{10} = (1 - e^{-\hbar\omega/kT})^{-1} \sigma_c \left[\frac{1}{(kT)^2} \int_0^\infty \sigma_{10}(E)\, E\, e^{-E/kT} dE\right]^{-1} \qquad (16)$$

SSH theory provides approximate formulas for the bracketed terms in the Eqs. (13) and (16) for ${}^1Z_{10}$ and Z_{10}. From the calculations presented in section III, we can calculate these terms exactly. We first consider the one-dimensional model of our three collision systems and then the three-dimensional model of the Cl_2—Cl_2 system.

The SSH formula for ${}^1Z_{10}$ is based on the following three approximations used in evaluating:

$$\frac{1}{kT} \int_0^\infty P_{10}(E)\, e^{-E/kT}\, dE. \qquad (17)$$

First, LJ can be replaced by either EXPA or EXPB. We will discuss only the SSH formulas using EXPA. From the discussion of section III, we would expect and our calculations show that the SSH formulas using EXPB are not as accurate as those using EXPA. Second, P_{10} can be replaced by the Jackson-Mott[9] formula for P_{10}^{DW}, the distorted wave probability for a head-on collision governed by an exponentially repulsive potential. Third, the integral of P_{10} over the Maxwell distribution can be evaluated by a modified method of steepest descent. Let us designate ${}^1Z_{10}^A$ as the SSH collision numbers for the EXPA fit to LJ. If the second and third approximations are exact, ${}^1Z_{10}^A$ should be identical to ${}^1Z_{10}^{EXPA}$. In Fig. 10 we plot for all three systems the $\log_{10}({}^1Z_{10}^A/{}^1Z_{10}^{EXPA})$ as a function of reduced temperature $kT/\hbar\omega$. One unit in reduced temperature is 2230°K for O_2—O_2, 810°K

for Cl_2-Cl_2, and 470°K for Br_2-Br_2. In Fig. 10, ${}^1Z_{10}^A/{}^1Z_{10}^{EXPA}$ varies rapidly at low temperatures for two systems and at higher temperatures tends to a constant considerably less than 1 for all three systems. The second and third approximations are in error. Examining the third approximation first, we find that the evaluation of the integral in expression (17) is obtained by expanding the integrand about its maximum value. In that expansion, the dependence of α on E is ignored; α is one of the potential parameters in EXPA [see Eq. (5)]. Although α is a weak function of E, the Jackson-Mott formula for P_{10}^{DW} is a very strong function of α, especially at low energies. In the SSH formula α_M is used where α_M is the value of α at the energy, E_M, for which the integrand has a maximum. Let us use in the expansion of the integrand

$$\alpha = \alpha_M + (E - E_M)\,\alpha'_M$$
$$\text{where } \alpha'_M = \frac{\partial \alpha}{\partial E}\,\Big|\, E = E_M \tag{18}$$

To first order in α'_M, we get the modified collision number ${}^1Z_{10}^{MA}$:

$${}^1Z_{10}^{MA} = (1 - \tfrac{1}{3}\beta v_M)\, e^{\frac{1+2\epsilon}{2kT}\beta v_M}\, {}^1Z_{10}^A$$
$$\text{where } \beta = \frac{\alpha'_M}{\alpha_M};\ v_M = \sqrt{\frac{2}{M}\,E_M} \tag{19}$$

β can be determined from α_M and the formula relating α to ϵ and σ for each value of E. In Fig. 11 we plot for all three systems $\log_{10}({}^1Z_{10}^{MA}/{}^1Z_{10}^{EXPA})$ as a function of $kT/\hbar\omega$. ${}^1Z_{10}^{MA}/{}^1Z_{10}^{EXPA}$ does not vary rapidly with reduced temperature. The second approximation can also be improved because the Jackson-Mott formula for P_{10}^{DW} is not as accurate as the

the exact formula for P_{10}^{DW} evaluated by Mies.[10] Secrest[11] has shown that P_{10}^{DW} is quite close to P_{10}^{EXPA} for several systems. Let ${}^1Z_{10}^{DWMA}$ designate the SSH collision number with both the second and third approximations improved upon. In Fig. 12 we plot for all three systems $\log_{10}({}^1Z_{10}^{DWMA}/{}^1Z_{10}^{EXPA})$ as a function of $kT/\hbar\omega$. The ratio ${}^1Z_{10}^{DWMA}/{}^1Z_{10}^{EXPA}$ is approximately 1 over the whole temperature range. Therefore, the second and third approximations suitably modified introduce little error into one-dimensional collision numbers. The effect of the first approximation is shown in Fig. 13 where $\log_{10}({}^1Z_{10}^{EXPA}/{}^1Z_{10}^{LJ})$ for all three systems is plotted as a function of $kT/\hbar\omega$. The low energy disagreement of P_{10}^{EXPA} with P_{10}^{LJ} discussed in section III appears as a low temperature disagreement of ${}^1Z_{10}^{EXPA}$ with ${}^1Z_{10}^{LJ}$. Figs. 10, 11, 12, and 13 show that, for a 1-dimensional model of our three collision systems, a modified form of SSH theory correctly predicts collision numbers except at temperatures low enough to make the effects of the well important.

The SSH formula for Z_{10} is based on an approximate evaluation of:

$$\frac{1}{(kT)^2}\int_0^\infty \sigma_{10}(E)\, E e^{-E/kT}\, dE \qquad (20)$$

This requires a fourth approximation not used in evaluating ${}^1Z_{10}$, i.e.

$$\left[\frac{1}{(kT)^2}\int_0^\infty \sigma_{10}(E)\, E\, e^{-E/kT}\, dE\right] = \pi r_M^2 \left[\frac{1}{kT}\int_0^\infty P_{10}(E) e^{-E/kT}\, dE\right] \qquad (21)$$

where r_M is the classical turning point for E_M, the value of E at which the integrand on the right hand side reaches a maximum. The integral

on the right hand side is expression (17) used in ${}^1Z_{10}$. In Fig. 14, we plot for the Cl_2-Cl_2 system both $\log_{10}(Z_{10}^{DWMA}/Z_{10}^{EXPA})$ and $\log_{10}({}^1Z_{10}^{DWMA}/{}^1Z_{10}^{EXPA})$ as a function of $kT/\hbar\omega$. If the fourth approximation is exact, the two curves should be identical. They are different with the greatest disagreement at low temperatures. In Fig. 15 we plot for the Cl_2-Cl_2 system $\log_{10}(Z_{10}^{EXPA}/Z_{10}^{LJ})$ and $\log_{10}({}^1Z_{10}^{EXPA}/{}^1Z_{10}^{LJ})$ as a function of $kT/\hbar\omega$. Because the well affects crossections less than probabilities, the first curve departs from zero less than the second. In Fig. 16 we plot for the Cl_2-Cl_2 system $\log_{10}(Z_{10}^{DWMA}/Z_{10}^{LJ})$ and $\log_{10}({}^1Z_{10}^{DWMA}/{}^1Z_{10}^{LJ})$ as a function of $kT/\hbar\omega$. The two curves are very similar, with the greatest departure from zero occurring at low temperatures. For the three-dimensional model, Figs. 14 and 15 indicate that the disagreement of Z_{10}^{DWMA} with Z_{10}^{LJ} at low temperatures is due equally to the inability of SSH theory to correctly include the effects of the well and to accurately infer crossections from probabilities. We have already shown that ${}^1Z_{10}^{DWMA}$ disagrees with ${}^1Z_{10}^{LJ}$ at low temperatures due mainly to the effects of the well. If the results shown in Fig. 16 are typical for many collision systems, then our conclusions about the accuracy of ${}^1Z_{10}^{DWMA}$ for the O_2-O_2 and the Br_2-Br_2 systems could equally well apply to Z_{10}^{DWMA} for these two systems. To the degree that the modeling described in section II is correct, we can conclude from these calculations that SSH theory accurately predicts collision numbers from known potential parameters except at low temperatures, where the theory incorrectly estimates well effects and crossections.

SSH theory can also be used to analyze experimental collision numbers for unknown potential parameters. If we consider ${}^1Z_{10}^{LJ}$ to be the experimental result, then we can adjust the potential parameters in the SSH theory so that ${}^1Z_{10}^{DWMA}$ becomes equal to ${}^1Z_{10}^{LJ}$. The resulting potential parameters can then be compared to the σ and ϵ which actually produced ${}^1Z_{10}^{LJ}$. Let us call σ_A the potential parameter in conjunction with ϵ that makes ${}^1Z_{10}^{DWMA}$ equal to ${}^1Z_{10}^{LJ}$. Let us call ϵ_A the potential parameter in conjunction with σ that makes ${}^1Z_{10}^{DWMA}$ equal to ${}^1Z_{10}^{LJ}$. In Figure 17, we plot $(\sigma_A/\sigma) \times 100$ and $(\epsilon_A/\epsilon) \times 100$ as a function of $kT/\hbar\omega$ for all three systems. Over this temperature range, σ_A is within 10% to 15% of σ. However, ϵ_A is never more than 70% of ϵ, even when ϵ is very large. For the O_2–O_2 system, no ϵ_A can be found which in conjunction with σ will make ${}^1Z_{10}^{DWMA}$ equal to ${}^1Z_{10}^{LJ}$. This is so because SSH theory does not properly estimate well effects. Even though SSH theory is more accurate at high temperatures, it is not because it more accurately predicts well effects, but because well effects are less important at high temperatures. There is no temperature range over which SSH theory will accurately predict the depth of the potential well for our three systems.

VI. CONCLUSION

Three conclusions can be drawn from this work. First, calculations of quantum mechanical crossections for vibrational scattering off of spherically symmetric potentials are currently practical. Efficient computational methods, suitably restrictive channel sets, and interpolation procedures help make the calculations feasible. Second, the comparison of probabilities and crossections between the Lennard-Jones potential and several "well-less" potentials emphasizes the adiabatic long-range nature of potentials with wells. The presence of the well washes out structure in the probabilities as a function of energy and produces probabilities and crossections less than that estimated by the acceleration approximation. Third, SSH theory reasonably accurately predicts collision numbers except at low temperatures where it incorrectly estimates well effects and crossections. SSH theory can not be used to accurately determine the depth of the well.

REFERENCES

[1] K. F. Herzfeld and T. A. Litovitz, Absorption and Dispersion of Ultrasonic Waves (Academic Press, New York, 1959), Chapt. VII, p. 260.

[2] B. Hartmann and Z. I. Slawsky, J. Chem. Phys. 47, 2491, (1966).

[3] D. J. Wilson, J. Chem. Phys. 54, 540 (1971).

[4] A. F. Wagner and V. McKoy, J. Chem. Phys. (to be published).

[5] V. P. Gutschick and V. McKoy, J. Chem. Phys. 54, 4807 (1970).

[6] D. Secrest and B. R. Johnson, J. Chem. Phys. 45, 4556 (1966).

[7] R. G. Gordon, J. Chem. Phys. 51, 14 (1969).

[8] A. S. Cheung and D. J. Wilson, J. Chem. Phys. 51, 4733 (1969).

[9] J. M. Jackson and N. F. Mott, Proc. Roy. Soc. (London), A137, 703 (1932).

[10] F. H. Mies, J. Chem. Phys. 40, 523 (1964).

[11] D. Secrest, J. Chem. Phys. 49, 2880 (1968).

Table I. System Parameters[1]

Parameter	O_2—O_2	Cl_2—Cl_2	Br_2—Br_2
ϵ	.0508	.441	1.106
σ	131.7	141.7	168.1
unit of energy: $\hbar\omega$ (°K)	2230	810	470
unit of length: $\frac{1}{2}\sqrt{\frac{\hbar\omega}{k_e}}$ (A°)	.02606	.02909	.02538

[1] K. F. Herzfeld and T. A. Litovitz, Absorption and Dispersion of Ultrasonic Waves (Academic Press, New York, 1959), p. 321.

Table II. The number of channels in the expansion set as a function of the number of open channels.

Open Channels	O_2–O_2	Cl_2–Cl_2	Br_2–Br_2
2	3	3	5
3	4	4	5
4	4	4	5
5	4	4	5
7	5	5	6
9	5	6	6
12	6	6	7
14	8	7	7

FIGURE CAPTIONS

Fig. 1. Coordinate System.

Fig. 2. $\text{Log}_{10}\ (P_{10}^{LJ})$ vs. E for O_2-O_2, Cl_2-Cl_2, and Br_2-Br_2.

Fig. 3. $\text{Log}_{10}\ (P_{10}^{EXPA}/P_{10}^{LJ})$ vs. E for O_2-O_2, Cl_2-Cl_2, and Br_2-Br_2.

Fig. 4. $\text{Log}_{10}\ (P_{10}^{EXPB}/P_{10}^{LJ})$ vs. E for O_2-O_2, Cl_2-Cl_2, and Br_2-Br_2.

Fig. 5. $\text{Log}_{10}\ (\sigma_{10}^{LJ})$ vs. E for Cl_2-Cl_2. σ_{10}^{LJ} is in Å^2.

Fig. 6. $\text{Log}_{10}\ (\sigma_{10}^{EXPA}/\sigma_{10}^{LJ})$ and $\log_{10}\ (P_{10}^{EXPA}/P_{10}^{LJ})$ vs. E for Cl_2-Cl_2.

Fig. 7. $\text{Log}_{10}\ (P_{10}^{LJC})$ vs. E for O_2-O_2, Cl_2-Cl_2, and Br_2-Br_2.

Fig. 8. $\text{Log}_{10}\ (P_{10}^{C})$ vs. E for O_2-O_2, Cl_2-Cl_2, and Br_2-Br_2.

Fig. 9. $\text{Log}_{10}\ (P_{10}^{LJC}/P_{10}^{LJ})$ vs. E for O_2-O_2, Cl_2-Cl_2, and Br_2-Br_2.

Fig. 10. $\text{Log}_{10}\ ({}^1Z_{10}^{A}/{}^1Z_{10}^{EXPA})$ vs. $kT/\hbar\omega$ for O_2-O_2, Cl_2-Cl_2, and Br_2-Br_2.

Fig. 11. $\text{Log}_{10}\ ({}^1Z_{10}^{MA}/{}^1Z_{10}^{EXPA})$ vs. $kT/\hbar\omega$ for O_2-O_2, Cl_2-Cl_2, and Br_2-Br_2.

Fig. 12. $\text{Log}_{10}\ ({}^1Z_{10}^{DWMA}/{}^1Z_{10}^{EXPA})$ vs. $kT/\hbar\omega$ for O_2-O_2, Cl_2-Cl_2, and Br_2-Br_2.

Fig. 13. $\text{Log}_{10}\ ({}^1Z_{10}^{EXPA}/{}^1Z_{10}^{LJ})$ vs. $kT/\hbar\omega$ for O_2-O_2, Cl_2-Cl_2, and Br_2-Br_2.

Fig. 14. $\text{Log}_{10}\ (Z_{10}^{DWMA}/Z_{10}^{EXPA})$ and $\log_{10}\ ({}^1Z_{10}^{DWMA}/{}^1Z_{10}^{EXPA})$ vs. $kT/\hbar\omega$ for Cl_2-Cl_2.

Fig. 15. $\text{Log}_{10}\ (Z_{10}^{EXPA}/Z_{10}^{LJ})$ and $\log_{10}\ ({}^1Z_{10}^{EXPA}/{}^1Z_{10}^{LJ})$ vs. $kT/\hbar\omega$ for Cl_2-Cl_2.

Fig. 16. $\text{Log}_{10}\ (Z_{10}^{DWMA}/Z_{10}^{LJ})$ and $\log_{10}\ ({}^1Z_{10}^{DWMA}/{}^1Z_{10}^{LJ})$ vs. $kT/\hbar\omega$ for Cl_2-Cl_2.

Fig. 17. 100 x σ_A/σ vs. $kT/\hbar\omega$ for O_2-O_2, Cl_2-Cl_2, and Br_2-Br_2; 100 x ϵ_A/ϵ vs. $kT/\hbar\omega$ for Cl_2-Cl_2 and Br_2-Br_2.

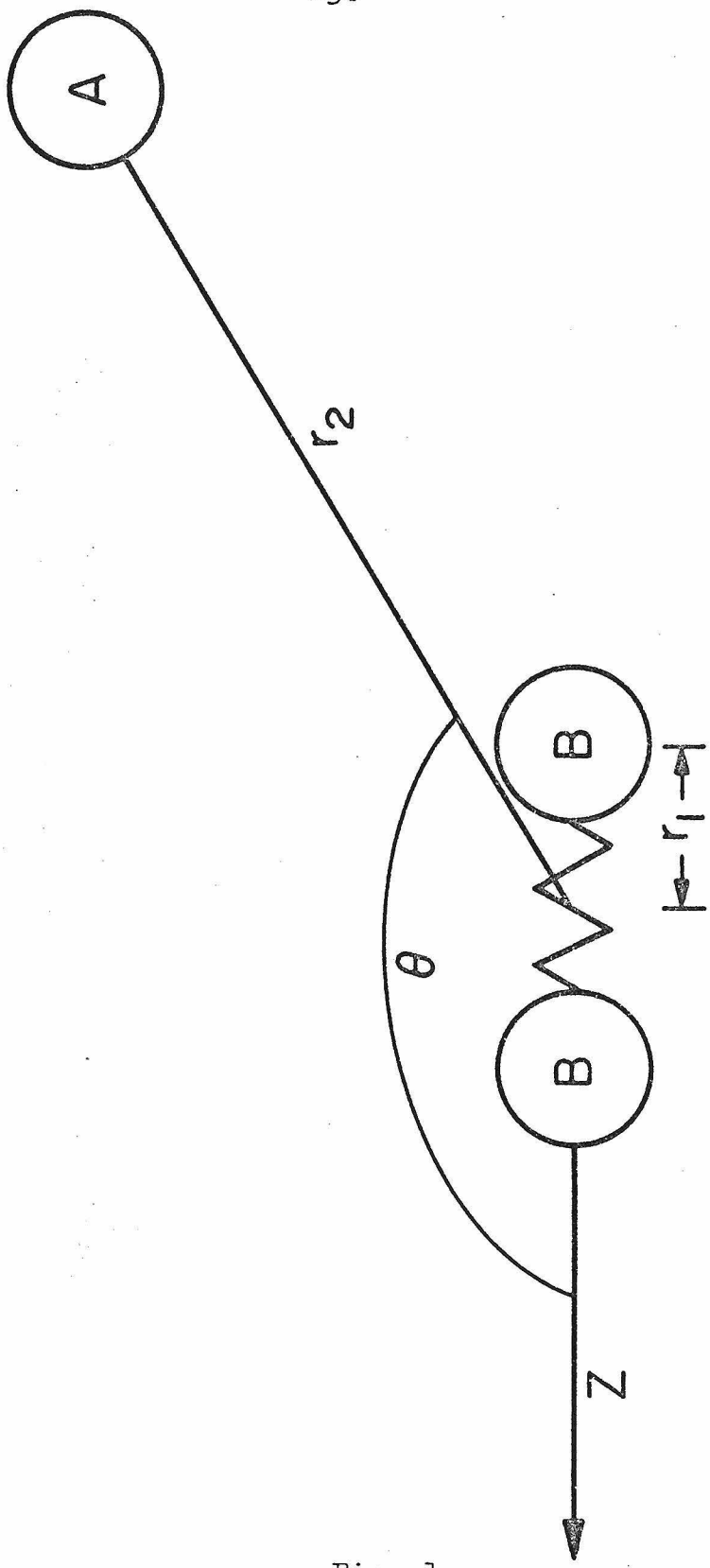

Fig. 1

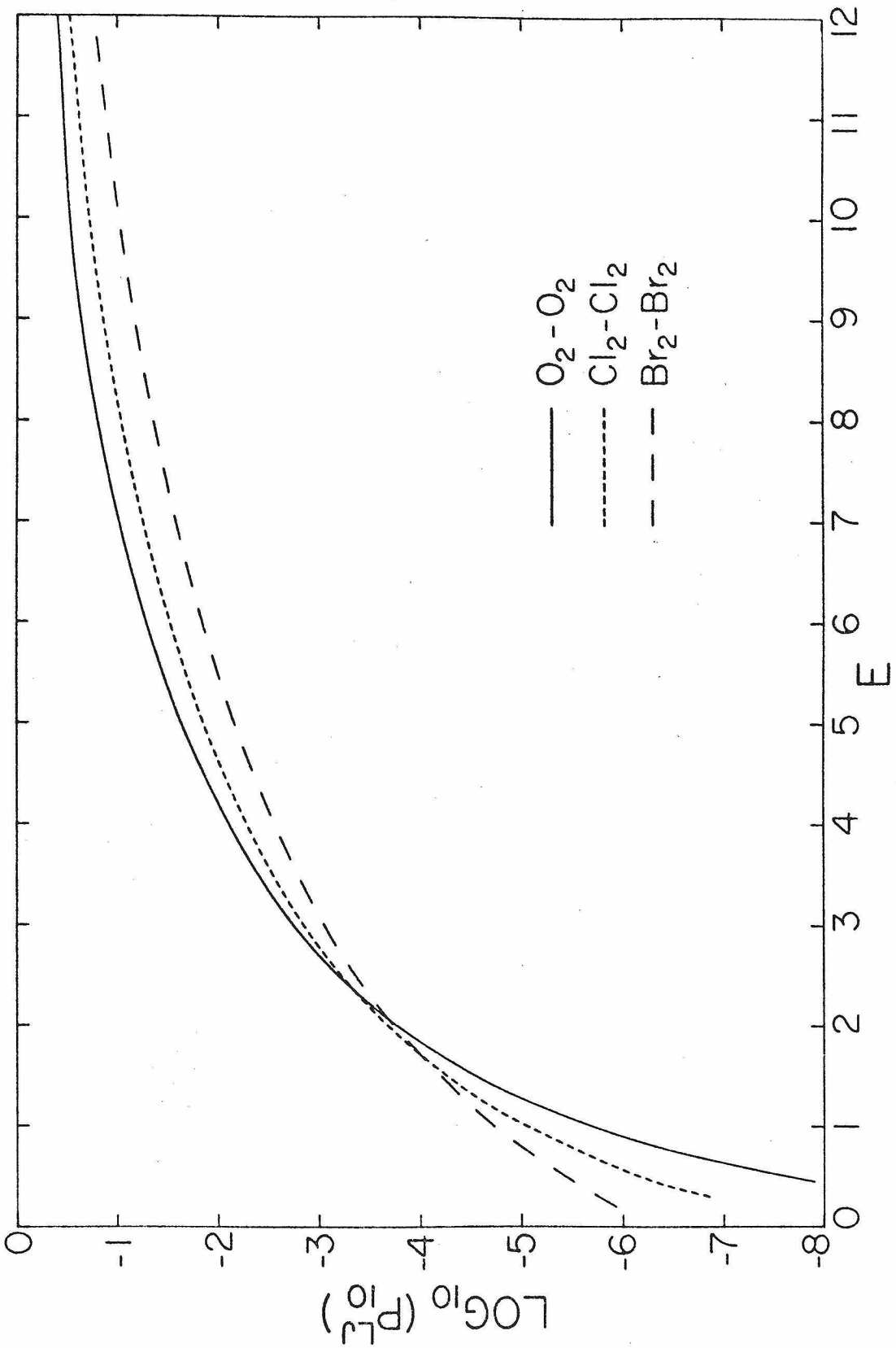
O_2-O_2
Cl_2-Cl_2
Br_2-Br_2
E
$LOG_{10}(P^{L_J}_{10})$
0
-1
-2
-3
-4
-5
-6
-7
-8
0
1
2
3
4
5
6
7
8
9
10
11
12

Fig. 2

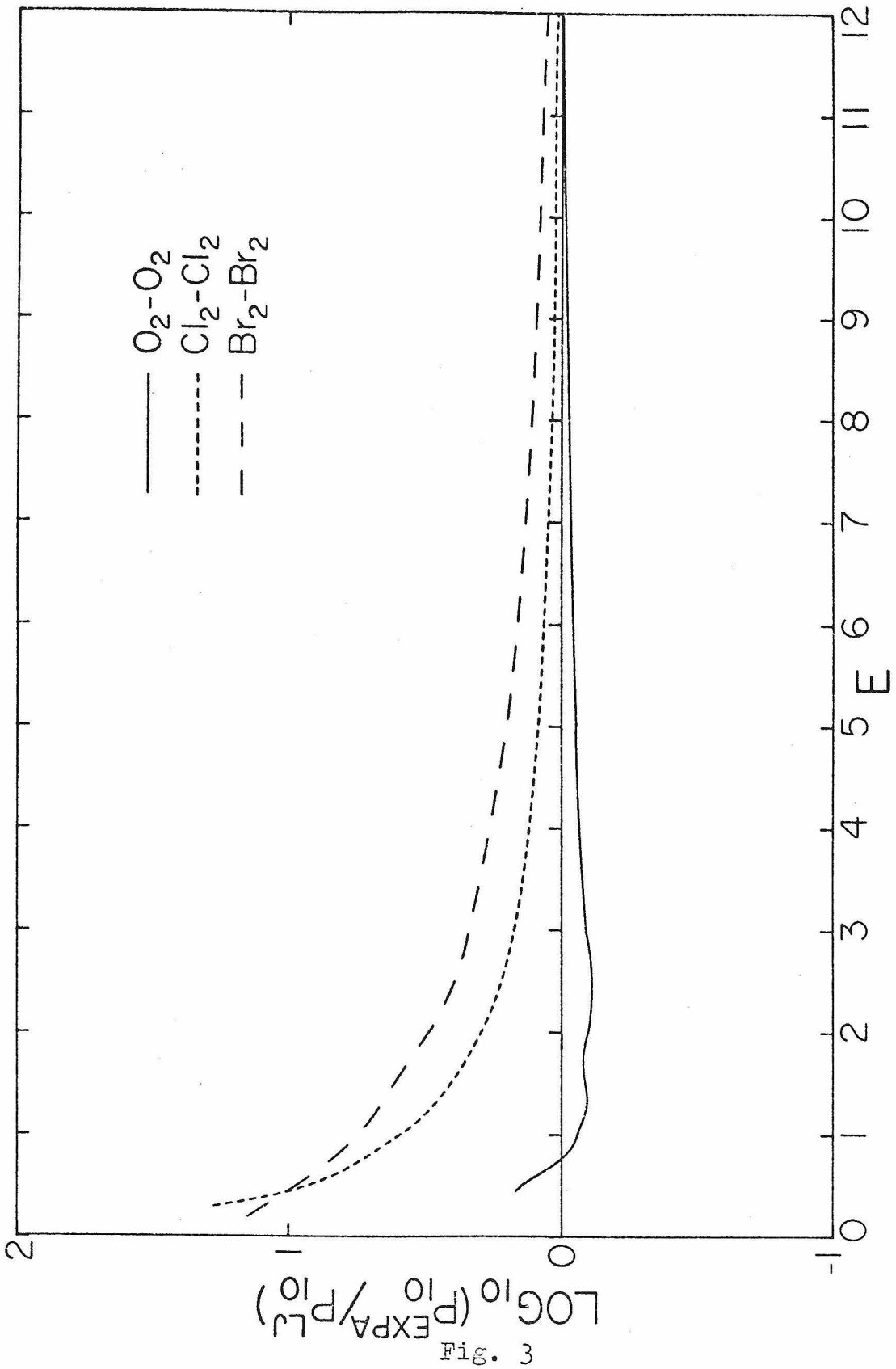
O_2-O_2
Cl_2-Cl_2
Br_2-Br_2
E
$LOG_{10}(P_{10}^{EXPA}/P_{10}^{LJ})$
2
1
0
-1
0
1
2
3
4
5
6
7
8
9
10
11
12

Fig. 3

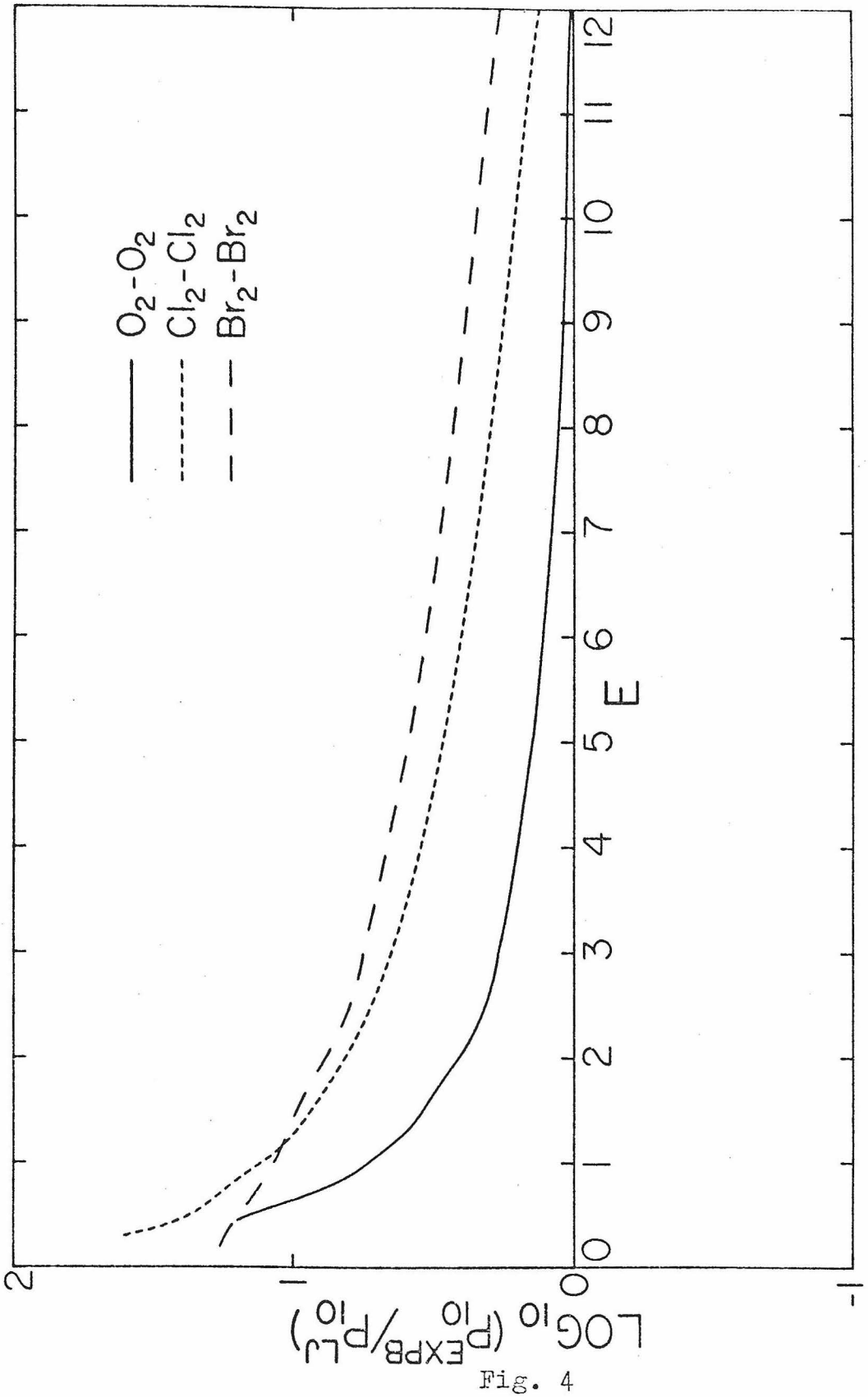
O_2-O_2
Cl_2-Cl_2
Br_2-Br_2
E
0
1
2
3
4
5
6
7
8
9
10
11
12
2
1
0
-1
LOG_{10} (P_{EXPB}/P_{10})

Fig. 4

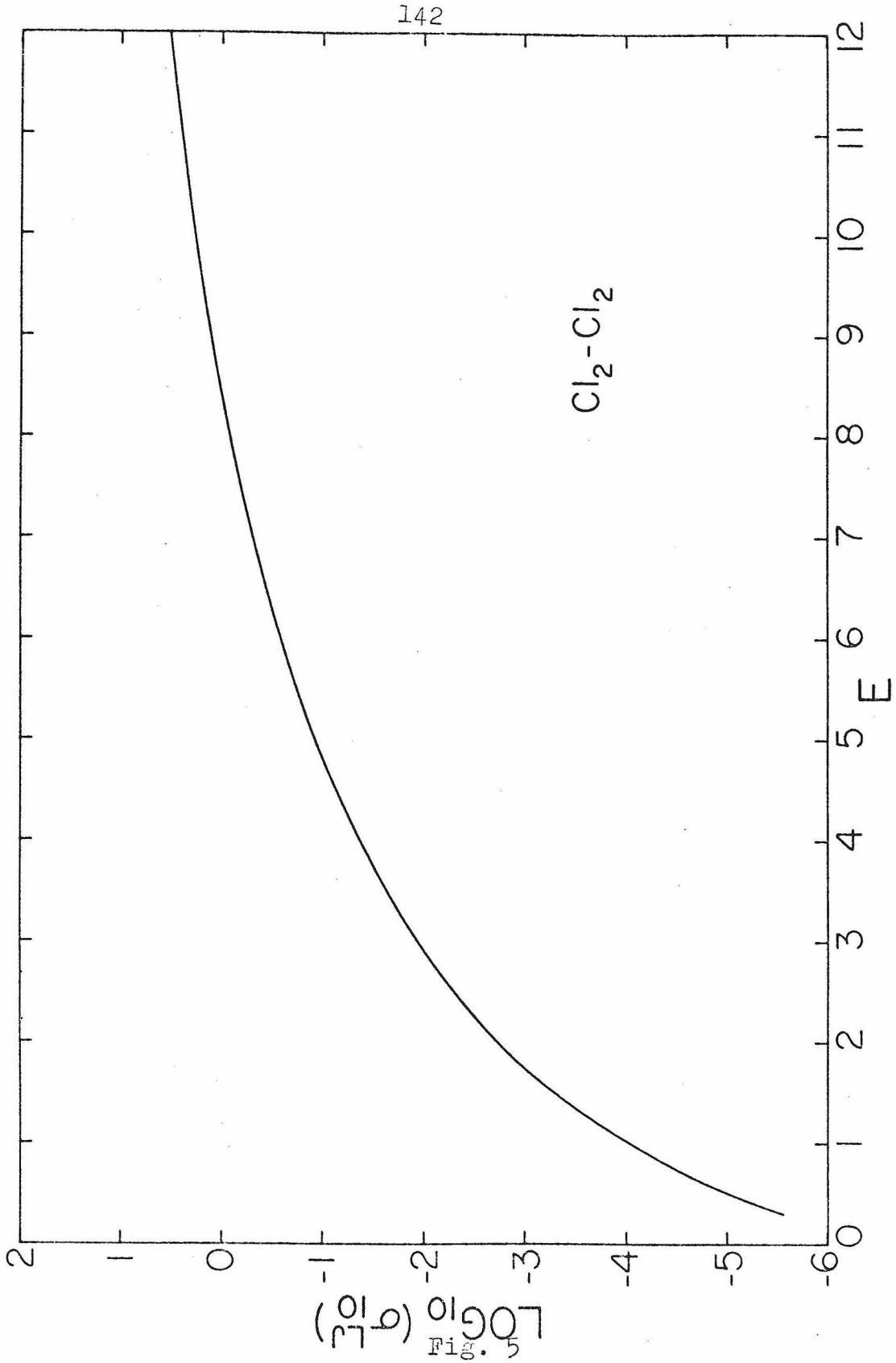

Fig. 5

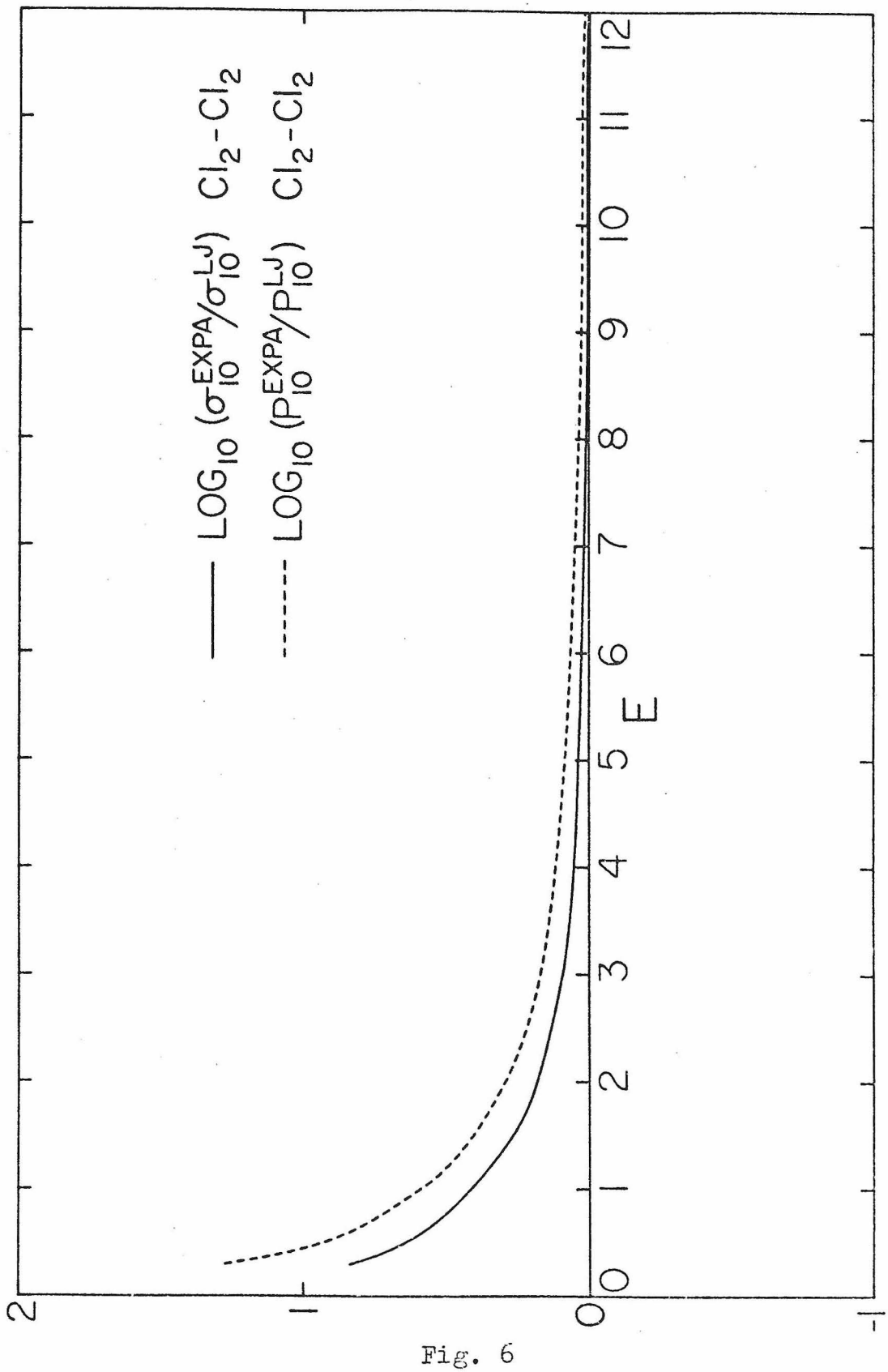
LOG10 (σ10EXPA/σ10LJ) Cl2-Cl2
LOG10 (P10EXPA/P10LJ) Cl2-Cl2
E
2
1
0
-1
0
1
2
3
4
5
6
7
8
9
10
11
12

Fig. 6

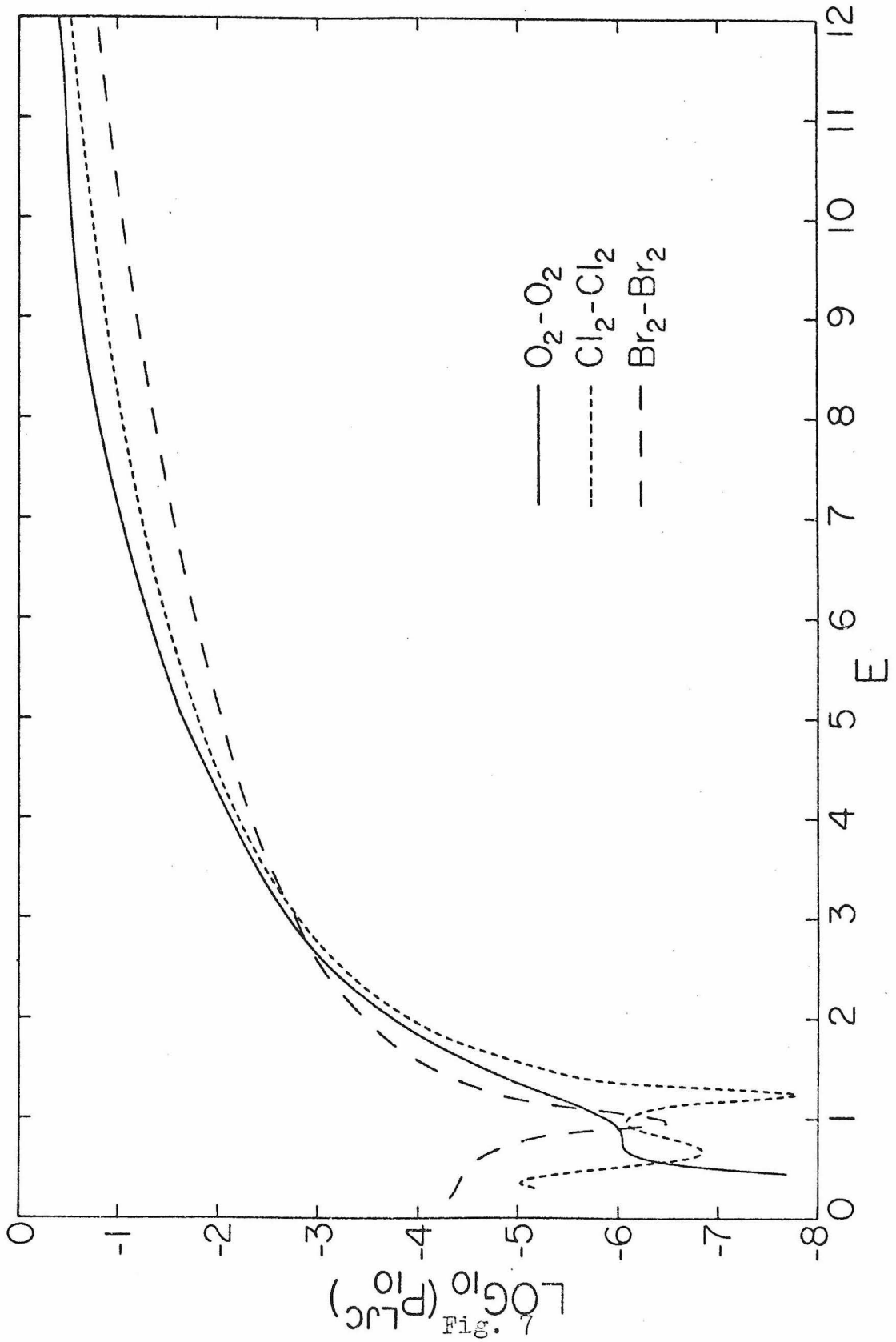
O_2-O_2
Cl_2-Cl_2
Br_2-Br_2
E
$LOG_{10}(P_{LIC})$
0
-1
-2
-3
-4
-5
-6
-7
-8
1
2
3
4
5
6
7
8
9
10
11
12

Fig. 7

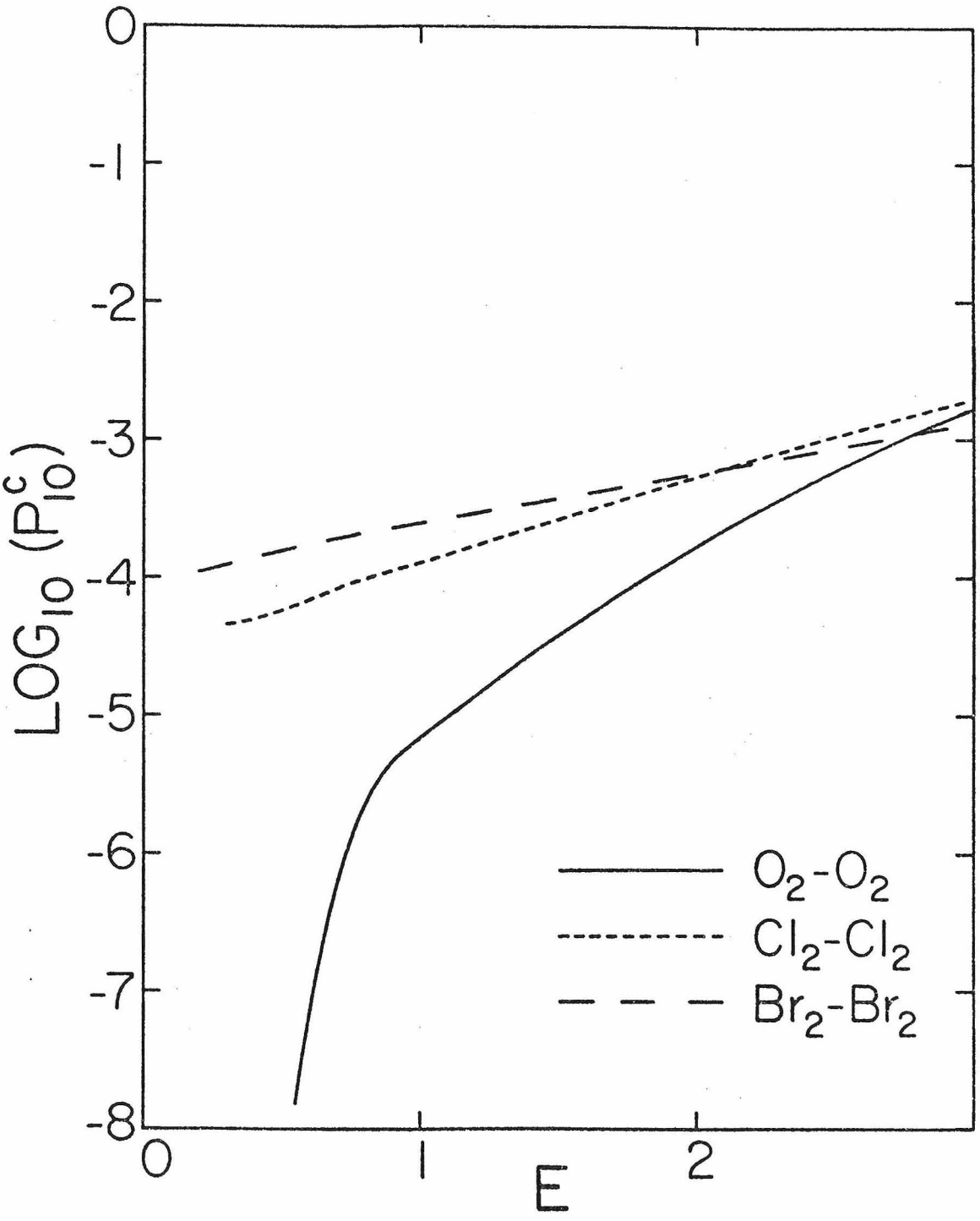

Fig. 8

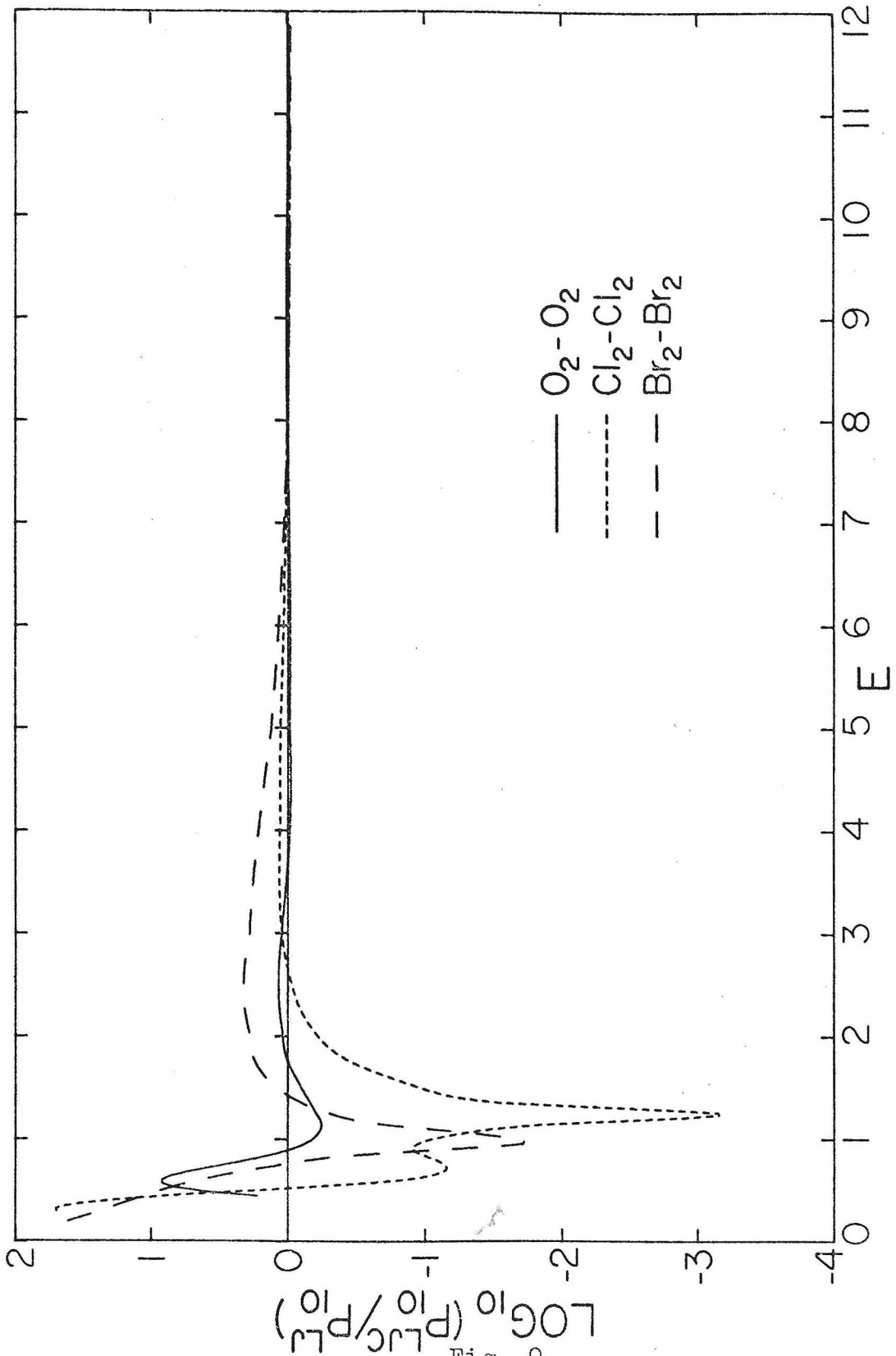

Fig. 9

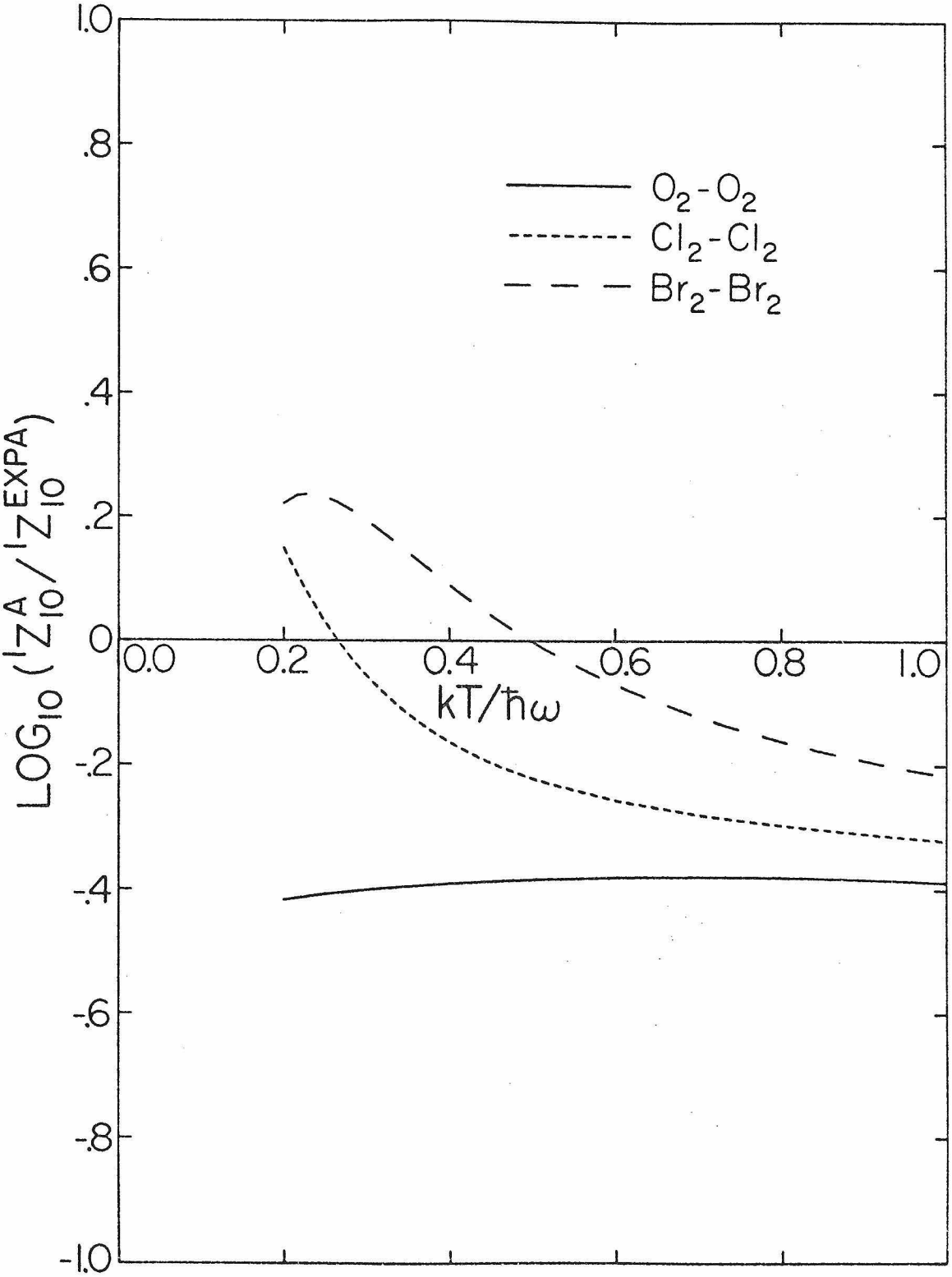
1.0
.8
.6
.4
.2
0
-.2
-.4
-.6
-.8
-1.0
0.0
0.2
0.4
0.6
0.8
1.0
kT/ħω
$LOG_{10}(^{1}Z^{A}_{10}/^{1}Z^{EXPA}_{10})$
O_2-O_2
Cl_2-Cl_2
Br_2-Br_2

Fig. 10

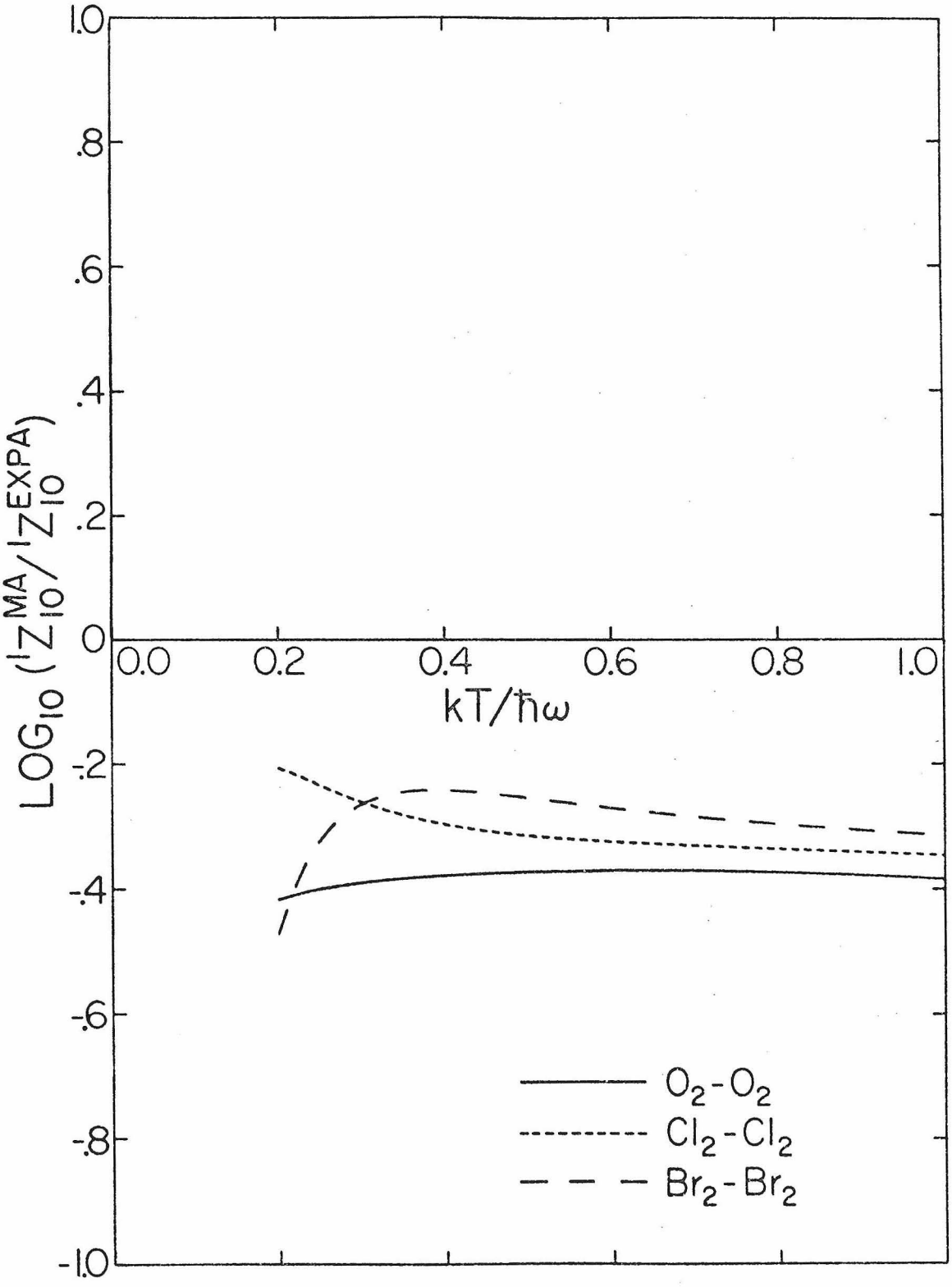
1.0
.8
.6
.4
.2
0
-.2
-.4
-.6
-.8
-1.0
0.0
0.2
0.4
0.6
0.8
1.0
kT/ħω
LOG10 (17Z10MA/17Z10EXPA)
O2-O2
Cl2-Cl2
Br2-Br2

Fig. 11

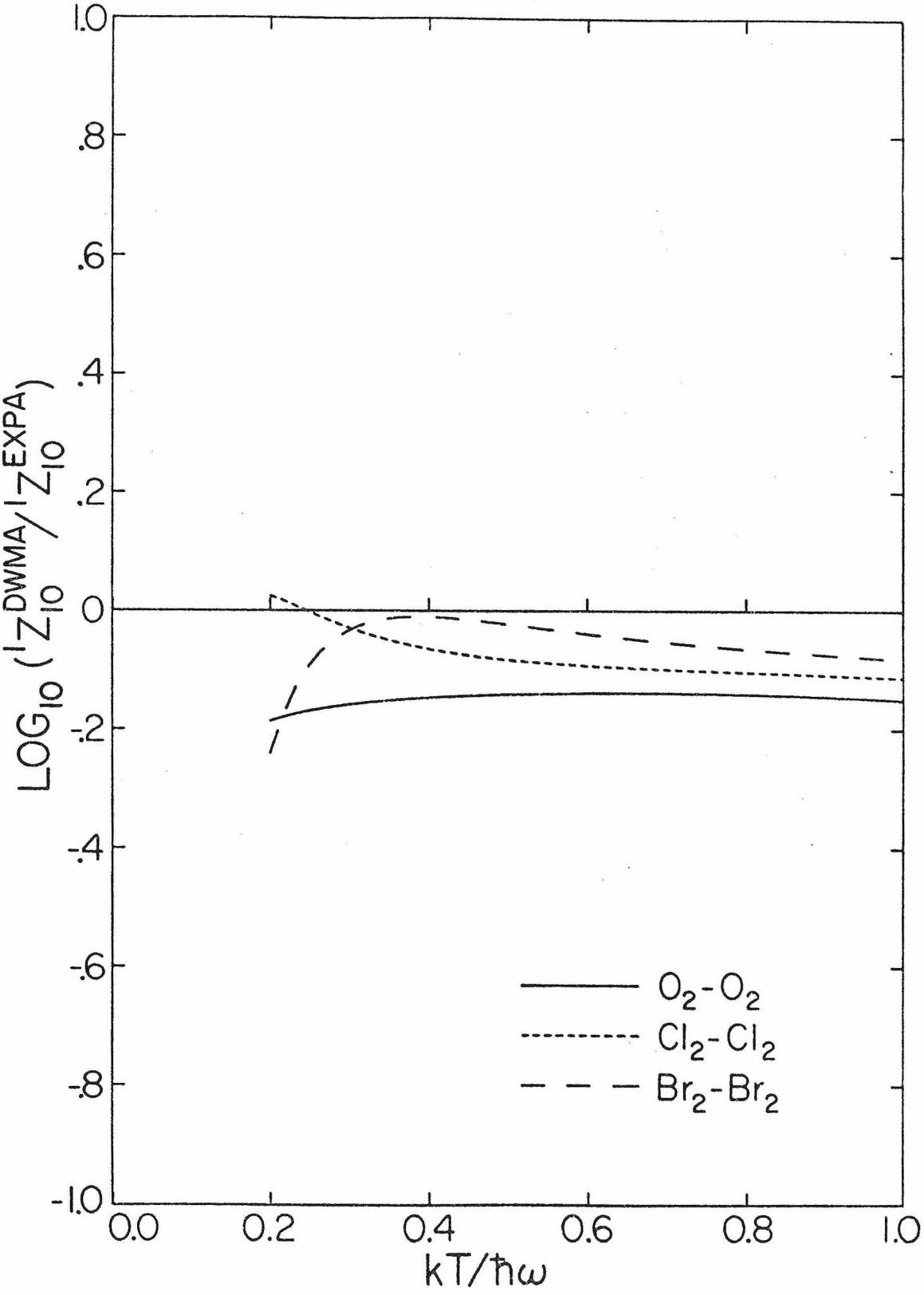
1.0
.8
.6
.4
.2
0
-.2
-.4
-.6
-.8
-1.0
0.0
0.2
0.4
0.6
0.8
1.0
$LOG_{10}(^{1}Z_{10}^{DWMA}/^{1}Z_{10}^{EXPA})$
$kT/\hbar\omega$
O_2-O_2
Cl_2-Cl_2
Br_2-Br_2

Fig. 12

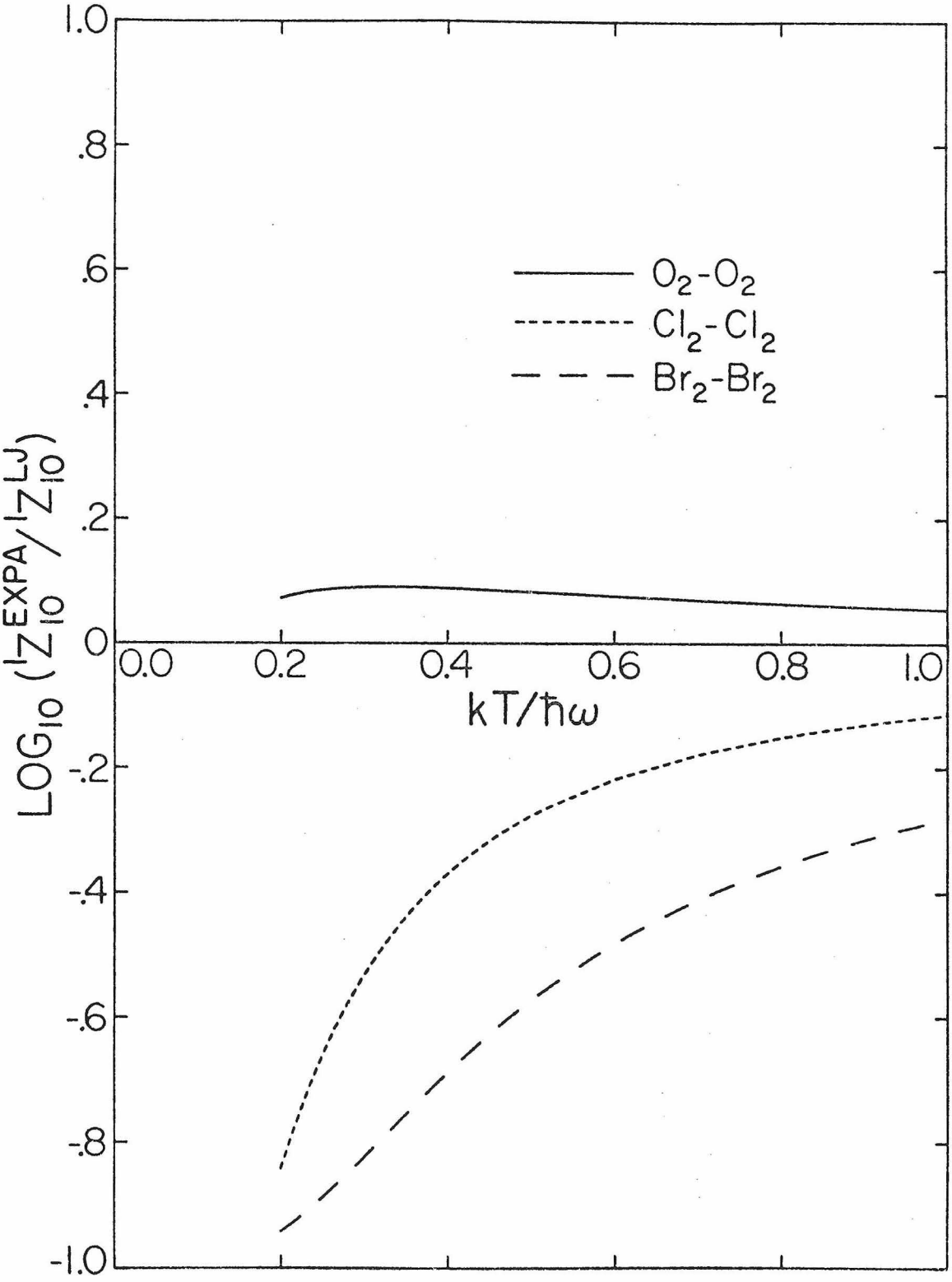
1.0
.8
.6
.4
.2
0
-.2
-.4
-.6
-.8
-1.0
0.0
0.2
0.4
0.6
0.8
1.0
kT/ħω
$LOG_{10}(^{I}Z_{10}^{EXPA}/^{I}Z_{10}^{LJ})$
O_2-O_2
Cl_2-Cl_2
Br_2-Br_2

Fig. 13

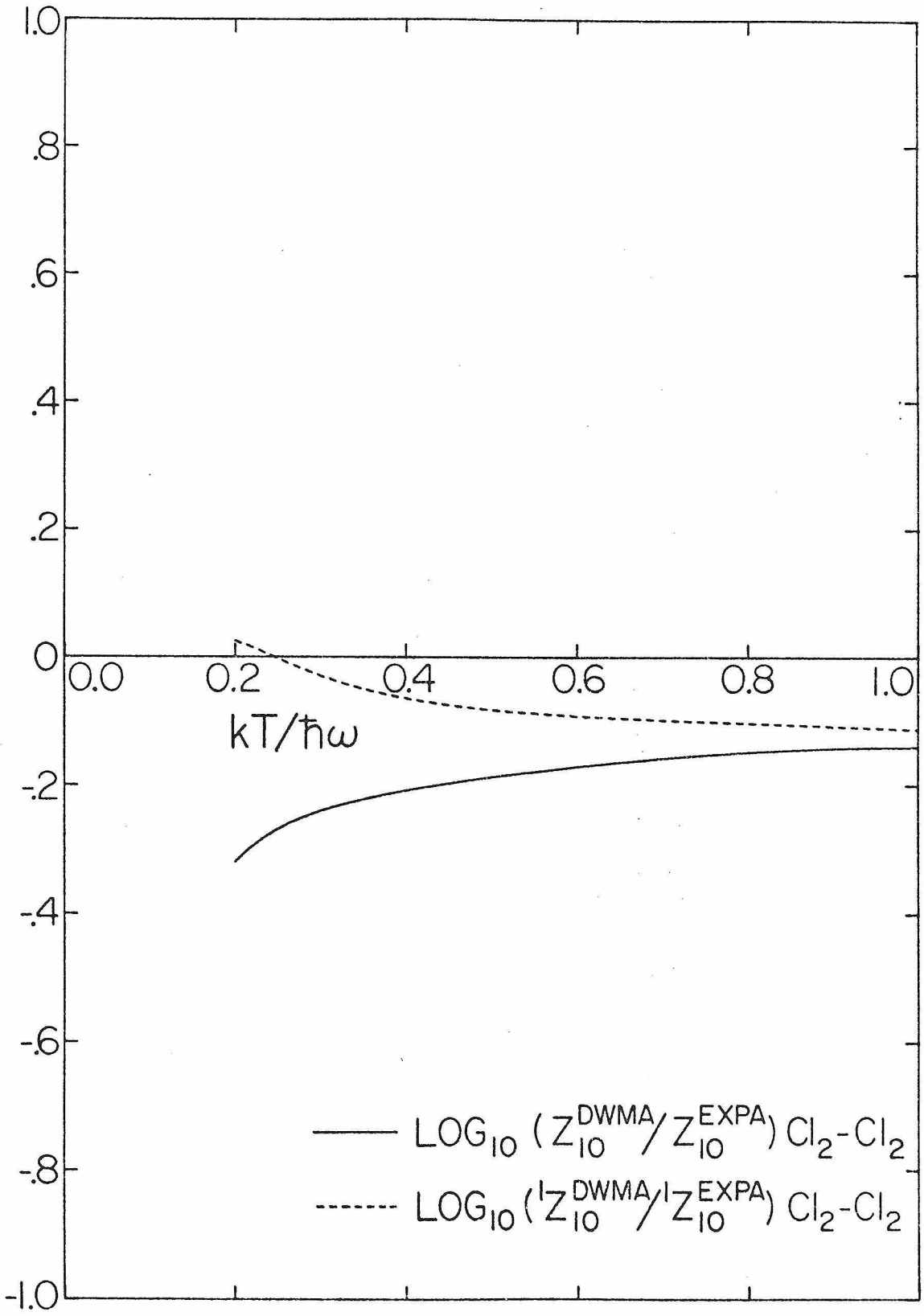
1.0
.8
.6
.4
.2
0
-.2
-.4
-.6
-.8
-1.0
0.0
0.2
0.4
0.6
0.8
1.0
kT/ħω
LOG10 (Z10DWMA/Z10EXPA) Cl2-Cl2
LOG10 (|Z10DWMA/|Z10EXPA) Cl2-Cl2

Fig. 14

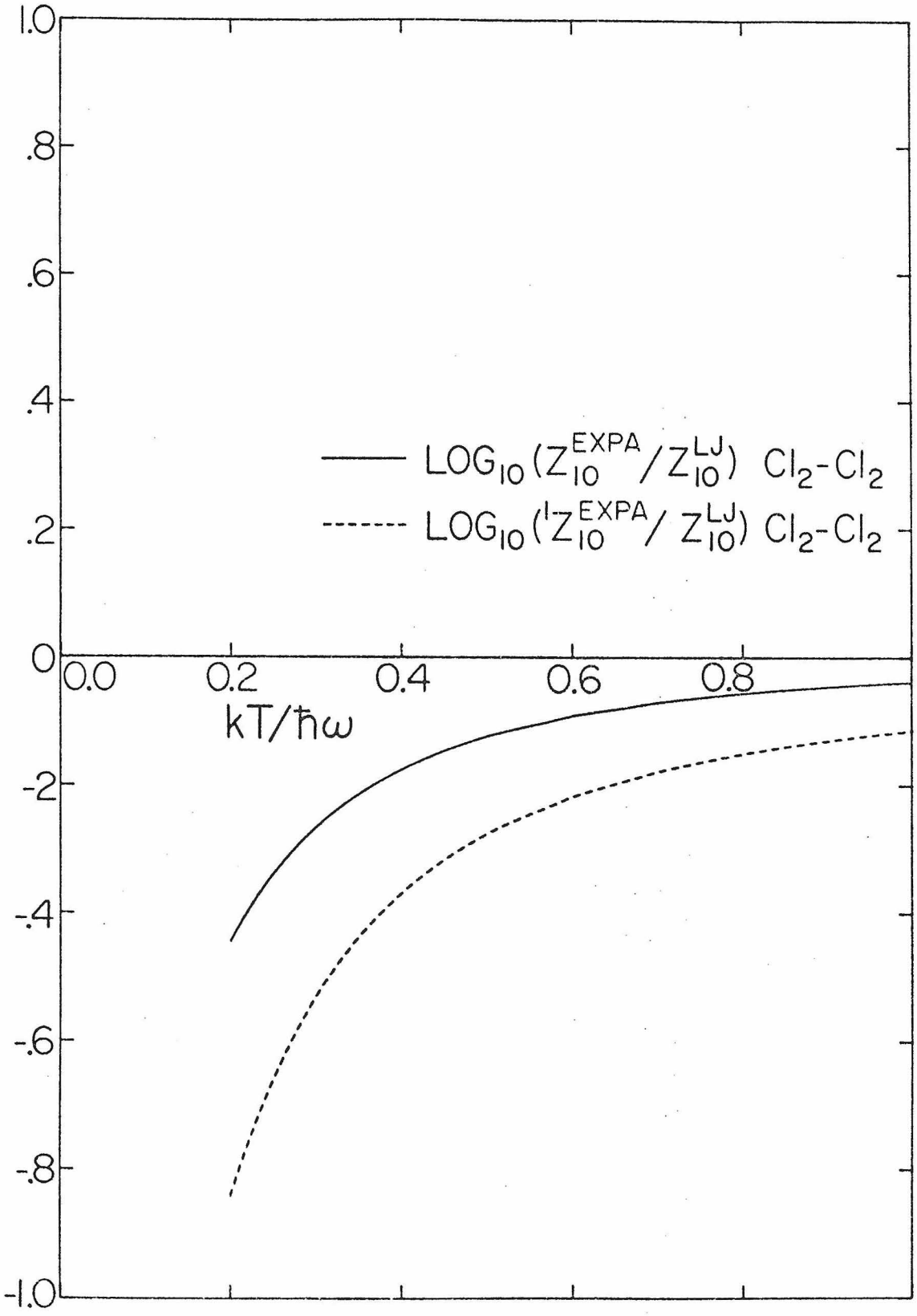
1.0
.8
.6
.4
.2
0
-.2
-.4
-.6
-.8
-1.0
0.0
0.2
0.4
0.6
0.8
kT/ħω
LOG10(Z10EXPA/Z10LJ) Cl2-Cl2
LOG10(1-Z10EXPA/Z10LJ) Cl2-Cl2

Fig. 15

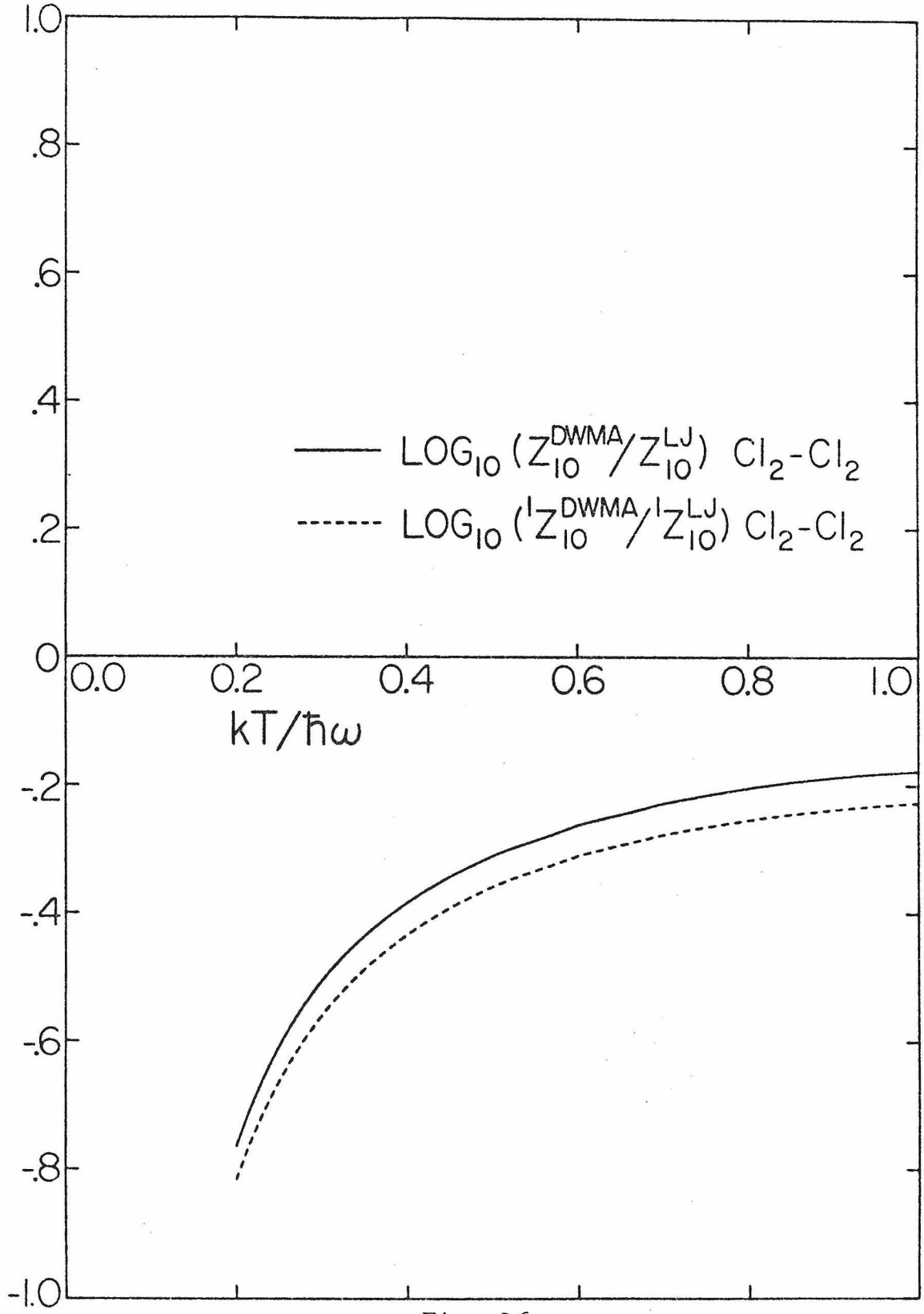
1.0
.8
.6
.4
.2
0
-.2
-.4
-.6
-.8
-1.0
0.0
0.2
0.4
0.6
0.8
1.0
kT/ħω
LOG10 (Z10DWMA/Z10LJ) Cl2-Cl2
LOG10 (1Z10DWMA/1Z10LJ) Cl2-Cl2

Fig. 16

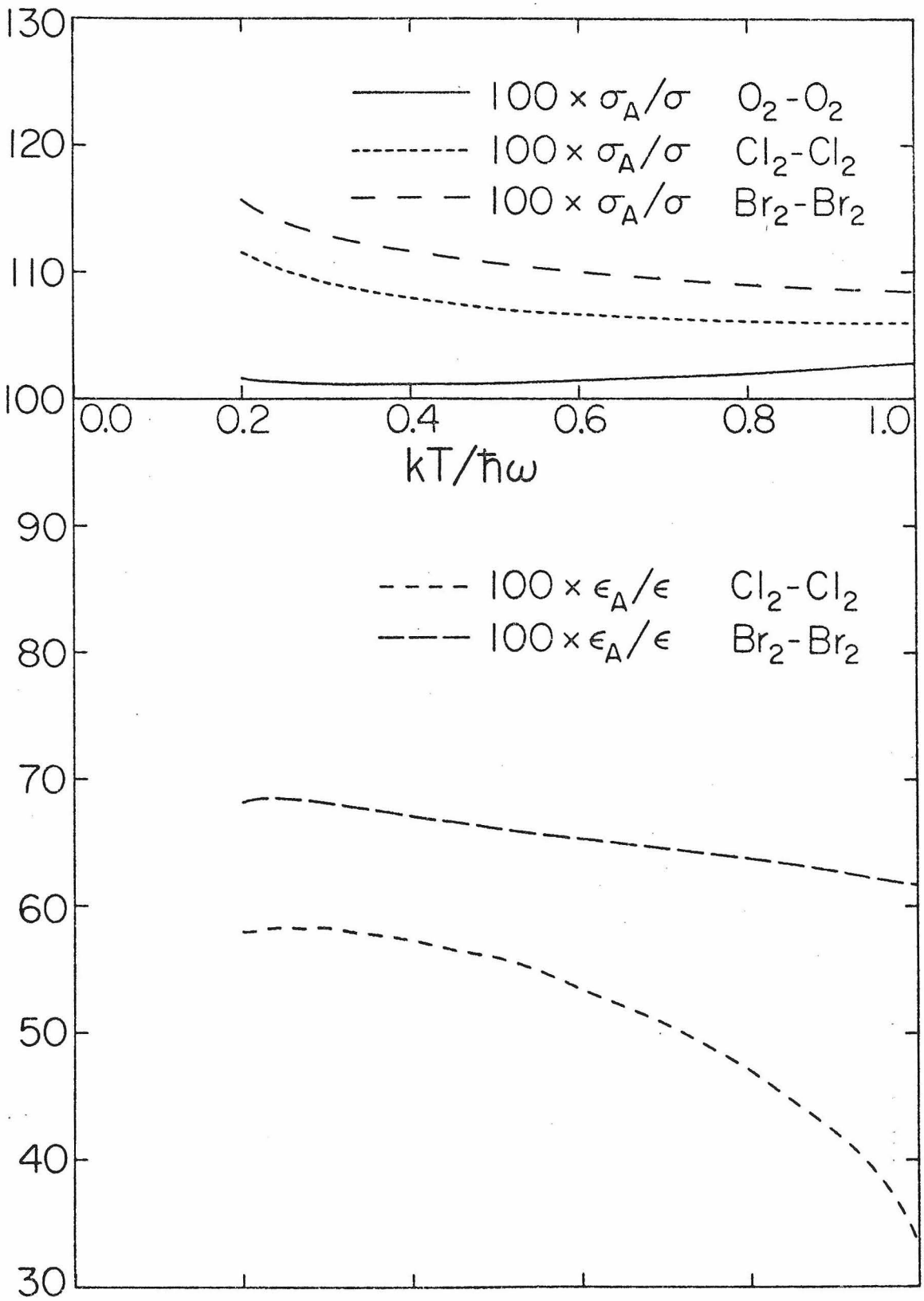
130
120
110
100
90
80
70
60
50
40
30
0.0
0.2
0.4
0.6
0.8
1.0
kT/ħω
100 × σA/σ O2-O2
100 × σA/σ Cl2-Cl2
100 × σA/σ Br2-Br2
100 × εA/ε Cl2-Cl2
100 × εA/ε Br2-Br2

Fig. 17